5-2010

Self-Assembly of Architecturally Complex Block Copolymers

Juan Hinestrosa
Clemson University, jhinest@clemson.edu

SELF-ASSEMBLY OF ARCHITECTURALLY COMPLEX BLOCK COPOLYMERS

A Dissertation
Presented to
The Graduate School of
Clemson University

In Partial Fulfillment
of the Requirements for the Degree
Doctor of Philosophy
Chemical Engineering

---

by
Juan Pablo Hinestrosa
May 2010

Accepted by:
Dr. Douglas E. Hirt, Committee Chair
Dr. S. Michael Kilbey, II
Dr. Anthony Guiseppe-Elie
Dr. Igor Luzinov

ABSTRACT

The term self-assembly denotes the formation of complex structures from simpler building blocks, resembling the manner in which Nature generates functional systems. In this pursuit, block copolymers present a great opportunity to study the interactions, dynamics and self-assembly of soft matter. Block copolymers have the ability to self-assemble into thermodynamically stable microphase segregated domains of precise shape and size, which are controlled by the chemistry of the constituent blocks, their size and connectivity, temperature and solvent conditions. Specifically, in this body of work two different types of branched copolymers with polystyrene (PS) and polyisoprene (PI) constituents are studied. The complex architectural arrangements studied include miktoarm block copolymers with a PS-PI-$(PI)_2$ configuration and symmetric $(PS)_n(PI)_n$ (A_nB_n) heteroarm star copolymers with an equal number of PS and PI arms emanating from a common junction point.

In the case of the miktoarm PS-PI-$(PI)_2$ block copolymers, the increase in complexity beyond a linear architecture clearly modifies the dynamics and structure of the macromolecules. I found by static and dynamic light scattering that these copolymers self-assemble into spherical micelles with cores composed of the unsolvated linear PS blocks and coronas formed by the well-solvated branched PI blocks. After thorough characterization of the micellization behavior, I followed the adsorption kinetics of these macromolecular ensembles using *in situ* phase modulated ellipsometry. In order to properly characterize their adsorption process from the initial fast adsorption to pseudo-equilibrium, a modeling framework that incorporates the effects of mass transport and

dynamic relaxation/reorganization events occurring at the solid/fluid interface is adopted. The results demonstrate commonality between adsorption of micelle-forming surfactant-like copolymers and biomimetic vesicles formed by small-molecule surfactants, both of which are systems whose adsorption behaviors are dominated by rearrangements on the surface.

The solution behavior of a set of A_nB_n heteroarm star copolymers was also examined. The systematic doubling of the number of arms in the symmetric $(PS)_n(PI)_n$ (A_nB_n) hetero-arm star copolymers results in a doubling of the total molecular weight while keeping the composition fixed. Dynamic light scattering experiments in n-hexane showed a loss of flexibility in the stars as the number of arms increase, an effect related to the increased intramolecular interactions as branching increases. Bimodal hydrodynamic size distributions for stars with 2 and 4 arms are observed, but only monomodal size distributions are observed for stars with 8 and 16 arms over the concentration range studied. Thus as the number of arms increases, the system becomes unable to self-assemble, mainly due to shielding posed by the longer PI blocks.

By studying these architecturally complex block copolymers, fundamental knowledge of how the structure and dynamics of polymeric materials can be modified by macromolecular design, solvent conditions and confinement is generated. This knowledge enhances our understanding of architecturally complex macromolecules and the role of chain architecture on behavior.

DEDICATION

This work is dedicated to my family and to Angela Montoya.

ACKNOWLEDGMENTS

First I want to acknowledge all the support and understanding from my family. Angela Montoya was a vital part of my time in graduate school with all her encouragement, listening and help. I want to thank my grandma Mariana, whose support was invaluable at the beginning of this journey.

I want to deeply thank my advisor Dr. S. Michael Kilbey, II whose guidance has made me a better researcher, a better colleague and a better person. All my committee members, Dr. Douglas Hirt, Dr. Anthony Guiseepi-Elie, Dr. Igor Luzinov have provided precious help to my development as a responsible member of the scientific community.

There are many people that I have had the pleasure to work with during these years and I am very thankful for the great times and for their support. At Clemson University, all the members of the Kilbey's group: Jose, Amit, Alaina, Santosh, Azi and Josh. At the Center for Nanophase Materials Sciences at Oak Ridge National Laboratory I have been fortunate to work with and befriend all of the members of the Macromolecular Nanomaterials group: Deanna, Joe, David, Peter, Kunlun, Lihong, Brad, Jamie, Rafael, Jihua, John, Jim, Candice, Erick and Chaitra. I have had also the good fortune to collaborate with professors from different institutions, including Prof. Jimmy Mays from University of Tennessee, Prof. Paul Russo from Louisiana State University and Prof. Masashi Osa from Kyoto University.

Finally I am thankful for the many friends I made during these years; I want to thank them for the good times and the great experiences - Eduardo, Marlon, Erick, Julian, Nizel, Dinora, Rodolfo, Christy, Natan, Rebecca, Greg, Thomas, Danielli and TJ.

TABLE OF CONTENTS

Table of Contents (Continued)

Page

Table of Contents (Continued)

Page

LIST OF TABLES

List of Tables (Continued)

Table Page

LIST OF FIGURES

List of Figures (Continued)

Figure Page

List of Figures (Continued)

Figure Page

List of Figures (Continued)

Figure Page

List of Figures (Continued)

Figure Page

List of Figures (Continued)

Figure Page

CHAPTER I

INTRODUCTION

The term self-assembly denotes the formation of complex structures from simpler building blocks, resembling the manner in which Nature generates functional systems. Nature demonstrates control over self-assembly on length scales ranging from molecular to cosmic and everything in between.[1] Humans on the other hand, have achieved control of self-assembly processes over a more limited scale, ranging from angstroms to meters, which has sparked the boom of nanotechnology in the last 20 years. Self-assembly depends on the ability to generate well-organized constructs by carefully controlling the interactions, size, shape and surface properties of the building blocks.[2] With self-assembly as a tool, chemistry can be employed to encode information into the molecules, giving rise to organized structures with defined properties and predictable interactions. By properly designing the materials in order to direct self-assembly, further processing and modifications can be avoided.[3]

Self-assembly processes can be further classified as either into static or dynamic, depending upon the energy state in each process. Static self-assembly is driven by energy minimization in order to reach a local equilibrium without any energy exchange. Examples of static self-assembly include the creation of molecular crystals,[4,5] formation of lipid bilayers,[6] and micellization of block copolymers.[7-9] On the other hand, dynamic self-assembly occurs in systems that reside in a local energy minimum allowing certain structures or patterns to prevail.[2] However, if the energy influx or dissipation is altered,

the system transitions to a new state, which could include disassembly.[1] Living organisms are a perfect example of dynamically self-assembled systems: if the influx of energy stops or increases beyond some upper limit, it triggers a series of physicochemical events that result in a loss of function such that life processes are no longer supported.[2] Thus the energy derived from the environment (in form of food or light for example) helps to maintain the dynamic self-assembly condition.

In the understanding of the dynamics, self-assembly and structure of soft matter, block copolymers present a great opportunity because as building blocks they are seen as simplified versions of complex systems found in Nature. Block copolymers have the ability to self-assemble into thermodynamically stable microphase segregated domains of well-defined shape and size.[3,10] Their dynamics and equilibrium properties are controlled by the nature of the constituent blocks, their size and connectivity, and temperature and solvent conditions.

1.1 Theoretical Considerations on Self-Assembly of Block Copolymers in Solution

Block copolymers in which the constituent blocks are incompatible, spontaneously self-assemble into micellar structures when dissolved in a solvent selective for one of the blocks.[11,12] This spontaneous assembly arises from the desire of one of the blocks to minimize contact with the thermodynamically unfavorable solvent. The phenomenon of self-aggregation has been extensively studied, and two different models for micellization - open association and closed association - have been proposed.[13]

The "open association" model describes systems where equilibrium exists between many different supramolecular species (M_2, M_3,…M_Q, where Q is the aggregation number). In this model the variety of stable aggregates are made, self-assembling by addition of individual molecules (or polymer chains), designated as M_1. The following set of equations describe the open association model:[14]

$$\begin{aligned} M_1 + M_1 &\rightarrow M_2 \\ M_2 + M_1 &\rightarrow M_3 \\ &\vdots \\ M_Q + M_1 &\rightarrow M_{Q+1} \end{aligned} \tag{1.1}$$

This model is mostly followed by small weight-average molecular weight, M_w, surfactants. Thus, under the open association model, there is a progression in the number of associated molecules, and aggregates of many sizes and Q are present in the medium.

On the other hand, the "closed association" model refers to systems that self-assemble into aggregates having a narrow size distribution and a well-defined Q. These aggregates are in equilibrium with individual molecules (or polymer chains) in the medium:[15]

$$M_1 \leftrightarrow QM_1 \tag{1.2}$$

Here the equilibrium properties are dictated by thermodynamic state, depending on variables such as solvent quality, temperature, block size and connectivity. Figure 1.1 shows the three characteristics zones of the closed association model expressed as the inverse of micellar molecular weight, $(M_{w,mic})^{-1}$, versus solution concentration, c. In zone I only free chains are present in solution. The concentration at which aggregates first appear is called the critical micelle concentration, *cmc*. After the *cmc* is reached, there is a small window (zone II) where micelles and free chains coexist. As c increases, the

number of aggregates increases until zone III is reached. In zone III virtually all of the chains in solution are incorporated into the ensembles. However, there is a certain amount of free chains (or particles) remaining in solution and their concentration is roughly equal to the *cmc*. Figure 1.2 depicts some of the micellar morphologies that can be obtained when a diblock copolymer is dissolved in a solvent selective for one of the blocks.

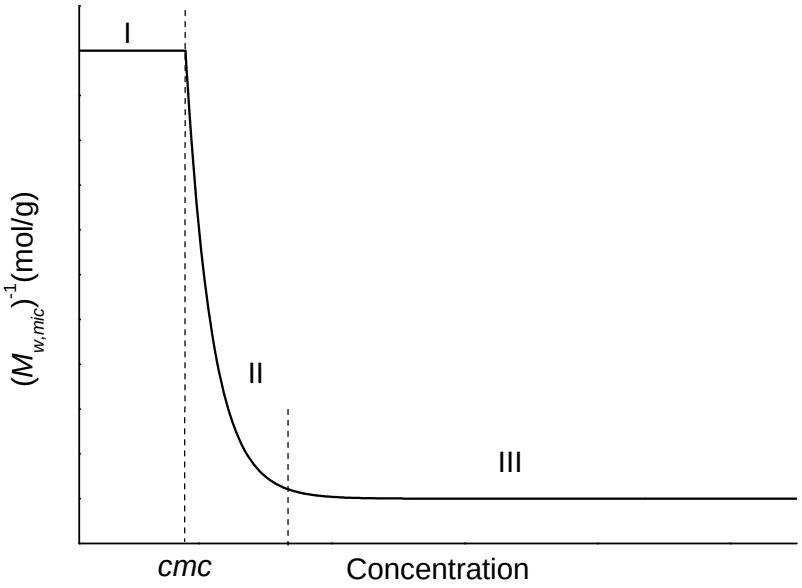

Figure 1.1. Inverse of micellar molecular weight, $(M_{w,mic})^{-1}$ versus concentration, c, for the closed association model. Only free chains exist in zone I. Zone II is marked by coexistence of free chains and aggregates, and in zone III the equilibrium is shifted towards self-assembled aggregates.

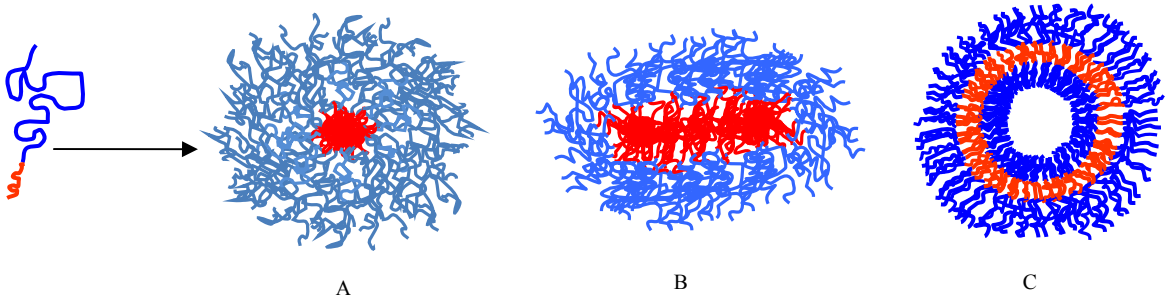

Figure 1.2. Illustration of the possible morphologies adopted by diblock copolymers upon self-assembly in a solvent that is selective for the blue block. Micelles can take the form of (A) spheres, (B) cylinders, or (C) vesicles.

Equilibrium properties of the self-assembled block copolymers such as total radius, R, coronal length, L_A, core radius, R_B, and interfacial area per monomer at the core/shell interface, A_c, have been theoretically predicted by several methods.[13] Initially the model developed by Daoud and Cotton for star-like homopolymers in good solvent was used to characterize the dimensions of spherical micelles in the limit of very long chains.[16] According to Daoud and Cotton, the total size, R, for a star homopolymer scales as:[16]

$$R \sim N^{3/5} f^{1/5} \tag{1.3}$$

where N is the degree of polymerization of each arm and f is the number of arms. Later, Zhulina and Birshtein identified four different regions based on block configurations for the case of diblock copolymers dissolved in a solvent that is selective for one of the blocks.[17] The scaling behavior of R_B, L_A, Q and A_c depend on the length of each block and the exponent v that scales the dependence of the radius of gyration, R_g, on the degree of polymerization of the soluble block, N_A: $R_g \sim N_A^v$. The four regions described by Zhulina and Birshtein are:[17]

- Region I describes the so-called 'crew-cut' micelles where the size of the core is much larger than the size of the corona. Here A_c, R_B and Q scale only with the degree of polymerization of the insoluble block, N_B.
- In region II the A blocks are larger, so there is some overlap of the soluble A chains, but the equilibrium properties are largely dependant on the insoluble block B.
- In region III, the soluble A blocks play an important role in the equilibrium properties and R_B and Q scale with both N_A and N_B.
- Region IV covers the so-called 'star-like' regime where N_A is much larger in comparison to N_B and the curvature of the core enables each soluble block to take a larger area at the core/corona interface forming star-like spherical aggregates.

Throughout the four regions, the solvent quality parameter v plays a key role, as seen in the exponents of N_A and N_B for the equilibrium properties. Table 1.1 summarizes the predictions for the four regions and Figure 1.3 presents illustrations of the regimes defined by Zhulina and Birshtein.[17]

Table 1.1. Scaling predictions for micellar characteristics of A-B diblock copolymers in a solvent selective for the A block.[17]

Region	Copolymer Composition	R_B	L_A	Q	A_c
I	$N_A < N_B^{v/6}$	$N_B^{2/3}$	N_A^{v}	N_B	$N_B^{1/3}$
II	$N_B^{v/6} < N_A < N_B^{(1+2v)/6v}$		$N_A N_B^{(v-1)/6v}$		
III	$N_B^{(1+2v)/6v} < N_A < N_B^{(1+2v)/5v}$	$N_B N_A^{-2v/(1+2v)}$	$N_A^{3v/(3v+1)}$	$N_B^{2} N_A^{-6v/(1+2v)}$	$N_A^{2v/(1+2v)}$
IV	$N_A > N_B^{(1+2v)/5v}$	$N_B^{3/5}$	$N_A^{v} N_B^{2(1-v)/5}$	$N_B^{4/5}$	$N_B^{2/5}$

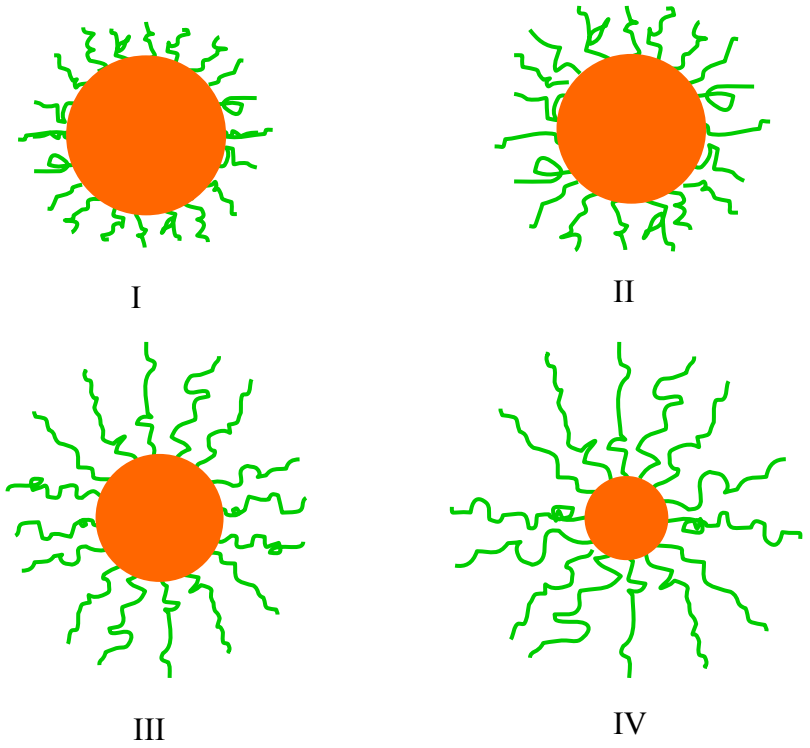

Figure 1.3. Illustration of the four regions predicted by Zhulina and Birshtein.[17] Orange represents the insoluble blocks that form the micellar core and green chains represent the soluble blocks that form the micellar corona.

Further developments in the prediction of equilibrium properties of self-assembled block copolymers, especially for region IV, have been made based on the minimization of the free energy which considers contributions from the packing of chains in the core, the creation of the core/corona interface and stretching of chains of the corona.[18] Additionally, predictions of equilibrium properties based on self-consistent fields models[19,20] and scaling arguments that conceptualize the micelles as spherical polymer brushes[21] basically agree with findings shown in Table 1.1. Recently Zhulina and coworkers have developed a theoretical framework, with numerical prefactors included, that predicts the thermodynamic stability and equilibrium properties of spherical,

cylindrical and lamellar micelles.[9] These developments will be discussed further in Chapter 2.

1.2 Experimental Results on Self-Assembly of Block Copolymers in Solution

Self-assembled block copolymers in solution are used in a variety of applications that include the solubilization of organic substances like perfluorinated compounds,[22] aromatic hydrocarbons,[23,24] and even large molecules such as fullerenes.[25] Block copolymer micelles are also useful as stabilizers in microemulsion polymerization, used to prepare hollow polystyrene (PS) nanospheres; thus, they can be used as nanoreactors.[26] Also PS-PI block copolymers, where PI stands for polyisoprene have been used as thermoplastic elastomers able to compatibilize blends of PS and PI.[27] One of the biggest fields of application for block copolymers is drug delivery.[28] In this case the core blocks need to be compatible with the drug that is loaded and carried in the micelle and the corona blocks need to be able to circulate thru the medium (blood stream), be biologically inactive in order to not stimulate the organism's immune response, and be able to recognize the target site for delivery and release the payload. One of the block copolymers used in drug delivery is PEO-PLA, where PEO is poly(ethylene oxide) and PLA is polylactic acid. PEO is a water soluble polymer that can be easily functionalized with ligand molecules that facilitate recognition. PLA is hydrophobic, biodegradable, and drugs can be readily loaded into it.[28] A full discussion of the wide variety of block copolymers explored and developed for drug delivery applications is beyond the scope of this chapter. The interested reader can find more information and additional references in

several interesting book chapters.[29,30] Due to the wide variety of applications and possibilities, it is important to understand how block copolymers self-organize in solution and how these properties can be controlled.

The solution behavior of linear amphiphilic block copolymers in a solvent selective for one of the blocks has been extensively studied in regard to the effects of block size, temperature and solvent conditions. Riess and coworkers[31,32] studied PS-PEO diblock copolymers in water, a solvent selective for PEO. Their copolymers formed spherical micelles, and by using a series of copolymers of fixed composition but different size, they found that Q (aggregation number) decreases as the length of the PEO block is increased. An empirical correlation between the hydrodynamic radius, R_h, and block sizes was found: $R_h = 1.77 N_{PS}^{0.09} N_{PEO}^{0.31}$. This result differs slightly from scaling predictions shown in Table 1.1; it is argued that due to the glassy state of the core forming blocks ($T_{g,PS}$ = 105°C),[33] thermodynamic equilibrium conditions are not fulfilled.[31,32] Burchard and coworkers studied the properties of micelles made from poly(2-vinylpyridine) (PVP) and PS in toluene, a solvent selective for PS.[34] The PVP core forming blocks of these micelles were loaded with $HAuCl_4$. They found that 'crew-cut' micelles are formed (see, for example, image I of Fig. 1.3) when the degree of polymerization (length) of the PVP block was similar to that of the PS block. On the other hand, micelles formed from PVP-PS diblocks with much larger PS blocks showed 'star-like' morphologies as depicted in image IV of Figure 1.3. At high concentrations ($c \approx 0.1$ mg/mL) spherical morphologies were observed; however, when c is reduced, the R_g/R_h ratio, which is an indication of the adopted morphology, increases from 0.77 to 2.2. The former value is typical for spherical

morphologies, while the latter suggests the formation of ellipsoidal or rod-like micelles. This change in morphology was attributed to the loss of control of micelle formation due to dilution.

Thermoresponsive and solvent transitions for polystyrene-polydimethylsiloxane (PS-PDMS) micelles were observed by Abbas et al.[35] Dioctyl phthalate (DOP), dibutyl phthalate (DBP) and diethyl phthalate (DEP) were used as a series of solvents that increase their selectivity towards PS. A sample with a PS block of 4000 g/mol and a PDMS block of 12000 g/mol was used. Dynamic light scattering experiments at constant temperature showed that when the solvent selectivity increases, there were transitions from free chains to spherical micelles to cylindrical micelles and finally to vesicles. The transitions were related to the decrease in curvature at the core/corona interface as the interfacial tension increases with solvent selectivity. This phenomenon is enhanced by the larger size of the insoluble PDMS block. They found that as temperature is increased, the solvent selectivity decreases, rendering an opposite series of transitions (vesicles to free chains). In both sets of experiments, coexistence between aggregates was observed which suggests that transitions from one morphology to another are not sharp. At a given concentration, the temperature at which micellar aggregates are first observed is called the critical micelle temperature, *cmt*. Abbas et al.[27] showed that these temperature-induced transitions are reversible, and this behavior has been attributed to the low T_g of PDMS ($T_{g,\mathrm{PDMS}}$ = -123°C).[33]

It has been argued that when the T_g of the core-forming blocks is above the temperature in which the solutions are kept, the micelles are “kinetically frozen” in a

non-equilibrium state.[7,36] This is especially a concern for micellar systems made from block copolymers having core-forming blocks that have a high T_g. One system that is widely investigated is PS-PI block copolymers in a solvent selective for PI. Nevertheless, experimental results have shown that there can be a coexistence of free chains and micelles in solution (zone II in the closed association model), which is a clear indication of micellar aggregates that are not kinetically frozen. For example, Woods and coworkers studied the effects of temperature on micelles made from PS-PI linear diblocks (25 wt % PS) in n-decane.[37] At low temperatures (T < 35°C) only spherical micelles are observed, whereas at high temperatures (T ≈ 75°C) the micelles break up into single chains. Interestingly, at intermediate temperatures (45°C < T < 55°C) an apparent equilibrium between the micellar aggregates and free chains in solution is observed. This suggests that the core is somewhat swollen by the solvent and that there is, in fact, a coexistence of chains between the micelles and the solution, as predicted by the closed association model. To examine the coexistence between micelles and free chains, Price et al. performed photon correlation spectroscopy on two PS-PI diblock copolymers in n-decane, with each having a total weight-average total molecular weight, $M_{w,tot}$, of 54000 g/mol.[38] One of the samples was a 52 wt % PS while the other was 24 wt % PS. There was a significant broadness of the micellar size distribution for the copolymer having larger PS blocks. On the other hand, micelles formed from the diblock having a smaller PS fraction appeared to be in equilibrium with free chains at a temperature of 23°C. As the solution concentration was increased from 0.6 mg/mL to 8.7 mg/mL, clusters of micelles formed, adopting either worm-like or globular morphologies.[38]

The effects of solvent selectivity were studied in a sequence of PS-PI diblock copolymers with an increasing mass fraction of PS using four different n-alkanes, which are known for being good solvents for PI and poor solvents for PS.[39] The micellar R_h values obtained in each solvent were very similar to one another, with R_h values in n-dodecane being slightly larger than those measured in n-hexane, n-heptane and n-decane, because it is a better solvent for PI. Q values of ~300 were observed and these aggregation numbers tended to increase as the mass fraction of PS and $M_{w,tot}$ increased; the same trend was observed for R_h. However, because both $M_{w,tot}$ and the mass fraction of PS were varied at the same time, a scaling analysis could not be made. Bluhm and Malhotra used small-angle x-ray scattering (SAXS) to find the scaling behavior $R_g \sim M_n^{0.5}$, where M_n is the number-average molecular weight, for spherical micelles made from PS-PI diblock copolymers having equal mass fraction of each constituent.[40] Although the SAXS technique allows one the determination of both R_g and R_B, the interference from the micellar corona and sample's polydispersity hindered the ability to properly determine R_B. Since the size and aggregation of the micelles are highly dependent on the length of each block, the scaling finding for R_g cannot be applied to samples with different mass fractions. Methylcyclohexane is another selective solvent for PI, and PS-PI diblock copolymers dissolved in it have been shown to adopt star-like morphologies.[41] Static and dynamic light scattering experiments at concentrations well below the overlapping concentration, c^*, calculated to be equal to 7 mg/mL for the copolymers investigated, showed repulsive interactions between micelles, i.e., a positive second virial coefficient, A_2. Likewise, the solution diffusion coefficient, D_s, was found to

be independent of c, which is an indication of the counterbalance between thermodynamic and hydrodynamic interactions. It was suggested that the soluble PI blocks adopt a Gaussian conformation instead of a stretched conformation.[41] At concentrations close to c^*, the micelles form a liquid-like phase due to interactions between micellar coronas and in this regime, D_s decreases with c. These experiments demonstrate the colloidal-like nature of micellized block copolymers.

Cylinder- and vesicle-like morphologies have also been observed for PS-PI linear block copolymers. Lodge and coworkers showed that for an asymmetric PS-PI diblock, with $M_{w,tot}$ of 74000 g/mol and 17.5 wt % PS, solvent selectivity plays an important role in the morphology adopted by the aggregates.[42] By increasing the selectivity of the solvent towards PI, which is accomplished from changing the solvent from dibuthyl phthalate to dimethyl phthalate, contacts between the solvent and the core are minimized because the interfacial tension at the core/corona interface is increased. Therefore, a transition from spheres to cylinders to vesicles is experienced as the solvent selectivity increases. Similar transitions were recently observed by small and ultra small angle x-ray scattering (SAXS and USAXS) and dynamic light scattering (DLS) for a PS-PI diblock with $M_{w,tot}$ = 36000 g/mol and 44wt % PS, both n-decane and in n-heptane.[43] These studies showed that there is a transition from spherical micellar aggregates to vesicles over the temperature range of 25°C to 90°C, and at higher temperatures the aggregates disintegrate into single chains. Interestingly, experiments at intermediate temperatures showed the coexistence morphologies. The reduction in solvent selectivity towards PS was responsible for the transitions from spheres to vesicles and such transitions were

observed to be reversible.[43] As the foregoing shonws, there has been an extensive range of work focused on the self-assembly of linear copolymers; however, there also have been limited efforts to characterize the solution behavior and aggregation of architecturally complex block copolymers.

Effects of Architecture. Architectural effects in block copolymers have a strong influence on the size and aggregation of the micellar structures. A great deal of work has been undertaken for BAB or ABA triblock copolymers, particularly copolymers with PEO and polybutylene oxide (PBO) constituents in the fashion PEO-PBO-PEO[44-46] and PBO-PEO-PBO.[45,47] When these triblock copolymers are dissolved in water, a solvent selective for PEO, the *cmc* is higher than in comparison to their linear PBO-PEO analogs having the same composition and $M_{w,tot}$.[48] In both situations, the insoluble PBO blocks tend to avoid contact with the solvent, resulting in chains forming 'loops' caused by the PBO blocks sticking together in the case PBO-PEO-PBO. For this block arrangement, as the concentration is increased, the loops aggregate, generating flower-like micelles, as seen in Figure 1.4A. The micelles formed from both triblock copolymer arrangements showed smaller Q and R_h values than their equivalent diblocks. Also, with the PBO-PEO-PBO triblocks there is the possibility of bridges forming between micelles as the triblock copolymers span between two different micellar aggregates (see Figure 1.4A). On the other hand, PEO-PBO-PEO triblocks adopt a spherical conformation with the PBO forming the core and the soluble PEO blocks forming the corona (see Figure 1.4B). In general, the micellization of triblock copolymers is entropically disfavored due to the

larger cost of organizing the chains into aggregates in comparison to linear diblocks having the same constituents and block sizes.[48]

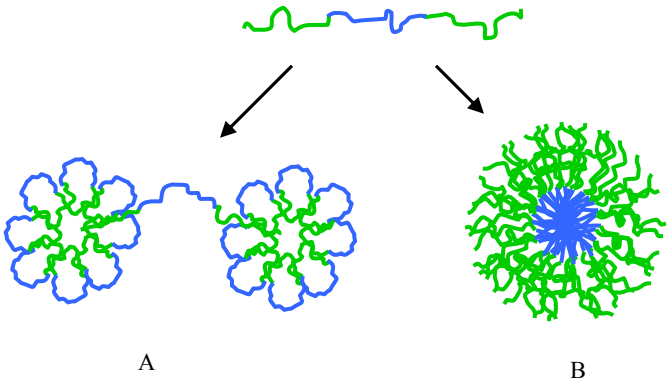

Figure 1.4. Self-assembly of ABA and BAB triblock copolymers. In (A), the solvent is selective for the middle block (blue), flower micelles are formed and there is a possibility of bridges forming between flowers. In (B), the solvent is selective for the two outer blocks (green), forming spherical micelles.

A closely related type of triblock copolymer made from PEO-PPO-PEO, where the middle block is poly(propylene oxide) (commercial name Pluronics), have been studied due to their ability to adopt different morphologies as temperature is varied.[49,50] SANS experiments on a 10 wt % solution of PEO_{26}-PPO_{40}-PEO_{26} (the subscripts denote the degree of polymerization of each block) in D_2O showed a transition from single chains at 20°C to spherical micelles at T = 30°C. As the temperature was gradually increased above 30°C, Q increased and the spherical morphology persisted with the PPO blocks forming the core of the micelles and the PEO blocks forming the corona. This increase in Q was explained in the light of a greater insolubility of the PPO blocks as temperature increases.

The emergence of anionic polymerization techniques in the last 20 years has provided the capability to synthesize architecturally complex block copolymers such as stars, grafts and combs. In most cases these copolymers are based on PS and PI constituents because the monomers are quite stable during polymerization.[51] For example, Iatrou et al. investigated the micellization of triblock copolymers in the fashion $(PI)_3$-dPS-$(PI)_3$ in n-decane, where dPS stands for deuterated polystyrene.[52] Here the subscripts denote the number of arms of each constituent. The micelles formed from this 'super-H' copolymer showed smaller Q values and higher stability when compared to a PS-PI of similar composition and $M_{w,tot}$. The equilibrium properties of micelles made from miktoarm (mixed-arm) stars of $(PI)_2$-PS and PI-$(PS)_2$ in n-decane were compared by Pispas and coworkers to the micelles formed from linear PS-PI copolymers in the same solvent.[53] With the increase in the number of arms, the elastic energy per molecule increases due to crowding at the junction and it becomes unfavorable for the micelles made from the miktoarm copolymers to have the same Q as micelles formed from the linear analog; therefore, they found that Q and R_h increase in the order PS-$(PI)_2$ < $(PS)_2$-PI < PS-PI, mainly due to the larger area per junction point at the core/corona interface for the micelles made from branched copolymers. A scaling theory based on thermodynamics shows that the free energy of the soluble blocks is the dominant contribution to the equilibrium state. The increase in the stretching energy of chains due to crowding multiple chains at the core/corona interface formed from PS-$(PI)_2$ leads to smaller Q compared to $(PS)_2$-PI and PS-PI.

Other types of branched block copolymers have also been studied by Hadjichristidis and coworkers.[54] They have synthesized $(PS)_8(PI)_8$ heteroarm stars (~ 45 wt % PS), where all of the arms emanate from a common junction point. When these samples were studied in solvents selective for PI, it was found that the aggregates formed by the stars have smaller Q and larger R_h values in comparison to micelles formed from an analogous linear PS-PI. The stars with symmetric arms (equal arm molecular weight) and lowest $M_{w,tot}$ formed elongated micelles as evidenced by a R_g/R_h = 1.13; however, for the $(PS)_8(PI)_8$ stars in which the size of the soluble PI blocks is larger than that of the insoluble PS block, spherical morphologies were observed, as evidenced by the R_g/R_h ratio of ≈ 0.6. The morphologies obtained were explained in light of a compromise between unfavorable interactions of the PS blocks with the solvent and stretching of PI chains: as the length of the PI blocks increases, the area per copolymer chain taken is larger for the PI blocks and the contributions from the PS chains are reduced; thus, a more spherical morphology is adopted. Roovers and coworkers also studied the solution behavior of $(PS)_8(PI)_8$ stars, both in toluene and THF, which are common good solvents, in cyclohexane, which is a good solvent for PI but a θ-solvent for PS, and in dioxane, which is a good solvent for PI but a marginal solvent for PS.[55] It was found that as $M_{w,tot}$ increases, the probability of contacts between PS and PI chains (that commonly try to avoid each other) increases. This causes expanded hydrodynamic and viscometric dimensions in comparison to $(PS)_2(PI)_2$ miktoarm and homopolymer stars of the same $M_{w,tot}$. This behavior was correlated to the increased hydrodynamic interactions arising when there are more heterogeneous arms attached to a common core. In all of the

solvents, the viscometric radius, R_v, of the stars increases with $M_{w,tot}$ and no evidence of micelization in cyclohexane nor in dioxane was observed. Slightly larger R_v values were observed in toluene and THF in comparison to those for cyclohexane and dioxane.

In addition, self-assembled block copolymers can be deposited or preferentially adsorbed onto different substrates, making them suitable in applications such as colloid stabilization,[56] advanced lithography for patterning electronic circuitry,[10] adaptive, stimuli-responsive layers that allows control adsorption events or flow through membranes,[57] and nanopattering of surfaces.[58] Therefore, it is important also to understand how block copolymers populate surfaces and interfaces.

1.3 Adsorption of Block Copolymers at the Solid/Fluid Interface

It is well know that the interactions of a surface or interface with its surroundings are largely due to its most external layer. A surface covered even with only a few nanometers of material can completely hide the chemical nature of the underlying surface - described by Rühe as the "stealth effect".[59] Therefore, the generation of polymer-modified surfaces with tailored structures and properties is attractive because it allows the material properties of the surface and the bulk to be optimized separately. There are two main approaches used to decorate surfaces with block copolymers, which are named "grafting to" and "grafting from".[59] The latter uses surface-initiated polymerization to grow polymer chains from a surface modified with initiators. By this approach, robustly anchored polymer layers can be created due to the formation of covalent bonds with the substrate. The grafting from approach has been recently reviewed by Klok and

coworkers.[60] On the other hand, the grafting to approach uses pre-made polymers, and there are two methods of attachment that are distinguished by how the chains are tethered. The first method of attachment relies on chemisorption, which implies that the polymer chains are grafted (tethered) by a covalent bond, usually formed when a reactive end-group of the polymer reacts with a surface site. The second method relies on di- or multi-block copolymers in which of the blocks wets the surface. This is called physisorption and in this case there is no involvement of a covalent bond for the tethering of the chains. Interactions such as van der Waals, electrostatic and hydrogen bonding are responsible for keeping the polymer chains tethered to the surface.[61,62]

One facile and commonly physisorption route used for the deposition of block copolymers onto surfaces is preferential adsorption from a solvent selective for one of the blocks. The basis of this fascinating process is the incompatibility of one of the blocks with the solvent and its desire to spread on the substrate. In the case of a linear diblock copolymer, the nonsolvated block tends to adsorb onto the surface, driven by its desire to minimize contacts with the solvent. The adsorption can be enhanced if there are favorable interactions between that 'anchor' and the substrate.[63] Additionally, this methodology is usually preferred for fundamental studies because the macromolecular materials can be characterized prior to the adsorption experiments. Consequently, the effects of connectivity, $M_{w,tot}$, asymmetry, and chemical nature of the constituent blocks can be studied. Surface modification by preferential adsorption is practical, scalable and there is the possibility of operating at ambient temperature and mild conditions using

commercially available solvents (toluene, THF, cyclohexane, etc.) as well as water, which is especially useful for polyelectrolytes and PEO based copolymers.

As seen in sections 1.1 and 1.2 block copolymers tend to self-assemble into micellar aggregates when dissolved in a selective solvent for one of the blocks. The micellization of these type of block copolymers in solution also has a strong effect in their preferential adsorption at the solid/fluid interface.[64,65] Therefore is it important to distinguish between preferential adsorption processes carried out below or above the *cmc*.

1.4 Preferential Adsorption of Block Copolymers below the Critical Micelle Concentration

The kinetics of preferential adsorption of amphiphilic block copolymers in solutions below the *cmc* is usually described as a two stage process. First, at very early times of the adsorption, the diffusion of material towards the solid/fluid interface is the driving force for the process.[66] In this stage, adsorption occurs as soon as a chain reaches the solid/fluid interface. The adsorbed amount, $\Gamma(t)$ as a function of time, t, is given by the flux of material towards the substrate:[66]

$$\Gamma(t) = 2C_0\sqrt{D_s t/\pi} \tag{1.4}$$

This equation is derived from Fick's second law, which depends upon the initial adsorbate concentration, C_0, and D_s. The second stage occurs when, as time progresses, more copolymer chains populate the surface and the adsorption rate decreases because the already adsorbed chains create a barrier to adsorption of the incoming ones. At this time, a deviation from the $\Gamma(t) \sim t^{1/2}$ scaling behavior is expected because of the increased

difficulty for the incoming chains to find an adsorption site on the surface. As the adsorption progresses, the osmotic pressure of the 'tethered' blocks increases, causing the chains to stretch away from the surface in order to alleviate local crowding. When the distance between tethering points, d, is smaller than the dimensions of the chains in solution ($2R_g$), the so-called 'polymer brush' is formed.[67] The entropic energy cost associated with the stretching of the solvated blocks is balanced by the enthalpic energy gain due to the adsorption of the insoluble blocks on the substrate.[67] This energy balance determines the equilibrium structure of the adsorbed layer.[62,66,67] Figure 1.5 shows an illustration of the preferential adsorption process for an amphiphilic diblock copolymer.

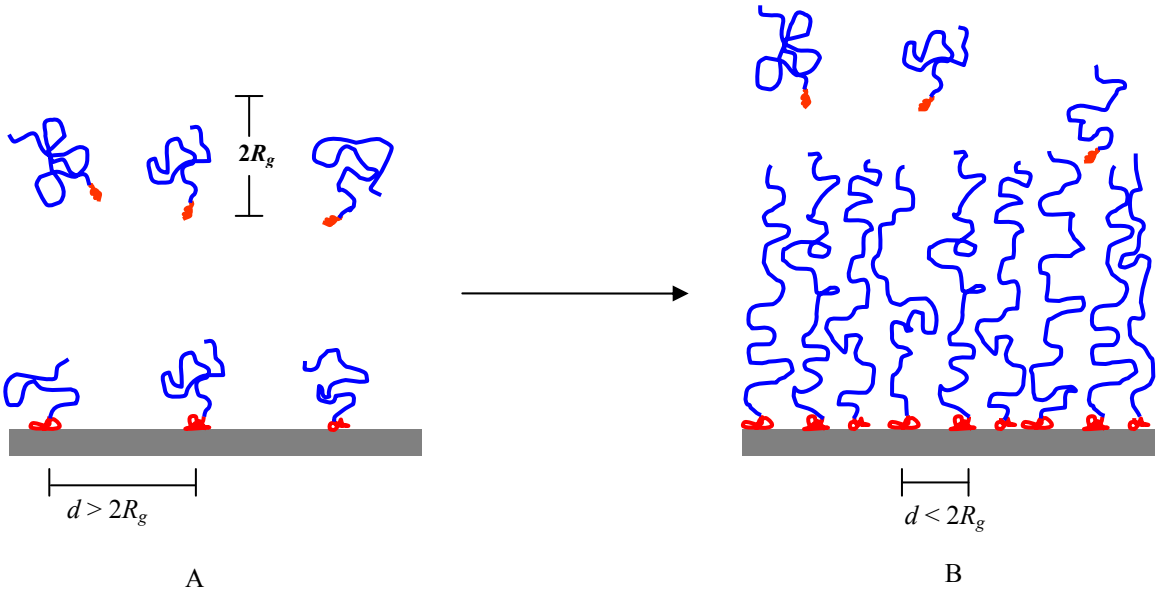

Figure 1.5. Preferential adsorption of an amphiphilic diblock copolymer from a solvent selective for the blue block. In (A), the initial stages of the process are shown. These stages are dominated by the mass transport of chains towards the surface. The grafting density is low, corresponding to $d > 2R_g$, and the tethered copolymers have dimensions similar to what they had in solution. As the grafting density increases, it is harder for the incoming chains to find an adsorption site on the surface, as shown in (B). The distance between grafting points is smaller than the dimensions of the chains in solution, $d < 2R_g$, and in order to alleviate the local crowding, the tethered chains stretch away from the surface forming a polymer brush.

Marques et al. presented a scaling theory for the influence of block size on the structure of AB diblock copolymers preferentially adsorbed on a solid substrate through the B blocks.[68] Four different regimes were predicted depending on the asymmetry ratio of the diblock, β, defined as:[68]

$$\beta = \frac{N_A^{3/5}}{N_B^{1/2}} \tag{1.5}$$

In the first regime, the Rollin regime, the adsorption depends on the spreading power of the insoluble B block. This regime exists only for very short 'anchor' B blocks. When $\beta \sim 1$, the adsorption and structure arise from a balance between the van der Waals forces of the adsorbing B blocks and the stretching energy of the soluble A block. This regime is known as the van der Waals-buoy regime. As the asymmetry between the blocks increases such that $\beta >> 1$, the elastic energy of soluble block *A* dominates the adsorption, the thickness of the 'anchor' layer is on the order of $R_{g,B}$ and the chains are said to exist in the buoy-dominated regime. If $\beta << N_B^{1/10}$ the stretching energy of the insoluble "anchor" block dominates the adsorption and the layer is said to be in the anchor-dominated regime. Tirrell and coworkers found good agreement between the theoretical predictions of Marques et al.[68] and the adsorption of PVP-PS diblock copolymers from toluene (selective for PS) onto oxidized silicon and mica substrates.[69] They found that for $10 < \beta < 100$ the surface coverage is dominated by the size of the insoluble PVP blocks, a result that resembles the van der Waals-buoy regime. As the asymmetry increases such that, $\beta > 100$, the layer structure is more dependent on the size of the soluble PS blocks and more or less insensitive to the length of the insoluble PVP block.

Studies of the effect of asymmetry on the adsorption kinetics onto solid substrates of PS-PEO block copolymers were made by Mostchmann et al.[70] These experiments were performed in toluene, which is mildly selective for PS. Their kinetics of adsorption experiments revealed a two-stage process, where at early times the adsorption process is governed by the diffusion of materials towards the solid/fluid interface and $\Gamma(t) \sim t^{1/2}$. As the adsorption progresses, the interactions of the incoming chains and the already adsorbed ones are stronger, making the adsorption rate, $\partial\Gamma(t)/\partial t$, decrease. It was found that as β increases, the maximum adsorbed amount, Γ_m, decreases. Thus, the surface coverage increases as the length of the insoluble block increases while keeping the length of the soluble block invariant. This is opposite to what was found by Parsonage et al.[69] Additionally, Mostchamnn et al.[70] found that it is easier for smaller chains, i.e., smaller $M_{w,tot}$, to penetrate the adsorbed layer in comparison to larger ones, allowing the adsorption to continue longer. Another interesting feature observed is that the $\Gamma(t) \sim t^{1/2}$ dependence predicted by Equation 1.4 is lost less than 200 seconds after the adsorption has started.[70] This result shows that Eq. 1.4 does not fully describe the adsorption process, likely because the model assumes that every chain that reaches the solid/fluid interface is adsorbed instantaneously and that there are no interactions between the incoming chains and those already adsorbed on the surface. Later, Toomey et al. used *in-situ* phase modulated ellipsometry to study the kinetics of adsorption of PVP-PS diblock copolymers from toluene solutions.[71] They analyzed the evolution of both $\Gamma(t)$ and the layer thickness, $H(t)$, from the initial stages of adsorption until the polymer brushes are formed when $\partial\Gamma(t)/\partial t$ reaches negligible values. The largest layer thickness is found for

the diblock copolymer samples with largest soluble PS block size. When the applicability of Eq. 1.4 was tested to characterize the adsorption profiles, a $\Gamma(t) \sim t^{0.84}$ dependence was found. They suggested that the strong repulsive interactions between adsorbing and tethered chains are responsible for the deviation from the $t^{1/2}$ scaling behavior predicted from Fick's second law. However, the injection protocol used to load the copolymer solution into the fluid cell utilized by Toomey et al.[71] can also influence the adsorption profiles, especially at early times of the process, as shown by Alonzo.[72] The experimental protocol used by Toomey et al.[71] consisted of the removal of a small amount of pure solvent from the fluid cell and replacing it with an equal volume of a concentrated stock solution. In this case C_0 is reached after the concentrated stock solution is diluted inside the fluid cell. However, any changes in chain conformation due to dilution are likely not instantaneous and these changes are not accounted for in the analysis of the kinetics of adsorption. When Alonzo et al. studied the adsorption kinetics of triblock copolymers using this protocol, they found considerable discrepancies from the $\Gamma(t) \sim t^{1/2}$ scaling behavior at early stages of the process.[73] By modifying the protocol such that all of the volume of pure solvent is removed from the fluid cell and replaced with an injection of a solution at the desired C_0, a $\Gamma(t) \sim t^{1/2}$ behavior is recovered showing that the adsorption kinetics are also dependant on factors such as how the polymer solution is loaded into the fluid cell.[72]

1.5 Preferential Adsorption of Block Copolymers above the Critical Micelle Concentration

The onset of micellization for block copolymers (*cmc*) in a selective solvent is rather small, and in the experimentally accessible concentration range, the presence of micelles

is likely. Therefore, many experimental studies of preferential adsorption of block copolymers have been made from micellar solutions.

Johner and Joanny used calculations of free energy in solution and at interfaces to study the preferential adsorption kinetics of block copolymers onto solid substrates, finding important physical results regarding the role of micelles and free chains in the layer formation.[65] First, they found that the micellar corona creates a potential barrier that hinders the adsorption of the insoluble core blocks on the surface; thus, only free copolymer chains in solution are able to adsorb. Second, they identified four regimes of the adsorption process: (i) The diffusion regime occurs at very early times of the adsorption, and here the process is dominated by the mass transport of free chains towards the surface and $\Gamma(t) \sim t^{1/2}$; (ii) The micelle limited regime starts when the local free chain concentration in the solution falls below the *cmc* due to the adsorption of free chains. This makes the micelles unstable and forces them to relax by releasing chains from the micellear ensemble. These chains eventually adsorb, driving the layer formation; (iii) The brush-limited regime is reached when the layer is sufficiently populated such that the adsorbed chains impose a barrier for the incoming ones. At this stage, $\Gamma(t) \sim (\log t)^{6/5}$, i.e., a very slow adsorption rate, and the layer is likely to adopt a brush conformation; and (iv) At even longer times the saturation regime is reached, where the already formed layer or brush relaxes towards equilibrium with the solution.

Despite the fact that the model of Johner and Joanny predicts that only free chains adsorb, experimentally it has been shown that micelles are able to adsorb and reorganize at the solid/fluid interface, playing an important role in the preferential adsorption

kinetics and the final layer structure.[74-78] For example Tassin et al. showed that for the adsorption of PVP-PS micelles from solution in toluene, the initial stages of the adsorption process are dominated by micelle adsorption, whereas at longer times free chains adsorb.[79] It was also found that the apparent $\partial\Gamma(t)/\partial t$ decreases with concentration, suggesting the strong effect of the micelles in the adsorption kinetics. For the PVP-PS micelles, Γ_m = 1 mg/m^2 at C_0 = 0.03 mg/mL, which is below the *cmc*, while at C_0 = 10 mg/mL, which is well above the *cmc*, Γ_m = 7.6 mg/m^2. In addition, the Γ_m is reached at longer times as the concentration is reduced. They also studied the effects of $M_{w,tot}$ and β on the adsorption kinetics. It was observed that a 10 fold increase in the length of the PVP block caused a decrease in Γ_m by four times. The largest Γ_m is found for the sample with the lowest $M_{w,tot}$, PVP_{47}-PS_{625}, whereas lower and similar values of Γ_m are found for PVP_{517}-PS_{576} and PVP_{517}-PS_{1730}. Later Munch and Gast studied the kinetics of preferential adsorption of PEO-PS diblock copolymers in cyclopentane, a solvent selective for PS, at concentrations both below and above the *cmc*.[80] Two diblocks were used, PEO_{170}-PS_{1730} and PEO_{83}-PS_{3470}. It was found that below the *cmc*, free chains create a more homogeneous layer in comparison to the layer formed from solutions above the *cmc*. After the *cmc* is crossed, both free chains and micelles participate in the adsorption and a micellar rearrangement in order to expose the PEO core blocks to the substrate was suggested. The more homogeneous coverage of the surface found below the *cmc* leads to higher Γ_m in comparison to those obtained at or above the *cmc*; nevertheless, the final layer structure is thought to be a polymer brush without any surface aggregates or the presence of surface micelles, regardless of the initial copolymer

concentration. The adsorption behavior of the two PS-PEO copolymers studied by Munch and Gast showed that as β increases Γ_m decreases,[80] which is the opposite trend of what was found by Tassin et al.[79]

The adsorption kinetics of PBu-PS (PBu stands for polybutadiene) micellized block copolymers in n-hexane were studied using *in-situ* null ellipsometry.[81] It was found that higher copolymer concentrations led to thicker layers and that the equilibrium layer thickness and adsorb amount depends on the interactions of the constituents with the substrate. This finding came from studies using silicon wafers covered with a PS film rather than bare silicon. In this situation, Γ_m was found to be 3.8 times greater, a behavior that was attributed to strong PS-PS interactions that further drive the adsorption of the insoluble blocks. The experiments performed above the *cmc* showed Γ_m values about one order of magnitude larger than those measured below the *cmc*. For these PBu-PS systems, Awan et al. argued that when single copolymer chains adsorb, the micelles relax and release chains into the solution in order to reestablish the equilibrium between micelles and single chains, thereby agreeing with what was proposed by Johner and Joanny.[65] However, micellar adsorption, through the PBu corona block was also considered to be a factor, followed by a quick rearrangement in order to expose the PS blocks to form a polymer brush.

Post-adsorption rearrangements from micelle adsorption were also discussed by Toomey et al., who examined for polyelectrolyte micelles made from poly(*tert*-butylstyrene-*b*-sodium-4-styrenesulfonate) ($PtBS_{15}$-$NaPSS_{438}$) in water, where the core is made by the PtBS blocks.[82] Their findings suggest that immediately after adsorbing

through the coronal arms, the micelles spread and rearrange, competing for the available adsorption sites. This may lead to surface micelles as has been theoretically predicted[83,84] and experimentally observed in several studies.[77,88,85] The adsorption kinetics for the polyelectrolyte micelles showed a strong dependence on concentration: as C_0 increases, Γ_m increases, confirming the influence of the aggregates on the adsorption process. Interestingly, they compared the behavior of the $PtBS_{15}$-$NaPSS_{438}$ micelles with block copolymer stars of similar $M_{w,tot}$ ($PtBS_{10}$-*star*-$NaPSS_{307}$), which can be considered as "frozen" micelles because all of the diblock arms are covalently attached at a common junction point. The adsorption profiles for the stars collapse onto a common curve at the four concentrations studied. In other words, they do not show a concentration dependence, which is opposite of what was found for the micelles. This behavior suggested that no post-adsorption rearrangements occur for the stars and their adsorption process resembles the so-called random sequential adsorption (RSA) process.[86]

Complex architectures, such as stars or triblocks, also affect the diffusion and preferential adsorption behavior of block copolymers at the solid/fluid interface. Efforts to characterize the adsorption kinetics of branched copolymers have been scarce but there a few interesting examples that are worth highlighting.

Effects of Architecture. Dorgan et al. studied the adsorption of PEO-PS-PEO triblock copolymers from toluene onto silicon substrates using null ellipsometry.[87] The kinetics of adsorption followed the classical two stage process: They found a fast initial adsorption regime marked by the scaling relationship of $\Gamma(t) \sim t^{1/2}$ followed by a second regime where $\partial\Gamma(t)/\partial t$ continuously decreases. They found that Γ_m was less than what is

expected for the equivalent PEO-PS diblock, which is formed by "cutting" the PEO-PS-PEO triblock in half at the middle. This behavior was attributed to the formation of PS loops on the surface, formed when both of the PEO blocks anchor to the silicon substrate. Dorgan et al.[87] analyzed the equilibrium coverage expressed by the grafting density, $\sigma = \Gamma_m/M_wN_{av}$, where N_{av} is Avogadro's number, as a function of β. It was found that $\sigma \sim \beta^{-2}$, implying that moderately symmetric triblocks behave as highly asymmetric diblocks. They also found that as c increases, Γ_m increases and that there may be extremely long lived non-equilibrium states, especially at intermediate concentrations. At the very early stages of the process and at low C_0, the $\Gamma(t)$ profiles are diffusion-limited (Eq. 1.4) up to $t \approx 100$ s; however, at intermediate concentrations an overshoot in the $\Gamma(t)$ profiles is observed and at higher concentrations this overshoot is almost undetectable. This overshoot phenomenon was attributed to the displacement of unfavorably adsorbed chains for ones that have a lower stretching energy; as the concentration increases there is a larger availability of chains and the chain replacement occurs very fast.

Cosgrove and coworkers studied the preferential adsorption of PEO-PPO-PEO triblock copolymers in water.[88] These triblocks, with $M_{w,tot} \approx 15000$ g/mol, absorb in a manner similar to PEO homopolymers and their adsorption kinetics follow the classical two stage process. However, they found that triblocks with up to 30 wt % PPO had similar adsorption kinetics profiles ($\Gamma(t)$ behaviors), reaching the same low value of Γ_m (~ 0.4 mg/m^2). Similarly to what was found by Tassin et al.,[79] Cosgrove and coworkers observed that Γ_m increases once the *cmc* has been reached.[88] They also examined the effects of micelization above and below the *cmt*. As T was increased above the *cmt*, a

sharp increase in $\Gamma(t)$ is observed during an adsorption experiment for a PEO-PPO-PEO triblock sample. This was attributed to the occurrence of surface micellization prior to solution micellization.

Another kinetic study of triblock copolymer adsorption was made by Alonzo et al.[73] In this case, PVP-PS-PVP triblocks were dissolved in toluene and preferentially adsorbed onto silicon substrates. All the adsorption profiles showed an initial period of fast adsorption followed by a transition to a region marked by a continuous slowing of $\partial\Gamma(t)/\partial t$ until pseudo-equilibrium is reached; here no further adsorption was observed. They suggested that both the PVP blocks attach to the substrate forming PS loops, a structure that was later confirmed by neutron reflectivity experiments.[89] It was also speculated that surface rearrangements are responsible for the final layer structure, helped by the slow nature of the adsorption process. The fast initial adsorption observed in the kinetics profiles does not follow the $t^{1/2}$ dependence, likely because the interactions between adsorbed layer and the incoming chains, and the fluid cell loading protocol. When comparing the adsorption behavior of the triblocks with an equivalent diblock copolymer of half the $M_{w,tot}$ and a similar PS/PVP ratio, it was found that the transition from the fast initial regime to the brush regime occurs at longer times and higher values of $\Gamma(t)$ for the triblock copolymers in comparison to the equivalent diblocks.

Despite the considerable amount of literature on the solution behavior of self-assembled PS-PI block copolymers, there are no studies of the kinetics of preferential adsorption of those materials onto solid substrates.

1.6 Research Objectives

It has been shown that block copolymers serve as model systems for studying the dynamics, structure and interactions of soft matter as well as the self-assembly in solution and preferential adsorption at the solid/fluid interface. The scientific focus of this dissertation is on understanding the effects of connectivity, molecular weight and solvent conditions of architecturally complex block copolymers. The main techniques used are static and dynamic light scattering, phase modulated ellipsometry and atomic force microscopy.

The overarching aim of this research is to understand how well-defined, architecturally complex block copolymers organize in solution and how they preferentially adsorb at the solid/fluid interface. Specific efforts focus on investigating how manipulating copolymer architecture, block size, molecular weight, and solvent conditions affect dynamics and self-assembly in solution, as well as the kinetics of preferential adsorption and the adsorbed structure at the solid/fluid interface. Particular systems of study include B-A-A_2 miktoarm and A_nB_n heteroarm star copolymers. The B-A-A_2 miktoarm copolymers can be thought of as linear diblocks with a single branch point, making then more complex than the well-studied linear architectures. These miktoarms can be used to provide information about how the placement of the branching point within one of the blocks and moving its location along the chain affects self-assembly processes. The heteroarm star copolymers are much more complex systems due to their connectivity. In these copolymers, the number of arms is increased while keeping the composition fixed; therefore, it is possible to learn how crowding around a common

junction point affects the structure and dynamics of these stars in solution. The specific goals of this project are:

i. To study the effects of architecture and concentration on the solution behavior of PS-PI-$(PI)_2$ miktoarm block copolymers in a solvent selective for the PI block.

ii. To compare the experimental findings from the miktoarm systems with theoretical predictions for the equilibrium properties, namely size and aggregation, of micellized linear block copolymers.

iii. To understand the effects architecture, micellization and surface relaxation/reorganization events on the kinetics of preferential adsorption onto solid substrates for PS-PI and PS-PI-$(PI)_2$ block copolymers.

iv. To elucidate how connectivity and crowding affect the solution behavior of $(PS)_n(PI)_n$ heteroarm star copolymers in a solvent selective for the PI block.

These objectives are accomplished through the work presented in the following chapters. Chapter 2 comprises the study of self-assembly in solution of PS-PI-$(PI)_2$ miktoarm block copolymers in n-hexane. Additionally in this chapter theoretical predictions made by Zhulina and coworkers[9] are tested against the experimental results both for a linear PS-PI diblock and the PS-PI-$(PI)_2$ miktoarm copolymers. Chapter 3 deals with the kinetics of preferential adsorption for the miktoarms onto silicon substrates and how the relaxation/reorganization events at the solid/fluid interface play a key role in the evolution of the adsorption profiles and the final layer structure. The solution studies of $(PS)_n(PI)_n$ heteroarm stars are presented in Chapter 4. These studies provide important

insights into how the size of each block and a systematic increase the number of arms affect the self-organization and dynamics of these systems in solution. Finally, Chapter 5 presents an overview of the scientific knowledge gained from these studies of architecturally complex block copolymers and some recommendations for future studies.

1.7 References

1. Ozin, G.; Hou, K.; Lotsch, B.; Cademartiri, L.; Puzzo, D.; Scotognella, F.; Ghadimi, A.; Thomson, J. *Materials Today* **2009**, *12*, 12.

2. Whitesides, G. M.; Grzybowski, B.; *Science* **2002**, *295*, 2418.

3. Klok, H-A.; Lecommandoux, S. *Adv. Mater.* **2001**, *12*, 1217.

4. Desiraju, J.R. *Crystal Engineering: The Design of Organic Solids*; Elsevier: New York, 1989.

5. Isaacs, L.; Chin, D.N.; Bowden, N.; Xia, Y.; Whitesides, G.M. in *Supramolecular Technology* Reinhoudt, D.N. Ed. Wiley: New York, 1999. pp 1-46.

6. Jones, M.N.; Chapman, D. *Micelles, Monolayers and Biomembranes*; Wiley-Liss: New York, 1995.

7. Riess, G.; *Prog. Polym. Sci.* **2003**, *28*, 1107.

8. Halperin, A.; Alexander, S. *Macromolecules* **1989,** *22,* 2403.

9. Zhulina, E.; Adam, M.; LaRue, I.; Sheiko, S.; Rubinstein, M. *Macromolecues* **2005**, *38*, 5330.

10. Hadjichristidis, N.; Pispas, S.; Floudas, G. *Block Copolymers : Synthesis Strategies, Physical Properties, and Applications*; Wiley-Interscience: Hoboken, 2003; p. 195.

11. Hamley, I.W.; Castelleto, V. *Prog. Polym. Sci.* **2004**, *29*, 909.

12. Abetz, V.; Simon, P. *Adv. Polym. Sci.* **2005**, *189*, 125.

13. Hamley, I.W. *Block Copolymers in Solution: Fundamentals and Applications*; Wiley: West Sussex, 2005.

14. Elias, H-G.; *J. Macromol. Sci. Chem.* **1973**, *7*, 601.

15. Tuzar, Z. in *Solvents and Self-Organization of Polymers*; Webber, J.; Tuzar, Z.; Munk, P. Eds. Kluwer Academic Publishing: Amsterdam, 1996 pp. 1.

16. Daoud, M.; Cotton, J.P. *J. Phys. France* **1982**, *43*, 531.

17. Zhulina, E.B.; Birshtein, T.M. *Polym. Sci. USSR* **1985**, *27*, 570.

18. Halperin, A. *Macromolecules* **1987**, *20*, 2943.

19. Noolandi, J.; Hong, K.M. *Macromolecules* **1983**, *16*, 1443.

20. Whitmoore, M.D.; Noolandi, J. *Macromolecules* **1985**, *18*, 657.

21. Leibler, L.; Orland, H.; Wheeler, J. *J. Chem. Phys.* **1983**, *79*, 3550.

22. Matsumoto, K.; Mazaki, H.; Nishimura, R.; Matsuoka, H.; Yamaoka, H. *Macromolecules* **2000**, *33*, 8295.

23. Hurter, P.N.; Hatton, T.A. *Langmuir* **1992**, *8*, 1291.

24. Paterson, I.F.; Chowdhry, B.Z.; Leharne, S.A.; *Langmuir* **1999**, *15*, 6187.

25. Jenekhe, S.A.; Chen, X.L. *Science* **1998**, *279*, 1903.

26. Jang, J.; Ha, H. *Langmuir* **2002**, *18*, 5613.

27. Bhowmick, A.K.; Stephens, H.L. *Handbook of Elastomers*, 2nd Edition; Marcel Dekker, Inc.: New York, 2001.

28. Otsuka, H.; Nagasaki, Y.; Kataoka, K. *Adv. Drug Deliv. Rev.* **2003**, *55*, 403.

29. Kavanov, A.V.; Alakhov, V. In *Amphiphilic Block Copolymers: Self-Assembly and Applications*; Alexandridis, P.; Lindman, B. Eds. Elsevier: Amsterdam, 2000. p 319.

30. Bae, Y.; Cabral, H.; Kataoka, K. In *Block Copolymers in Nanoscience*; Lazzari, M.; Liu, G.; Lecommandoux, S. Eds. Wiley-VCH: Weinheim, 2006; p. 73.

31. Calderara, F.; Hruska, Z.; Hurtez, G.; Lerch, J.P.; Nugay, T.; Riess. G. M *Macromolecues* **1994**, *27*, 1210.

32. Jada, A.; Hurtez, G.; Siffert, B.; Riess, G. *Macromol. Chem. Phys.* **1996**, *197*, 3697.

33. Andrews, R. J. Grulke, E. A.; Glass Transition Temperatures for Polymers. In *Polymer Handbook*, 4th Edition; Brandrup, J.; Immergut, E.; Grulke, E., Eds.; Wiley-Interscience: New York, 1999.

34. Mössmer, S.; Spatz, J.; Möller, M.; Aberle, T.; Schmidt, J.; Burchard, W. *Macromolecues* **2000**, *33*, 4791.

35. Abbas, S.; Li, Z.; Hassan, H.; Lodge, T. *Macromolecues* **2007**, *40*, 4048.

36. Gohy, J-F.; *Adv. Polym. Sci.* **2005**, *190*, 65.

37. Price, C.; McAdam, J.D.G.; Lally, T.P.; Woods, D. *Polymer* **1974**, *15*, 228.

38. Price, C.; Canham, P. A.; Duggleby, M.C.; Naylor, T.; Rajab, N.; Stubbersfield, R.B. *Polymer* **1979**, *20*, 615.

39. Bahadur, P.; Sastry, N.V.; Marti, S.; Riess, G. *Colloids Surface* **1985**, *16*, 337.

40. Bluhm, T.L.; Malhotra, S.L. *Eur. Polym. J.* **1986**, *22*, 249.

41. Adam, M.; Carton, J.P.; Corona-Vallet, S.; Lairez, D. *J. Phys. II France* **1996**, *6*, 1781.

42. Bang, J.; Jain, S.; Li, Z.; Lodge, T.; Pedersen, J.; Kesselman, E.; Talmon, Y. *Macromolecules* **2006**, *39*, 1199.

43. Di Cola, E.; Lefebvre, C.; Deffieux, A.; Narayanan, T.; Borsali, R. *Soft Matter* **2009**, *5*, 1081.

44. Yang, Y-W.; Deng, N.; Yu, G-E.; Zhou, Z-K.; Attwood, D.; Booth, C. *Langmuir* **1995**, *11*, 4703.

45. Yang, Z.; Packard, S.; Deng, N.; Barlow, R.; Attwood, D.; Booth, C. *Macromolecules* **1994**, *27*, 2371.

46. Luo, Y. Z.; Nicholas, C.; Attwood, D.; Collet, J.H.; Price, C.; Booth, C. *Colloid. Polym. Sci.* **1992**, *270*, 1094.

47. Yang, Y-W.; Yang, Z.; Zhou, Z-K.; Attwood, D.; Booth, C. *Macromolecules* **1996**, *29*, 670.

48. Booth, C.; Yu, G-E.; Nace, V. M.; In *Amphiphilic Block Copolymers: Self-Assembly and Applications*, Alexandridis, P.; Lindman, B. Eds. Elsevier: Amsterdam, 2000. pp 57.

49. Hammouda, B. *The SANS Toolbox;* National Institute for Standards and Technology: Gaithersburg, MD, 2004.

50. Slawecki, T.; Glinka, C.; Hammouda, B. *Phys. Rev. E* **1998**, *58*, 4084.

51. Hadjichristidis, N.; Pitsikalis, M.; Pispas, S.; Iatrou, H. *Chem. Rev.* **2001**, *101*, 3747.

52. Iatrou, H.; Wilner, L.; Hadjichristidis, N.; Halperin, A.; Richter, D. *Macromolecules* **1996**, *29*, 581.

53. Pispas, S.; Hadjichristidis, N.; Potemkin, I.; Khokhlov, A. *Macromolecues* **2000**, *33*, 1741.

54. Pispas, S.; Poulos, Y.; Hadjichristidis, N. *Macromolecules* **1998**, *31*, 4177.

55. Pispas, S.; Avgeropoulos, A.; Hadjichristidis, N.; Roovers, J. *J. Polym. Sci., Part B : Polym. Phys.* **1999**, *37*, 1329.

56. Napper, D.H. *Polymeric Stabilization of Colloidal Dispersion*; Academic Press: New York, 1983.

57. Geoghegan, G.; Jones, R. In *Block Copolymers in Nanoscience*; Lazzari, M.; Liu, G.; Lecommandoux, S. Eds. Wiley-VCH: Weinheim, 2006; pp. 275 -290.

58. Kim, S.H.; Misner, M.J.; Xu, T.; Kimura, M.; Russell, T. P. *Adv. Mater.* **2004**, *16*, 226.

59. Rühe, J. In *Polymer Brushes*; Advincula, R., Brittain, W., Caster, K., Rühe, J., Eds.; Wiley-VCH: Weinheim, 2004; pp. 1 -31.

60. Barbey, R.; Lavanant, L.; Paripovic, D.; Schüwer, N.; Sugnaux, C.; Tugulu, S.; Klok, H-A. *Chem. Rev.* **2009**, *109*, 5437.

61. Halperin, A.; Tirrell, M.; Lodge, T.P. *Adv. Polym. Sci.* **1992**, *100*, 31.

62. Zhao, B.; Brittain, W.J. *Prog. Polym. Sci.* **2000**, *25*, 677.

63. Kilbey, S.M.; Watanabe, H.; Tirell, M. *Macromolecules* **2001**, *34*, 5249.

64. van Lent, B.; Scheutjens, J.M.H.M. *Macromolecules* **1989**, *22*, 1931.

65. Johner, A.; Joanny, J.F. *Macromolecules* **1990**, *23*, 5299.

66. Fleer, G.H.; Cohen Stuart, M.A.; Scheujens, J.M.H.M.; Cosgrove, T.; Vincent, B. *Polymers at Interfaces*; Chapman & Hall: London, 1993.

67. Milner, S.T. *Science* **1991**, *251*, 905.

68. Marques, C.; Joanny, J.F.; Leibler, L. *Macromolecules* **1988**, *21*, 1051.

69. Parsonage, E.; Tirrell, M.; Watanabe, H.; Nuzzo, R. *Macromolecules* **1991**, *24*, 1987.

70. Motschmann, H.; Stamm, M.; Toprakcioglu, C. *Macromolecules* **1991,** *24*, 3681.

71. Toomey, R.; Mays, J.; Tirrell, M. *Macromolecules* **2004,** *37,* 905.

72. Alonzo, J. Kinetics of Preferential Adsorption and Equilibrium Properties of Interfacial Layers Formed from Polymer Chains that Tether by Multiple Ends. Ph.D. Dissertation, Clemson University, Clemson, SC, 2008.

73. Alonzo, J.; Huang, Z.; Liu, M.; Mays, J.; Toomey, R.; Dadmun, M.; Kilbey, S.M. *Macromolecules* **2006,** *39,* 8434.

74. Toomey, R.; Mays, J.; Holley, D.; Tirrell, M. *Macromolecules* **2005,** *38*, 5137.

75. Albrecht, K.; Mourran, A.; Moeller, M. *Adv. Polym. Sci.* **2006**, *200*, 57.

76. Bijsterbosch, H.; Cohen Stuart, M.; Fleer, G. *Macromolecules* **1998,** *31,* 9281.

77. Sakai, K.; Smith, E.; Webber, G.; Schatz, C.; Wanless, E.; Bütün, V.; Armes, S.; Bigss, S. *J. Phys. Chem. B* **2006**, *110*, 14744.

78. Hamley, I.W.; Connell, S.; Collins, S. *Macromolecules* **2004**, *37*, 5337.

79. Tassin, J.F.; Siemens, R.; Tang, W.; Hadziioannou, G.; Swalen, J.; Smith, B.; *J. Phys. Chem.* **1989**, *93*, 2106.

80. Munch, M.; Gast, A. *Macromolecules* **1990**, *23*, 2313.

81. Awan, M.; Dimonie, V.; Ou-Yang, D.; El-Aasset, M. *Langmuir* **1997**, *13,* 130.

82. Toomey, R.; Mays, J.; Yang, J.; Tirrell, M. *Macromolecules* **2006,** *39*, 2262.

83. Ligoure, C. *Macromolecules* **1991,** *24,* 2968.

84. Zhan, Y.; Mattice, W. *Macromolecules* **1994**, *27*, 683.

85. Gragson, D.E.; Manes, J.P.; Smythe, J.E.; Baker, S.M. *Langmuir* **2003**, *19*, 5031.

86. Talbot, J.; Tarjus, G.; van Tassel, P.R.; Viot, P. *Colloids Surf. A* **2000**, *165*, 287.

87. Dorgan, J.; Stamm, M.; Toprakcioglu, C.; Jérôme, R.; Fetters, L. *Macromolecules* **1993,** *26*, 5321.

88. Malmstem, M.; Linse, P.; Cosgrove, T. *Macromolecules* **1992**, *25*, 2474.

89. Huang, Z.; Alonzo, J.; Liu, M.; Ji, H.; Yin, F.; Smith, G.; Mays, J.W.; Kilbey, S.M.; Dadmun, M. *Macromolecules* **2008**, *41*, 1745.

CHAPTER 2

SOLUTION BEHAVIOR OF POLYSTYRENE-POLYISOPRENE MIKTOARM BLOCK COPOLYMERS IN A SELECTIVE SOLVENT

2.1 Introduction

Amphiphilic block copolymers are widely studied due to their ability to form organized aggregates in solution and various microphase segregated morphologies in bulk, and because their surfactant-like nature promotes self-assembly onto solid substrates. The morphologies of the aggregates in solution depend on the chemical nature of the blocks, their size and connectivity (chain architecture), temperature and solvent conditions.[1,2] Applications for those self-organized structures include the generation of templates for inorganic membrane synthesis, separation agents for removal of contaminants water and delivery of therapeutics.[1] These and other applications as well as preparation techniques for block copolymers aggregates have been reviewed recently by Gohy[3] and Riess.[4]

In addition to technological applications, interest in the self-organization of amphiphilic block copolymers springs from conceptual ties to biology: Self-assembly is used by Nature to create useful and functional structures such as lipid and cell membranes, and virus particles.[1] Due to the intrinsic characteristics of block copolymers, they serve as simple models for more complex systems; consequently, by studying their behavior it is possible to comprehend how sequence, topology and composition impact self-assembly, structure and dynamics in soft matter. In particular, copolymers based on

polystyrene (PS) and polyisoprene (PI) constituents are widely studied because these monomers are perhaps the best behaved in living anionic polymerization, providing control over key molecular variables such as composition, block size and polydispersity, and enabling complex, non-linear architectures to be synthesized. The solution behavior of micellized linear PS-PI diblock copolymers in a selective solvent for PI has been thoroughly studied in relation to the effects of block size, solvent quality and temperature.[5-12] In this chapter, we focus on the self-assembly and aggregation properties of micelles made from architecturally complex block copolymers having PS and PI blocks (see Fig. 2.1), which in comparison have been studied to a much more limited extent.

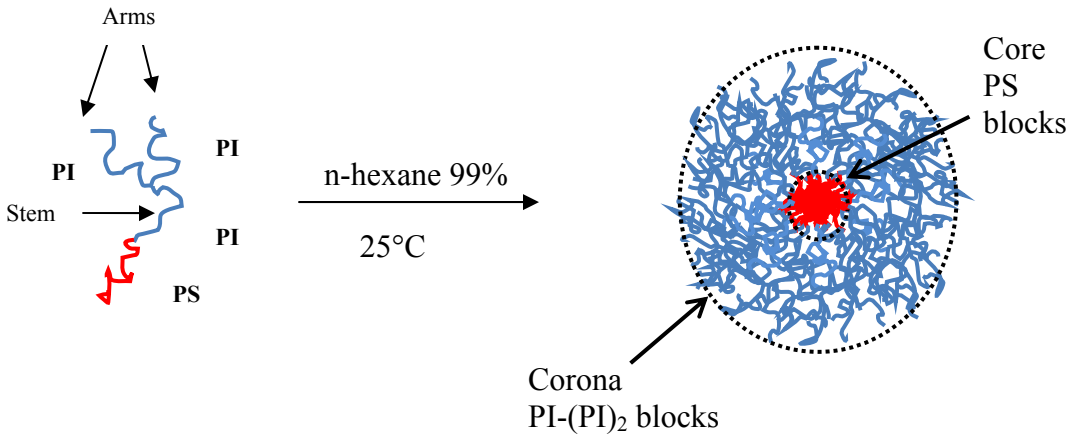

Figure 2.1. Illustration of single chains of PS-PI-$(PI)_2$ miktoarm block copolymers and their self-assembly into spherical micelles.

Lazzaroni and coworkers investigated the effect of cyclization by comparing the solution structure of linear and cyclized PS-PI copolymers of the same molar mass and composition in n-heptane, a selective solvent for PI.[13] They found that the linear copolymer self-organizes into a 'classical' spherical morphology with the PS blocks

trapped inside the core of the micelle and the corona formed by the PI chains. However, the cyclic version of the copolymer self-assembles into a sunflower configuration at low concentrations (~ 0.01 mg/mL), while at intermediate and high concentrations (~ 1 mg/mL), these sunflowers tend to undergo supramolecular assembly and create large wormlike micelles. Borsali et al. studied the solution behavior of graft copolymers consisting of poly(chloroethyl vinyl ether) backbones with grafted PS-PI side chains with similar degrees of polymerization of both the PS and the PI blocks. [14] Selective solvents for PI, n-heptane and n-decane, were used and it was found that these comb-like structures exist as isolated unimers in the concentration range of 0.5 to 5 mg/mL.[14] The complex architecture prevents any type of aggregation mainly due to the large entropic penalty incurred by bringing the insoluble blocks together. They also found that if the PI block was smaller than the PS block, the graft copolymer was insoluble in solvents that are selective for PI.[14]

Pispas and coworkers have worked extensively with star copolymers made by connecting PS and PI chains to a central core.[15,16] They studied the micellization behavior of $(PS)_2$-PI and PS-$(PI)_2$ block copolymers in n-decane, comparing the micelle properties of those 3-arm stars to those formed from linear PS-PI block copolymers.[15] Samples were synthesized by anionic polymerization to produce polymers having the same weight-average total molecular weight, $M_{w,tot}$, and PS mass fraction. They found that micelles made from miktoarm star copolymers were smaller in size compared to those formed from the linear analogs. The hydrodynamic radius, R_h, and aggregation number, Q, were found to increase in the order PS-$(PI)_2$ < $(PS)_2$-PI < PS-PI. This trend was attributed to

the micelles formed from PS-$(PI)_2$ having the largest area per junction point at the core/corona interface and the micelles formed from PS-PI having the smallest. All of the micellar aggregates had spherical morphologies with the PI blocks adopting a stretched conformation in comparison to their unperturbed size. The same group later studied PS-$(PI)_3$ miktoarm stars in n-decane.[16] Static and dynamic light scattering experiments revealed spherical aggregates with narrow hydrodynamic size distributions. They found that keeping the degree of polymerization of the soluble block, N_A, constant while increasing the degree of polymerization of the insoluble block, N_B, tends to increase Q. They also showed that Q increases when N_A is reduced and N_B is kept constant. For the PS-$(PI)_3$ stars, the trends in R_h and Q as N_A and N_B are changed are in agreement with what has been theoretically predicted for spherical micelles made from linear diblock copolymers.[17-19] When the effects of concentration were explored, it was found that at high concentrations (~ 10 mg/mL) the equilibrium shifts towards monodisperse micelles, but at low concentrations (~ 0.9 mg/mL) a coexistence between unimers and micelles is observed.[16]

The study of the self-assembly of novel branched block copolymers is of significant interest because branching introduces conformation-induced constraints that impact the relaxation dynamics and self-organization.[20] Additionally, branched chains provide a greater number of end-groups, which allows an enhancement of interfacial chemistry and reactivity.[21,22] Understanding the solution behavior of these novel miktoarm (mixed arm) copolymers also helps to further comprehend the process of preferential adsorption at the solid/fluid interface, a study that has been published separately and is presented in

Chapter 3 of this dissertation.[23] In this chapter, the solution behavior of model PS-PI-$(PI)_2$ block copolymers is studied using static and dynamic light scattering techniques. The aim is to provide further insight into the effect of architecture and molecular asymmetry on the self-assembly in solution of these precisely designed materials, as well as to compare the results with theoretical predictions for micelles made from equivalent linear block copolymers in dilute solution.[18]

2.2 Experimental

Materials and Sample Preparation. Miktoarm PS-PI-$(PI)_2$ block copolymers were synthesized via anionic polymerization using chlorosilane coupling to graft two PI anions and a PS-PI diblock copolymer at a junction (see Fig. 2.1). This scheme exploits methods pioneered by Mays and Hadjichristidis, whereby living macroanions are coupled using chlorosilanes to afford branched architectures, which was reviewed recently.[24] Here a poly(styrene-*block*-isoprenyl)-lithium anion is reacted with a considerable excess of trichlorosilane. After recovery of the dichlorosilane end-capped PS-PI diblock, the separately made poly(isoprenyl)-lithium "arms" are introduced and allowed to react to give the mikto-arm product. This method not only allows the constituents to be characterized, but styrene and isoprene monomers are among the best behaved monomers for living anionic polymerization, producing well-defined structures that promote fundamental studies of effects such as polymer architecture, block size, composition and solvent quality. Also a PS-PI diblock copolymer and a PI homopolymer were obtained from Polymer Source, Inc. (Montreal, Canada) in order to allow useful comparisons

because their block molecular weights, M_w, are very similar to those of the miktoarm copolymers. Table 2.1 shows the properties of all the copolymers used, with the molecular weights of each block of the PS-PI-PI_2 copolymers given, in kg mol^{-1}, following the sample identification string.

Table 2.1. Properties of PS-PI and PS-PI-$(PI)_2$ miktoarm block copolymers with block molecular weights given in kDa.

Sample ID and block M_w's		M_w PS (kDa)	M_w PI (kDa)	N_{PS}	N_{PI}	*PDI*	dn/dc^b
DB[a]	PS-PI 26/141	26	141	250	2073	1.09	0.224
MA1	PS-PI-$(PI)_2$ 33/32/$(14)_2$	33	60	317	882	1.01	0.219
MA3	PS-PI-$(PI)_2$ 29.6/70/$(43)_2$	29.6	156	284	2294	1.17	0.207
MA4	PS-PI-$(PI)_2$ 33/33/$(57.8)_2$	33	148.6	317	2185	1.14	0.199

[a]obtained from Polymer Source, Inc.; [b]measured at λ = 658 nm.

The solvent used in these studies is n-hexane, which is selective for PI. The solubility parameters (in $(cal/cm^3)^{1/2}$) are δ_{PS} = 9.1, δ_{PI} = 8.1, and $\delta_{n\text{-hexane}}$ = 7.3.[25] Calculations of interfacial energy, γ, for the PI-n-hexane pair show smaller values of γ in comparison for the PS-n-hexane pair (see Appendix A), which indicates better solubility of PI in the solvent. Stock solutions in n-hexane were prepared gravimetrically by adding solvent to the bulk polymer in dust-free vials. The n-hexane was filtered through Millipore 0.2 μm PTFE filters prior to solution preparation. Stock solutions were equilibrated at room temperature for at least a week. 48 to 72 hours prior to a light scattering experiment, an aliquot was taken from the stock solution and diluted with filtered n-hexane (0.2 μm PTFE) to achieve the concentration desired. Concentrations of 30 and 3 μg/mL (0.03 and 0.003 mg/mL) were used.

Static and Dynamic Light Scattering. Light scattering measurements were performed on a four detector ALV goniometer equipped with a linearly polarized 22 mW HeNe laser operating at a wavelength, λ, of 632.8 nm. The signal is processed using an

ALV 5000 multiple tau digital correlator with an initial sampling time of 125 ns. The temperature is maintained at 25 ± 0.1°C in all experiments. The copolymer solutions were contained in dust-free 10 mm borosilicate glass cuvettes that were sealed with a Teflon cap and the total volume used was 1.5 mL. All of the samples were filtered using a 0.2 μm PTFE filter immediately before filling the glass cuvettes.

A total of 16 angles ranging from 20° to 146° are used in the dynamic light scattering (DLS) experiments. A counting time of 600 seconds is used at each angle in order to obtain reliable statistics for the light intensity autocorrelation function, $g_2(q,\tau)$, defined by the Siegert relation as:[26]

$$g_2(q,\tau) = 1 + g_1(q,\tau)^2 = \frac{\langle I(q,t)I(q,t+\tau)\rangle}{\langle I(q,t)^2\rangle} \tag{2.1}$$

where $I(q,t)$ is the scattered light intensity at time t and $g_1(q,\tau)$ is the first-order electric field time correlation function, which depends on the delay time τ and the scattering wave vector, q. The latter is experimentally determined from the scattering angle θ, λ and the solvent refractive index, n_D, as $q = (4\pi n_D/\lambda)\sin(\theta/2)$. As an example, the autocorrelation function profiles, expressed as $[g_2(q,\tau)\text{-}1]^{1/2}$ versus τ, are shown in Figure 2.2 for all of the copolymer solutions studied at 30 μg/mL and θ = 96°. The autocorrelation functions determined at each scattering angle were analyzed first by the CONTIN[27] algorithm (built into the ALV software) to determine the distribution of decay rates, $A(\Gamma)$, which provides insight into the population(s) of scatterers in solution. CONTIN uses a regularization method in order to resolve $A(\Gamma)$ such that it satisfies the expression[28]

$$\left[g_2(\tau) - 1\right]^{1/2} = g_1(\tau) = \int_0^\infty A(\Gamma) e^{-\Gamma\tau} d\Gamma \tag{2.2}$$

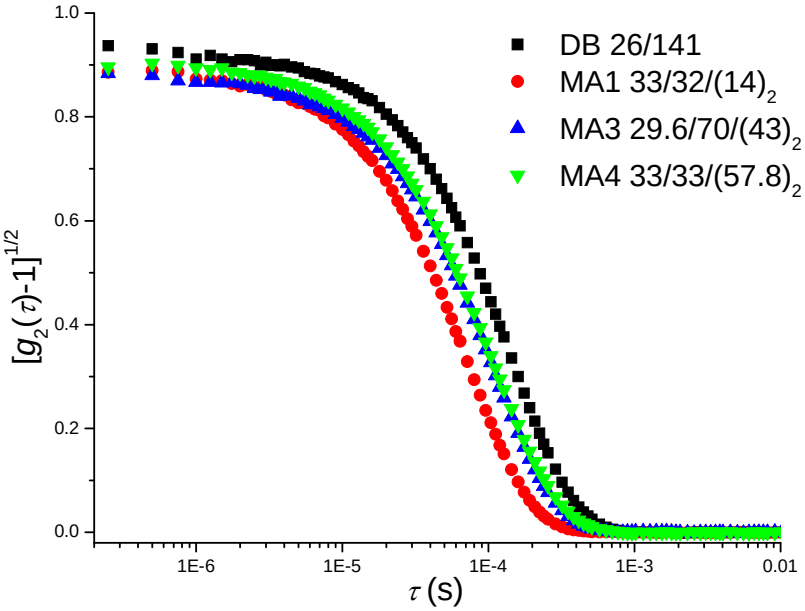

Figure 2.2. Light intensity autocorrelation function for all of the miktoarm copolymers at 30 μg/mL in n-hexane at $\theta = 96°$. The legend shows the sample ID strings and molecular weights (in kDa) of each copolymer studied.

For systems where the CONTIN analysis shows one peak in the distribution of decay rates, the method of cumulants[29] is used to resolve the mean decay rate or first cumulant, Γ_1, and the variance, μ_2/Γ_1^2, at each scattering angle according to:

$$\frac{1}{2}\ln\left[g_2(\tau)-1\right] = \Gamma_0 - \Gamma_1\tau + \frac{\mu_2}{2}\tau^2 \tag{2.3}$$

Γ_0 is a constant independent of τ. Systems exhibiting two decay modes are analyzed using a double exponential distribution:[28]

$$\left[g_2(\tau)-1\right]^{1/2} = A_1\exp\left(-\Gamma_1\tau\right) + A_2\exp\left(-\Gamma_2\tau\right) \tag{2.4}$$

Here A_1 and A_2 are the relative amplitudes of each characteristic decay mode, Γ_1 and Γ_2. Data and fitting results (up to 90% of the correlation function decay) using the method of cumulants are shown in Appendix B for sample MA1 at 30 μg/mL at four scattering angles. Once the characteristic decay rates are obtained, the apparent diffusion

coefficient, D_{app}, from a population having a mean decay rate of Γ_i can be determined by:[30]

$$D_{app}(q) \equiv \Gamma_i / q^2 \tag{2.5}$$

The "true" z-average diffusion coefficient, $\langle D \rangle_Z$, is obtained by extrapolating $D_{app}(q)$ to zero scattering angle ($q^2 \rightarrow 0$), where nondiffusional processes such as rotation or polymer segment fluctuations do not contribute to $g_1(q,\tau)$.[26] After determining $\langle D \rangle_Z$, the hydrodynamic radius, R_h, is calculated using the Stokes-Einstein equation, $R_h = kT/6\pi\eta_o\langle D \rangle_Z$, where k is the Boltzmann constant, T is the absolute temperature and η_o is the solvent viscosity (η_o = 0.293 cp for n-hexane at 25°C).[26]

Static light scattering (SLS) experiments were also carried out using the ALV system. A total of 44 scattering angles ranging from 20° to 152° were surveyed and toluene was used as the calibration standard. The apparent molecular weight, $M_{w,app}$, and z-average radius of gyration, $R_g \equiv [<S^2>_z]^{1/2}$, were determined using the truncated form of the virial expansion for the scattered intensity:[26]

$$\frac{Kc}{\Delta R} = \frac{1}{M_{w,app}P(q)} + 2A_2c \tag{2.6}$$

Here c is the solution concentration, ΔR is the normalized absolute scattering intensity, A_2 is the second virial coefficient and $P(q)$ is the so-called particle form factor. K is the contrast factor, which is defined as:[26]

$$K = \frac{16\pi^2}{\lambda^4 N_{av}} n_D^2 \left(\frac{dn}{dc}\right)^2 \tag{2.7}$$

where N_{av} is Avogadro's number and dn/dc is the refractive index increment, which was measured using a Wyatt OptiLab Rex differential refractometer at λ = 658 nm. Results from those dn/dc measurements are shown in Table 2.1. Due to the low concentrations studied and the low values of A_2 typically observed (~ 10^{-5} cm^3mol/g^2),[15,16] the second term of Eq. (2.6) can be neglected. For comparatively small particles ($q^2R_g^2 << 1$), $P(q)$ can be expressed as:[26]

$$P(q) = 1 + \frac{q^2 R_g^2}{3} \tag{2.8}$$

The aggregation number, Q, is obtained by comparing the $M_{w,app}$ determined by SLS with the molecular weight of the single block copolymer chains: $Q = M_{w,app}/M_{w,tot}$ where $M_{w,tot} = M_{w,PS} + M_{w,PI}$ ($M_{w,PS}$ and $M_{w,PI}$ values are listed in Table 2.1). This parameter provides an estimate of the number of single chains self-assembled into the micellar aggregate.

2.3 Results and Discussion

Hydrodynamic size distributions obtained for samples at 30 μg/mL from the CONTIN regularization method (see Figure 2.3) show narrow monodisperse behavior, which is characteristic of well-defined micellar aggregates of block copolymers,[31] and the normalized amplitude $A(\Gamma)/A(\Gamma)_{max}$ allows direct comparison of their R_h distributions. The fact that the R_h values range from 40 nm for sample MA1 to 90 nm for sample DB provides an indication that these block copolymers are in an aggregated state, as these sizes are too large for single PS-PI-$(PI)_2$ chains in solution (see analysis in Appendix C). The hydrodynamic size distributions obtained by DLS suggest that these copolymers self-

assemble in solution, most likely to due to the low solubility of the PS blocks in n-hexane. Because the R_h distributions determined at each scattering angle for all of the samples at 30 μg/mL show only one narrow distribution peak, the method of cumulants (Eq. 2.3) can be used to determine the mean decay rate Γ_1 from the $[g_2(\tau)\text{-}1]^{1/2}$ profiles. The resulting Γ_1 as a function of q^2 are shown in Figure 2.4, where it is observed that all of the systems studied at 30 μg/mL display a linear dependence on q^2 and intersect the y-axis at $\Gamma_1 \approx 0$. This behavior is expected for particles solely controlled by diffusive processes; thus, the diffusion coefficient can be obtained from the slope of the line.[26] Further information from the DLS results can be obtained by plotting D_{app} versus q^2, which is shown in Figure 2.5. It is observed that D_{app} has no q-dependence over the range studied, and a linear fit and extrapolation to $q^2 \rightarrow 0$ provides $\langle D \rangle_Z$. This q independency is an indication of hard-sphere diffusive behavior.[32] The R_h for each sample can be calculated from $\langle D \rangle_Z$ using the Stokes-Einstein equation and the values of $\langle D \rangle_Z$ and R_h obtained are reported in Table 2.2. It is worth noting that the $\langle D \rangle_Z$ found by extrapolation to $q^2 \rightarrow 0$ are within 3% of the diffusion coefficients obtained from a linear fit of the results shown in Figure 2.4 (with the fit forced through $\Gamma_1 = 0$).

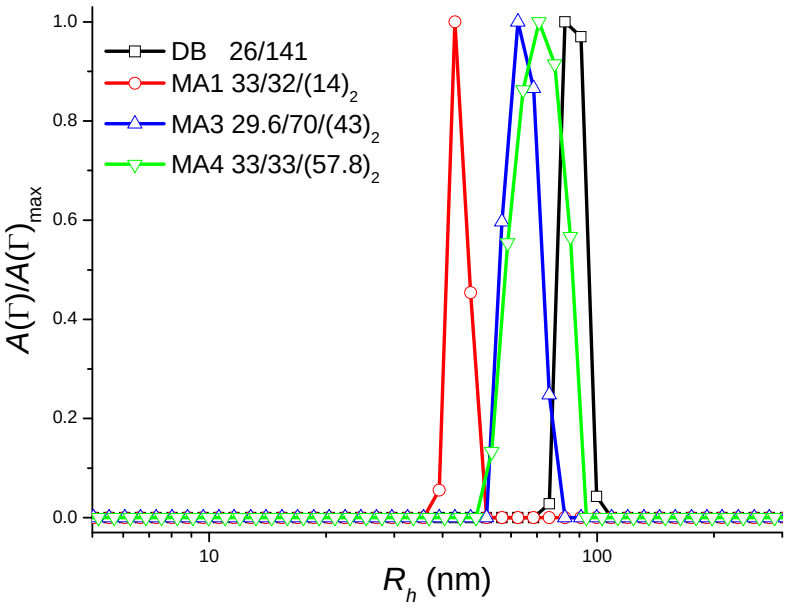

Figure 2.3. Hydrodynamic radii, R_h, distributions obtained from CONTIN regularization method for PS-PI-$(PI)_2$ miktoarm and PS-PI linear block copolymers at c = 30 μg/mL and θ = 96°. One narrow size distribution is observed for each sample, which is commonly found for micellized block copolymers.

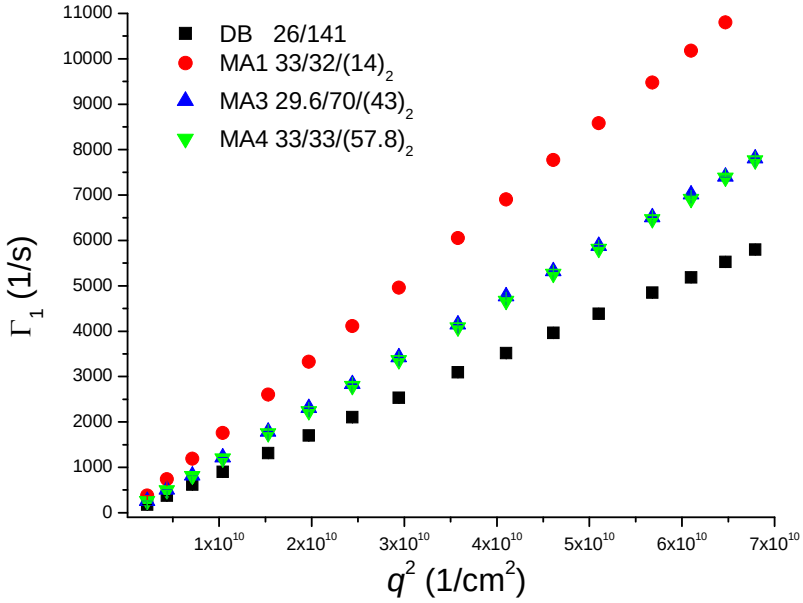

Figure 2.4. First cumulant Γ_1 versus q^2 for micellized PS-PI-$(PI)_2$ miktoarm and PS-PI linear block copolymers studied at c = 30 μg/mL in n-hexane. The linear dependence of Γ_1 with respect to q^2 allows the diffusion coefficient to be determined from the slope of the line.

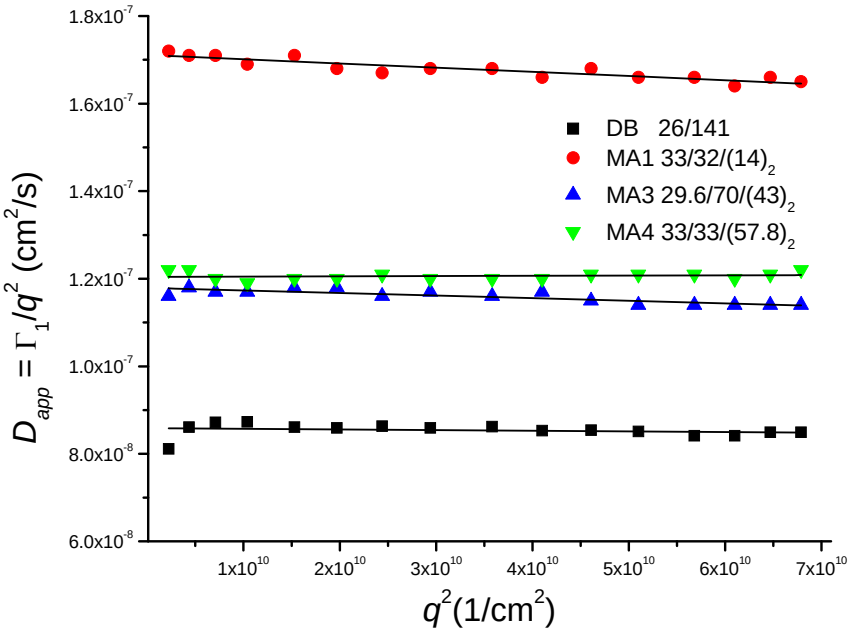

Figure 2.5. Apparent diffusion coefficient D_{app} versus q^2 for micellized PS-PI-$(PI)_2$ miktoarm and PS-PI linear block copolymers at c = 30 μg/mL in n-hexane. Linear fits are shown as solid black lines. The independence of D_{app} with respect to q^2 suggests hard-sphere diffusive behavior.

Table 2.2. Solution properties at c = 30μg/mL for PS-PI and PS-PI-$(PI)_2$ miktoarm block copolymers in n-hexane.

Sample ID and block M_w's		$\langle D \rangle_Z$ (cm^2/s)	R_h (nm)	R_g (nm)	$M_{w,app}$ (kDa)	R_g/R_h	Q
DB	PS-PI 26/141	8.66×10^{-8}	86.0	67.1	1.43×10^4	0.78	85
MA1	PS-PI-$(PI)_2$ 33/32/$(14)_2$	1.71×10^{-7}	43.6	26.6	1.31×10^4	0.61	140
MA3	PS-PI-$(PI)_2$ 29.6/70/$(43)_2$	1.18×10^{-7}	63.2	46.2	1.43×10^4	0.73	77
MA4	PS-PI-$(PI)_2$ 33/33/$(57.8)_2$	1.15×10^{-8}	64.8	47.2	2.52×10^4	0.73	139

It is seen clearly from Figures 2.4 and 2.5 that the aggregates formed from sample MA1, the smallest (lowest $M_{w,tot}$) branched copolymer, diffuse at a faster rate than the aggregates formed by the larger branched copolymers MA3 and MA4 and the linear DB sample. Samples MA3 and MA4 have very similar dynamic behaviors despite having different sized "arms" and "stems", as seen from Table 2.2. Their linear analog, sample DB, which has an $M_{w,tot}$ and composition similar to MA3 and MA4 has a much slower

diffusion rate, implying a larger hydrodynamic size. This pattern of behavior was also observed in the near-surface (effective) diffusion coefficients determined from studies of the kinetics of adsorption of these macromolecular ensembles at the solid/fluid interface as will be discussed in the next chapter.[23] As expected, micelles formed from sample DB have the smallest $\langle D \rangle_Z$ (largest R_h) while samples MA3 and MA4 have similar R_h values of ≈ 64 nm. It is interesting to compare samples MA3 and MA4 with sample DB, since their $M_{w,tot}$ and N_{PS} and N_{PI} values are similar. Branching in the PI blocks of MA3 and MA4 makes the micelles more compact in terms of size compared to those formed from the linear analog, sample DB. This behavior is in agreement with the findings of Pispas and coworkers, where the micelles formed from PS-$(PI)_2$[15] and PS-$(PI)_3$[16] miktoarm block copolymers in n-decane were compared to the micelles formed from linear PS-PI copolymers of similar composition and $M_{w,tot}$.

Figure 2.6 shows the SLS results for the PS-PI and PS-PI-$(PI)_2$ samples at 30 μg/mL. The near-linear relationship of $(Kc/\Delta R)^{1/2}$ over the q-range studied allows $M_{w,app}$ and R_g to be determined using Eq. (2.6), and those values are presented in Table 2.2. The R_g/R_h ratio offers an indication of the aggregate morphology and as reported in Table 2.2, all of the values are around 0.7, which is expected for spherical aggregates.[32] This result along with the behavior shown in Figure 2.5 confirm that these novel miktoarm block copolymers self-assemble into spherical "star-like" micelles, having cores that consist of the insoluble PS blocks and coronas made of the well-solvated PI-$(PI)_2$ blocks, as illustrated in Figure 2.1. Similar to what was observed from the R_h values, the linear DB sample has a larger R_g compared to samples MA3 and MA4 and sample MA1 has the

smallest R_g. Aggregation numbers, Q, for all of the copolymers studied are shown in Table 2.2.

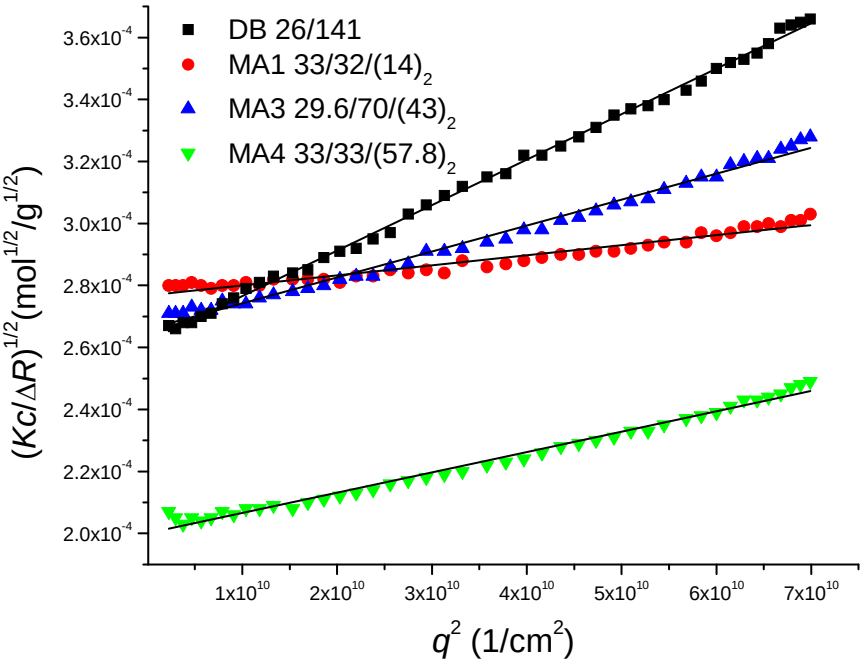

Figure 2.6. Berry plot from SLS experiments for all samples studied at c = 30 μg/mL. The linear behavior over the q-range studied allows Eq. 2.6 to be used to properly fit the data (solid black lines).

The results presented here also show that samples MA1 and MA4 have very similar Q values despite differences in the sizes of their soluble PI blocks. This shows the strong influence of the degree of polymerization of insoluble PS block, N_{PS}, on the self-assembly of block copolymers. In particular, samples MA1 and MA4 both feature PS blocks and PI stems of similar M_w; thus, their size difference must spring from the degree of polymerization and arrangement of the well-solvated outer $(PI)_2$ blocks, which are likely to adopt a stretched conformation towards the outer edge of the corona. On the other hand, while MA3 and MA4 have similar $M_{w,tot}$ and R_h, their aggregation properties are rather different: for sample MA3 Q = 77, while for sample MA4 Q = 139. Although

the large difference in aggregation number seems surprising at first, it has been theoretically predicted[17] and later experimentally confirmed [18] that $Q \sim N_B^{4/5}$, where N_B is the degree of polymerization of the insoluble block. Thus, sample MA4, which has a larger PS block, has the tendency to incorporate more chains into the macromolecular ensemble than MA3.

The influence of the relative sizes of the stem and arms on the arrangement of the branched PI chains of the micellar corona cannot be resolved at this point. Denser packing of chains at the core/corona interface may promote stretching of both PI arms outward from the micelle, similar to the outer region of a multi-arm polymer star.[12,33,34] Less compact arrangements may allow one of the arms to configure itself such that it points back toward the core/corona interface – an arrangement revealed through a mean-field treatment of branched polymer brushes that is owed to the branched brush being able to maximize its conformational entropy at a cost of stretching the tethered stem.[35] When taking into account the properties of the micelles formed from the linear DB sample, it can be seen that Q is smaller than for MA4 and slightly larger than for MA3. This again shows the stronger effects of N_B on the micellar aggregation. However, if N_B was the only parameter determining the number of chains incorporated into the ensemble, Q for sample DB would be lower than Q for MA3 because N_B is smaller for sample DB. As this is found to be not true, it stands to reason that the linear soluble PI blocks of sample DB allow more copolymer chains to self-assemble into the micelle, suggesting that the presence of the branching point in the miktoarms reduces the ability of the branched PI chains to pack, similar to what was found by Pispas et al.[15,16] This behavior

likely arises from a larger entropic cost associated with the aggregation of branched copolymers in comparison to linear ones, which may lead to a larger area per chain at the core/corona interface, even though the branch point is distal from the interface.

Effects of Dilution. To examine whether the critical micelle concentrations, *cmc*, could be detected for these systems, the solutions at 30 μg/mL were successively diluted by factors of 10 to generate 3, 0.3 and 0.03 μg/mL solutions; however, incoherent scattering became problematic at concentrations below 3 μg/mL. Results from the regularized fitting of the autocorrelation function (using the CONTIN algorithm) measured at c = 3 μg/mL are presented in Figure 2.7. Here it is seen that the distributions of hydrodynamic radii are much broader in comparison to the results obtained at 30 μg/mL, suggesting that at 3 μg/mL the copolymer aggregates have a looser structure. (The same x-axis scale is used in Figures 2.3 and 2.7.) The linear DB sample retains the narrowest R_h distribution among the samples studied despite having the smallest PS block. In addition, sample MA3 shows two distinct peaks, indicating the presence of two populations of scatterers, each having its own characteristic decay rate and hydrodynamic size. The larger of the two peaks corresponds to micellar aggregates (main population) and the smaller to the presence of small aggregates or single chains in accordance with the model of closed association.[31] In this case, because there are fast and slow diffusing populations, a double exponential decay is used to fit the autocorrelation function (Eq. 2.4), while samples DB, MA1 and MA4 at this concentration were analyzed by the method of cumulants (Eq. 2.3). As shown in Fig. 2.8, D_{app} is independent of q^2 for the large micellar aggregates (as they were at 30 μg/mL) suggesting a spherical arrangement

and hard-sphere diffusive behavior. The R_h values obtained for DB, MA1, MA4 and for the slow mode of MA3 are slightly smaller than those determined at 30 μg/mL, perhaps because the aggregates are less strongly packed, as reflected in the broader hydrodynamic radii distributions shown in Figure 2.7. These results seem to differ from the decrease in D_{app} (increase in R_h) observed by Pispas et al. for PS-$(PI)_2$ block copolymers in n-decane as c was decreased.[15] However, the concentration range they studied was from 1 μg/mL to 1000 μg/mL, with only two concentrations below 400 μg/mL.[15] For the fast mode measured for MA3, there is more uncertainty in the estimation of $\Gamma_i(q)$ at each q due to the lower scattered intensity arising from smaller particles. Nevertheless and as shown in Figure 2.8, the data appear to vary around a central value that yields $\langle D \rangle_Z = 4.96\times10^{-7}$ cm^2/s. Table 2.3 summarizes $\langle D \rangle_Z$, R_h, R_g, $M_{w,app}$, R_g/R_h and Q values obtained for the samples studied at 3 μg/mL.

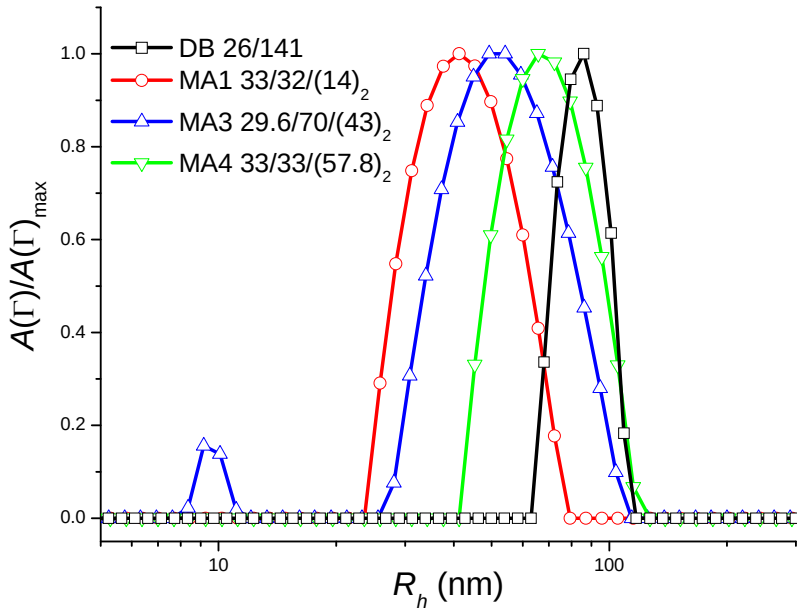

Figure 2.7. Hydrodynamic radii, R_h, distributions for PS-PI and PS-PI-$(PI)_2$ miktoarm block copolymers at c = 3 μg/mL in n-hexane, θ = 78°. The same x-axis scale is used in Figures 2.3 and 2.7, allowing the breadth of the distributions to be compared.

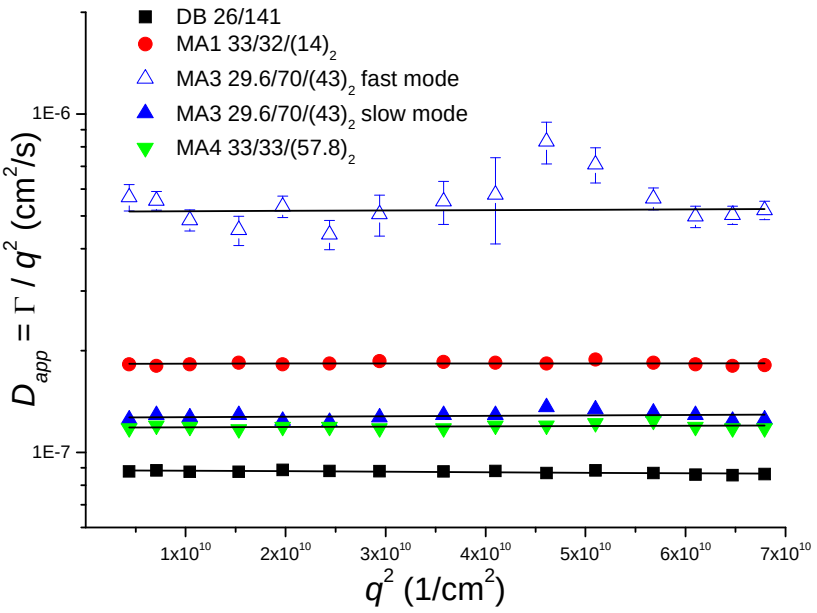

Figure 2.8. Apparent diffusion coefficient D_{app} versus q^2 for all samples studied at c = 3 μg/mL in n-hexane. Linear fits are shown by the solid black lines. The large error bars for the fast mode observed in sample MA3 are likely due to the low scattered light intensity from the smaller aggregates.

Table 2.3. Solution properties at c = 3μg/mL for PS-PI and PS-PI-$(PI)_2$ miktoarm block copolymers in n-hexane.

Sample ID	$\langle D \rangle_Z$ (cm^2/s)	R_h (nm)	R_g (nm)	$M_{w,app}$ (kDa)	R_g/R_h	Q
DB	8.86×10^{-8}	84.1				
MA1	1.83×10^{-7}	40.8	31.6	1.43×10^4	0.77	153
MA3 slow	1.27×10^{-7}	58.7	47.1	2.34×10^4	0.80	126
MA3 fast	4.96×10^{-7}	15.0	31.8	2.29×10^3	2.12	12
MA4	1.18×10^{-8}	62.9	43.3	1.84×10^4	0.69	101

To properly determine R_g and Q for both distribution peaks observed in sample MA3, is it necessary to account for the fraction of $I(q)$ resulting from each population. This is done by calculating the normalized amplitudes of the fast and slow diffusive modes, A_f and A_s, respectively.[36-38] Once $A_f(q^2)$ and $A_s(q^2)$ are determined from DLS results (see Appendix D), they can be applied to the SLS results to estimate the contributions from the slow and fast diffusing modes in $I(q)$. The outcome of this treatment is shown in the Berry plot for the miktoarm samples at c = 3 μg/mL (Figure 2.9), and the fitting results are given in Table 2.3. The R_g/R_h ratio for samples MA1, MA4 and the slow mode of MA3 are ~ 0.7, which along with the $D_{app}(q)$ behavior suggest that the micelles remain in a spherical, star-like morphology at this ultra low concentration. On the other hand, the fast diffusive mode of MA3 yields an R_g = 31.8 nm, which is much larger than the 11 nm predicted for single MA3 chains in n-hexane (see Appendix C). The calculated R_g/R_h ratio associated with this mode is 2.12, which is larger than the values theoretically predicted for linear monodisperse random coils (1.78) and also for linear polydisperse random coils in good solvent (2.05).[32] Additionally the experimentally obtained result of Q = 12 suggests that the fast mode is due to the presence of small aggregates in solution rather than single MA3 chains.

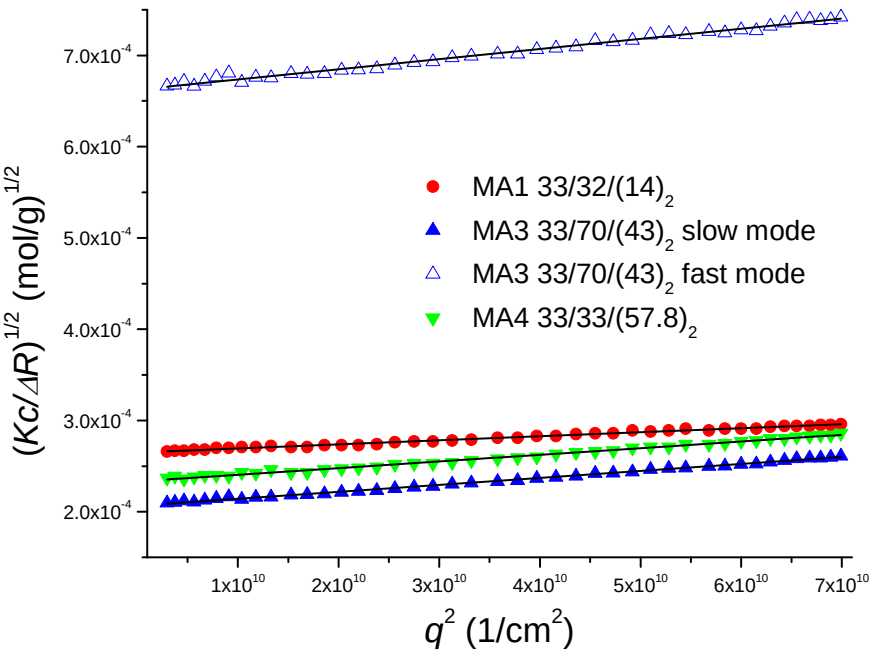

Figure 2.9. Berry plot for PS-PI-$(PI)_2$ miktoarm block copolymers at c = 3 μg/mL in n-hexane. Solid black lines are fits obtained using Eq. 2.6. The relative contributions of the fast and slow diffusing modes observed in MA3 were determined from DLS measurements (see Appendix D).

The Q values determined for the spherically micellized samples MA1, MA3 and MA4 at c = 3 μg/mL are slightly different than the ones determined at 30 μg/mL. For MA1 Q = 153, which is somewhat greater than at 30 μg/mL, suggesting the ability of the ensembles to incorporate more chains as the system is diluted. An increase in aggregation number upon dilution is also observed for the micelles formed from copolymer MA3: Q changes from 77 to 126; on the other hand, copolymer MA4 shows an opposite trend, with Q decreasing from 137 to 101 upon dilution. The differences in solution behavior of the micelles formed from MA3 and MA4 at c = 3 μg/mL are also reflected in their preferential adsorption at the solid/fluid interface: As described in Chapter 3, at lower concentration, the preferential adsorption process is dominated by surface

relaxation/reorganization events, rather than by transport of micelles in the near-surface region.[23] At this moment, we are uncertain as to why Q changes upon dilution, increasing for MA1 and MA3 but decreasing for MA4, while the R_h values remain nearly constant. When the concentration is reduced and approaches the stability limit for the micelles, i.e., the *cmc*, the driving force for the self-assembly process decreases, impacting both aggregation and size. The breadth of the hydrodynamic size distribution indicates looser macromolecular ensembles and these may be undergoing a rapid exchange of chains or smaller aggregates with the bulk solution as described by the closed association model.[31] However it is seen that R_h does not show a significant change from 30 μg/mL to 3 μg/mL; thus, if we conceptualize these spherical micelles as polymer stars with Q number of arms, a variation in Q should not drastically affect R_h, as has been shown for star homopolymers in good solvents where their size becomes practically independent of the number of arms, f, after $f \geq 8$.[12,32]

Comparison with Predictions for Spherical Diblock Copolymer Micelles. Zhulina and coworkers have developed a comprehensive theoretical framework for examining the dilute solution behavior of diblock copolymer micelles.[18] Their model elucidates and predicts the range of thermodynamic stability and equilibrium properties for spherical, cylindrical and lamellar morphologies, with experimental verification coming from light scattering and small angle neutron scattering (SANS) experiments on linear PS-PI diblock copolymers in n-heptane. As the PS-PI-$(PI)_2$ miktoarm copolymers studied here self-assemble into spherical micelles, the attention is focused on comparisons to predictions for spherical morphologies.

According to Zhulina et al.,[18] the free energy for a spherical block copolymer micelle in solution, F_3, having the insoluble blocks trapped inside the micellar core and the corona arms formed from the solvated blocks can be written as:[18]

$$\frac{F_3}{kT} = \frac{3\pi^2 r_3^2}{80 p_B N_B} + \gamma_i \frac{3N_B}{\varphi r_3} + \nu \hat{C}_F r_3^{3/2} \left(\frac{\varphi}{3N_B} \right)^{1/2} \ln\left[1 + \frac{1}{\nu} \left(\frac{a_A}{a_B} \right)^{1/\nu} \hat{C}_H N_A r_3^{(1-3\nu)/2\nu} \left(\frac{3N_B}{\varphi} \right)^{(\nu-1)/2\nu} \right] \quad (2.9)$$

In Eq. 2.9 the first term corresponds to the free energy of the core blocks (denoted by the subscript *B*), the second term represents the free energy of the core/corona interface and the third term accounts for the free energy of the solvated corona (denoted by the subscript *A*). The free energy depends on a variety of parameters: p_A and p_B are the stiffness parameters and a_A and a_B are the monomer sizes for the corona and core constituents, respectively. r_3 is the dimensionless core radius, which is defined as $r_3 = R_3/a_B$, where R_3 is the core radius; φ is the volume fraction of polymer inside the core ($\varphi = 1$ means that the core is in the melt state) and ν is the solvent quality parameter from the relationship of the radius of gyration, R_g, with the degree of polymerization of the soluble block, N_A, as $R_g \sim N_A^{\nu}$. γ_i is the surface tension at the core/corona interface, which varies with temperature according to:[18] $\gamma_i/\varphi^{2/3} = 0.14 - 1.07\times10^{-3}\mathrm{T(°C)}$. Finally $\hat{C}_F$ and $\hat{C}_H$ are solvent quality dependent numerical prefactors that are expressed in terms of p_A and the excluded volume and three-body interaction parameters, υ and ω, respectively:[18]

$$\hat{C}_H = \begin{cases} C_H p_A^{1/3} \upsilon^{1/3}, \nu = 3/5 \\ C_H p_A^{1/4} \omega^{1/4}, \nu = 1/2 \end{cases} \quad ; \quad \hat{C}_F = \begin{cases} C_F, \nu = 3/5 \\ C_F p_A^{-3/4} \omega^{1/4}, \nu = 1/2 \end{cases} \quad (2.10)$$

Here C_H and C_F are numerical constants of order unity that were determined from light scattering and SANS experiments on a series of linear PS-PI block copolymers.[18] In the

case of good solvent conditions (ν = 3/5), υ = 0.05 and this can be incorporated into the C_H constant. At θ-solvent conditions, ω is incorporated into the values of C_H and C_F.[18]

By minimizing F_3 with respect to r_3 ($\partial F_3/\partial r_3$), a non-linear equation for r_3 is obtained:

$$\frac{3\pi^2 r_3}{40 p_B N_B} - \gamma_i \frac{3N_B}{\varphi r_3^2} + \frac{3}{2}\nu\hat{C}_F\left(\frac{\varphi}{3N_B}\right)^{1/2} r_3^{1/2} \ln\left[1+\frac{1}{\nu}\left(\frac{a_A}{a_B}\right)^{1/\nu}\hat{C}_H N_A r_3^{(1-3\nu)/2\nu}\left(\frac{3N_B}{\varphi}\right)^{\nu-1/2\nu}\right]$$
$$+\frac{\hat{C}_F\hat{C}_H N_A\left(\frac{a_A}{a_B}\right)^{1/\nu}\left(\frac{3N_B}{\varphi}\right)^{-1/2\nu}\left(\frac{1-3\nu}{2\nu}\right)r_3^{(1-2\nu)/2\nu}}{1+\frac{1}{\nu}\left(\frac{a_A}{a_B}\right)^{1/\nu}\hat{C}_H N_A r_3^{(1-3\nu)/2\nu}\left(\frac{3N_B}{\varphi}\right)^{\nu-1/2\nu}} = 0 \qquad (2.11)$$

Equation 2.11 can be numerically solved for the dimensionless core radius r_3, This allows R_3 to be calculated, and also the corona thickness, H_3:[18]

$$H_3 = R_3\left[\left(1+\frac{1}{\nu}\left(\frac{a_A}{a_B}\right)^{1/\nu}\hat{C}_H N_A r_3^{(1-3\nu)/2\nu}\left(\frac{3N_B}{\varphi}\right)^{\nu-1/2\nu}\right)^{\nu} - 1\right] \qquad (2.12)$$

Subsequently, the total size of a spherical micelle, R_3^{tot}, and Q are given by:[18]

$$R_3^{tot} = H_3 + R_3 \qquad (2.13)$$

$$Q = \frac{4\pi r_3^3 \varphi}{3N_B} \qquad (2.14)$$

However, as stated by Zhulina and coworkers,[18] to compare the experimental R_h values with the ones predicted for spherical micelles, R_h^s, it is necessary to account for the fact that the solvent drains through the macromolecular ensemble on the same scale as the size of the last blob at the periphery of the micelle, ξ_{last}. Thus the hydrodynamic size of a spherical block copolymer micelle, R_h^s, can be predicted as [18]

$$R_h^s = R_3^{tot} - C_\xi \xi_{last} = R_3^{tot}\left(1 - \frac{C_\xi}{\sqrt{Q}}\, p_A^{3/4}\right) \tag{2.15}$$

where C_ξ is a numerical constant of order unity. In my calculations C_ξ is set equal to 1.

To make comparisons between Zhulina's et al. theory and my experimental results, it is necessary to consider that the copolymers studied here have branched coronas with PI-$(PI)_2$ arrangements; therefore, the parameter N_A needs to be modified to account for the smaller size of the branched blocks forming the corona. As shown in the Appendix C, calculations of radius of gyration based on chain statistics for single branched chains of PS-PI-$(PI)_2$ miktoarm copolymers in n-hexane, $R_{g,br}$, show that the Flory branching parameter, g, is ≈ 0.8 for three different approaches evaluated. Accordingly, to calculate R_h^s and Q using the framework developed by Zhulina et al.[18], the N_A values used here were 'rescaled' as $N_A = 0.8N_{PI}$, where N_{PI} are the values given in Table 2.1. In a sense, this provides insight into whether the equivalent size linear chain forms a micelle with similar properties, namely hydrodynamic size and aggregation number, as the one experimentally found for the corresponding branched miktoarm block copolymer. The parameters and numerical prefactors used in the present calculations are listed in Table 2.4.

Table 2.4. Parameters used for Predictions of Dilute Solution Spherical Micelles[a]

a_A (Å)	a_B (Å)	p_A	p_B	C_F	C_H
5.0	5.6	1.6	1.5	1.38	0.68

[a] the same parameters were used by Zhulina et al.[18]

Another important parameter for the prediction is polymer volume fraction inside the core, φ. Often it is assumed that PS-PI micelles have solvent-free PS cores, $\varphi = 1$, because of the high glass transition temperature for PS.[10,15,16] However Zhulina et al.[18]

determined that there is some solvent inside the core, and used a value of $\varphi = 0.70$ in their theoretical model. Recently, LaRue et al. used light scattering and x-ray small angle scattering to determine $\varphi = 0.85$ for linear PS-PI diblock copolymers in heptane.[19] In the comparisons done here, it is decided to make the calculations using φ values of 0.70, 0.85 and 1. The solvent quality, thru the v parameter, also plays a role in the equilibrium free energy of spherical micelles. According to Zhulina et al.,[18] in a PS-PI micellar solution in n-heptane, the solvent behaves as a θ-solvent. On the other hand, from the determination of R_g for PI homopolymers in n-hexane, it is known that $v = 0.57$, indicating nearly good solvent conditions (see Appendix C); therefore, the comparisons are done for both θ- and good-solvent conditions. Tables 2.5 and 2.6 show comparisons of the experimental results at $c = 30$ μg/mL and the calculated values for R_h^s and Q.

Table 2.5. Solution properties at $c = 30$ μg/mL in n-hexane and predictions at θ-solvent conditions ($v = 0.5$) for PS-PI and PS-PI-$(PI)_2$ miktoarm block copolymers.

Sample ID	*Experimental Results*		*φ = 0.70*		*φ = 0.85*		*φ = 1.00*	
	R_h (nm)	Q	R_h^s (nm)	Q	R_h^s (nm)	Q	R_h^s (nm)	Q
DB	86.0	85	37.2	72	36.6	69	36.2	68
MA1	43.6	140	30.1	155	29.4	150	28.8	145
MA3	63.2	77	37.7	87	37.1	84	36.6	82
MA4	64.8	139	38.8	101	38.2	99	37.7	95

Table 2.6. Solution properties at $c = 30$ μg/mL in n-hexane and predictions at good-solvent conditions ($v = 0.57$) for PS-PI and PS-PI-$(PI)_2$ miktoarm block copolymers.

Sample ID	*Experimental Results*		*φ = 0.70*		*φ = 0.85*		*φ = 1.00*	
	R_h (nm)	Q	R_h^s (nm)	Q	R_h^s (nm)	Q	R_h^s (nm)	Q
DB	86.0	85	31.8	55	31.2	53	30.8	51
MA1	43.6	140	25.9	141	25.1	135	24.5	129
MA3	63.2	77	32.2	68	31.5	67	31.0	65
MA4	64.8	139	33.2	80	32.5	77	31.9	74

At both solvent conditions the theoretical predictions from Zhulina and coworkers[18] follow the same trend as the experimental findings in this study; i.e., micellar hydrodynamic size increases with $M_{w,tot}$, and Q is highly dependent on and increases with N_B. As anticipated, the Q values decrease as solvent quality increases. When there are no excluded volume interactions among chains, i.e., θ-solvent conditions, the area per chain at the core/corona interface is smaller, which allows more chains to pack into the micellar ensemble. The increased crowding in the micellar corona makes R_h^s values larger compared to those calculated for good solvent conditions. However, the calculated R_h^s differ from the measured R_h for each of the samples studied while the Q values are somewhat close to the ones obtained from SLS experiments. The differences seen in hydrodynamic radii might arise from the organization of the branched blocks, due to additional stretching of the stem in the corona blocks that is not conceived in the model and/or from using the numerical prefactors, C_H and C_F, resulting from fits of experimental results of micelles formed from linear block copolymers, although it should be noted that these parameters are not architecturally dependent. As expected, the largest R_h^s values are achieved using $\varphi = 0.70$ due to the presence of solvent inside the micellar core; however, neither R_h^s nor Q change significantly as φ increases. Despite the correction in N_A introduced to account for branching (see Appendix C), the calculated R_h^s values for MA3 and MA4 are slightly larger that the one predicted for sample DB at both solvent conditions. This behavior differs considerably from our experimental results in which micelles formed from the linear PS-PI block copolymer have much larger R_h, as expected, since branched chains are more compact than their linear analogs.

Regarding the aggregation number, the largest Q values predicted are those for sample MA1, which has a larger N_B and the smallest ratio of PI to PS in comparison to samples MA3 and MA4. These observed behaviors reflect the theoretical prediction that the micelle is able to accommodate fewer chains into the ensemble as the length of the soluble block is increased for a given insoluble block size.[17] Contrary to this, however, the experimentally found Q values for MA1 and MA4 are very similar, despite significant differences in N_A and in their dynamic behavior. For samples MA1 and MA3, the Q values calculated assuming good solvent conditions and $\varphi = 0.70$ agree reasonably well with experimental results; however, the R_h^s values are rather different. On the other hand, it is intriguing that the predictions for R_h^s and Q for our linear PS-PI diblock, sample DB, (N_A = 2073, N_B = 250) differ so much from the experimental results. A plausible explanation for these differences may come from the fact that SANS experiments are typically run at concentrations of 1% wt (~ 6 mg/mL), which is three orders of magnitude greater than the concentrations used in this study. Therefore, the effects of concentration play an important role in the equilibrium structure of the spherical micelles as observed in previous studies[8,16] and in the current work. This suggests that these theoretical predictions may not work in the proximity of the micellar stability, i.e., at ultra low concentrations approaching the *cmc*.

It is also compelling to consider these micellar aggregates as a type of polymer brush, where the core/corona interface is the surface to which the branched PI chains are tethered.[39] Using a melt brush, Milner showed that the phase boundaries of asymmetric A_nB copolymer architectures depend substantially on the number of arms (n), due to the

competition between bending of the A-B interface and stretching of the blocks away from the crowded interface.[40] Carignano and Szleifer also stated that the stretching of a solvated branched brush depended sensitively on the number of arms tethered at a single point set at the solid/fluid interface and also on the location of the branch point,[35] as alluded to earlier. In consideration of these works as well as those of Pispas et al.,[15,16] it is likely that the organization of the branched PI-$(PI)_2$ blocks of the corona is different from the organization of chains in a corona made of linear PI chains. Moreover, and although the branch point is away from the core/corona interface, branching affects the size and aggregation of the whole ensemble, as observed from comparisons of samples DB, MA3 and MA4 presented herein.

2.4 Conclusions

Polystyrene (PS)-polyisoprene (PI) miktoarm block copolymers with a PS-PI-$(PI)_2$ architecture self-assemble into spherical micelles having PS cores and branched PI coronas when dissolved in n-hexane at concentrations of 30 μg/mL and 3 μg/mL. These spherical micelles have hard-sphere diffusive behavior, as evidenced by the steady value of the apparent diffusion coefficient obtained along the q-range studied, and as with micelles made from the linear block copolymers, aggregation number is strongly influenced by the degree of polymerization of the insoluble block. However, through comparisons with predictions from theory and properties of micelles formed from a diblock of similar total molecular weight and composition, it seems that while the micelles having branched coronal chains are more compact in hydrodynamic size, fewer

chains can be accommodated in the ensemble. We attribute this behavior to the influence of branching in the corona, even though the branch point is not at the core/corona interface. Experiments at lower concentration (3 μg/mL) show similar patterns of behavior in micelle properties, but broader hydrodynamic distributions: A bimodal distribution is observed for sample MA3, suggesting the coexistence of spherical micelles and smaller aggregates of block copolymers. Comparison of the results with theoretical predictions based on the spherical micelles made of equivalent diblock copolymers show discrepancies in hydrodynamic size and aggregation number. These discrepancies may arise from the different internal arrangement of the branched blocks of the micellar corona, or from the use of experimentally determined numerical prefactors found for linear self-assembled systems.

2.5 References

1. Hamley, I.W. *Block Copolymers in Solution: Fundamentals and Applications*; Wiley: West Sussex, 2005.

2. Zana, R. ed. *Dynamics of Surfactant Self-Assemblies Micelles, Microemulsions, Vesicles and Lyotropic Phases* Taylor and Francis: Boca Raton, 2005.

3. Gohy, J-F. *Adv. Polym. Sci.* **2005**, *190*, 65.

4. Riess, G. *Prog. Polym. Sci.* **2003**, *28*, 1107.

5. Bluhm, T.; Malthora, S. *Eur. Polym. J.* **1986**, *22*, 249.

6. Bahadur, P.; Sastry, N.; Marti, S.; Riess, G. *Colloid Surface* **1985**, *16*, 337.

7. Price, C.; Canham, M.; Duggleby, M.; Naylor, T.; Rajab, N.; Stubbersfield, R. *Polymer* **1979**, *20*, 615.

8. Adam, M.; Carton, J-P.; Corona-Vallet, S.; Lairez, D. *J. Phys. II (France)* **1996**, *6*, 1781.

9. Bang, J.; Viswanathan, K.; Lodge, T. *J. Chem. Phys.* **2004**, *121*, 11489.

10. Bang, J.; Jain, S.; Li, Z.; Lodge, T.; Pedersen, J.; Kesselman, E.; Talmon, Y. *Macromolecules* **2006**, *39*, 1199.

11. Di Cola, E.; Lefebvre, C.; Deffieux, A.; Narayanan, T.; Borsali, R. *Soft Matter* **2009**, *5*, 1081.

12. Farago, B.; Monkenbush, M.; Richter, D.; Huang, J.; Fetters, L.; Gast, A. *Phys. Rev. Lett.* **1993**, *71*, 1015.

13. Minatti, E.; Viville, P.; Borsali, R.; Schappecher, M.; Deffieux, A.; Lazzaroni, R. *Macromolecues* **2003**, *36*, 4125.

14. Lason, D.; Schappecher, M.; Deffieux, A.; Borsali, R. *Macromolecules* **2006**, *39*,

7107.

15. Pispas, S.; Hadjichristidis, N.; Potemkin, I.; Khokhlov, A. *Macromolecules* **2000**, *33*, 1741.

16. Sotiriou, K.; Nannou, A.; Velis, G.; Pispas, S. *Macromolecules* **2002**, *35*, 4106.

17. Halperin, A.; Alexander, S. *Macromolecules* **1989,** *22,* 2403.

18. Zhulina, E.; Adam, M.; LaRue, I.; Sheiko, S.; Rubinstein, M. *Macromolecues* **2005**, *38*, 5330.

19. LaRue, I.; Adam, M.; Zhulina, E.; Rubinstein, M.; Pisikalis, M.; Hadjichistidis, N.; Ivanov, D.; Gearba, R.; Anokhin, D.; Sheiko, S. *Macromolecues* **2008**, *41*, 6555.

20. Hult, A.; Johansson, M.; Malmström, E. *Adv. Polym. Sci.* **1999**, *143*, 1.

21. Chen, C-C. *Langmuir* **2005**, *21*, 5605.

22. Gestwicki, J.; Cairo, C.; Strong, L.; Oetjen, K.; Kiessling, L. *J. Am. Chem. Soc.* **2002**, *124*, 14922.

23. Hinestrosa, J.P.; Alonzo, J.; Mays, J.; Kilbey, S.M. *Macromolecules* **2009**, *42*, 7913.

24. Uhrig, D.; Mays, J.W. *J. Polym. Sci. Part A: Polym. Chem.* **2005**, *43*, 6179.

25. *Polymer Handbook, 4th edition*; Brandrup, J.; Immergut, E.; Grulke, E., Eds.; Wiley-Interscience: New York, 1999.

26. Schärtl, W. *Light Scattering from Polymer Solutions and Nanoparticle Disperions*; Springer: Berlin, 2007.

27. Provencher, S. *Comput. Phys. Commun.* **1982**, *27*, 229.

28. Chu, B. *Laser Light Scattering: Basic Principles and Practice*; Dover: Mineola, 2007; p. 248.

29. Koppel, D. *J. Chem. Phys.* **1972**, *57*, 4814.

30. Galinski, G.; Burchard, W. *Macromolecules* **1997**, *30*, 6966.

31. Tuzar, Z.; Kratochvil, P. In *Light Scattering: Principles and Development*; Brown, W., Ed.; Oxford University Press: Oxford, 1996; p. 327.

32. Burchard, W. *Adv. Polym. Sci.* **1999**, *143*, 113.

33. Semenov, A.; Vlasopoulos, D.; Fytas, G.; Vlachos, G.; Fleisher, G.; Roovers, J. *Langmuir* **1999**, *15*, 358.

34. Daoud, M.; Cotton, J-P. *J. Phys. (France)* **1982**, *43*, 531.

35. Carignano, M.A.; Szleifer, I. *Macromolecules* **1994**, *27*, 702.

36. Kanai, S.; Muthukumar, M. *J. Chem. Phys.* **2007**, *127*, 244908.

37. Kawaguchi, T.; Kobayashi, K.; Osa, M.; Yosizaki, T. *J. Phys. Chem. B.* **2009**, *113*, 5440.

38. Russo, P. *Macromolecules* **1985**, *18*, 2733.

39. Halperin, A.; Tirell, M.; Lodge, T.P. *Adv. Polym. Sci.* **1992**, *100*, 31.

40. Milner, S. *Macromolecules* **1994**, *27*, 2333.

CHAPTER 3

PREFERENTIAL ADSORPTION OF POLYSTYRENE-POLYISOPRENE MIKTOARM BLOCK COPOLYMERS AT THE SOLID/FLUID INTERFACE

3.1 Introduction

The adsorption of complex soft materials at interfaces is relevant to a variety of chemical and biological phenomena and central to the promise of preferential adsorption as a scalable and robust method of materials processing. Self-assembly has been proposed as an enabling technology, suitable for fabrication of a variety of next-generation devices and systems, such as nanopatterned resists for advanced lithography electronic circuitry and biomimetic constructs.[1] In this pursuit, block copolymers having incompatible blocks are often used because rigorous and controlled synthetic strategies can be employed to tailor how chemical information is encoded into the molecule by tuning composition, connectivity and chemical constituents.[2] In a selective solvent, block copolymers spontaneously self-assemble into complex microphase segregated ensembles.

In this chapter we investigate the kinetics of preferential adsorption of self-assembled macromolecular ensembles onto solid substrates and the kinetic processes leading to formation of tethered polymer layers, which in contrast to the thermodynamic behaviors of micellar systems in solution,[1-6] is dealt with in a largely phenomenological manner. It is generally agreed that when micellar systems self-assemble at the solid/fluid interface, there is a dynamic relaxation/reorganization of the micelles in order to expose the solvophobic core blocks to the surface, which ultimately leads to the tethering of

individual chains and micellar structures.[5,7-13] Rearrangement processes that may occur include break-up of the entire micelle, releasing single chains that will preferentially adsorb, or adsorption of micellar coronal arms that then undergo a redistribution of the core blocks in order to populate the surface and relieve the local crowding.[8] It is also speculated that in situations where there is a high energy barrier between the coronal arms and the substrate, the micelles never adsorb, but act only as reservoirs, supplying free chains to the solution that may eventually tether, driving the layer formation process.[5]

Despite the agreement on the complexity of the phenomena and possible mechanisms at play during adsorption, these dynamic events are basically omitted from any mathematical description of the adsorption process. Oftentimes the classical diffusion-controlled model, $\Gamma(t) = 2C_0\sqrt{Dt/\pi}$, derived from Fick's second law, which depends upon the initial adsorbate concentration, C_o, and the diffusion coefficient D, is assumed to apply and used to describe how the adsorbed amount Γ changes with time t during early stages.[14,15] However, almost no attention is placed on identifying the true terminus of the diffusion-limited regime, verifying the $t^{1/2}$ time-dependence, or properly describing adsorption behaviors at the intermediate or long times of the adsorption process. Moreover, assumptions of no interactions between approaching and adsorbed chains, and that every polymer chain that reaches the surface is adsorbed immediately are dramatic simplifications and particularly problematic for large adsorbing molecules and molecular aggregates that have numerous conformational states and are in dynamic equilibrium with single chains. As a result, values of D extracted by fitting the experimental data at

early stages of the self-assembly process often deviate substantially, sometimes by several orders of magnitude, from values typically expected.[1,3,7-11,16-18] While successful for describing the adsorption of single polymer chains[14,15] and the sequential adsorption of homopolymers,[19] the diffusion-controlled model has been proven unsuccessful for linear diblock copolymers forming polymer brushes[16] and more complex systems such as high molecular weight, M_w, triblock copolymers[17] and polyelectrolyte micelles.[11] To examine the importance of dynamic relaxation/reorganization processes occurring at the solid/fluid interface, preferential adsorption of polymer micelles onto Si/SiO_2 surfaces was monitored *in situ* by phase modulated ellipsometry. This allows the study their adsorption kinetics at the solid/fluid interface.

3.2 Experimental

Materials and Sample Preparation As outlined in the previous chapter, PS-PI-$(PI)_2$ miktoarm block copolymers were synthesized via anionic polymerization using chlorosilane coupling to graft two PI anions and a PS-PI diblock copolymer at a single junction (see Fig. 3.1). Here trichlorosilane is used to produce a 3-arm product. The identification strings used to refer to the various copolymers as well as the M_w of each block and polydispersities are shown in Table 3.1.

Table 3.1. Properties of polystyrene-polyisoprene (PS-PI) diblock and PS-PI-$(PI)_2$ miktoarm copolymers with results form light scattering experiments.

Sample ID and block M_w's		M_w PS (kDa)	M_w PI (kDa)	*PDI*	*dn/dc*	$\langle D \rangle_Z$ (cm^2/s)[b]	(R_g/R_h)[b]
DB[a]	PS-PI 26/141	26	141	1.09	0.224	8.66×10^{-8}	0.78
MA1	PS-PI-$(PI)_2$ 33/32/$(14)_2$	33	60	1.01	0.219	1.71×10^{-7}	0.61
MA3	PS-PI-$(PI)_2$ 29.6/70/$(43)_2$	29.6	156	1.17	0.207	1.18×10^{-7}	0.73
MA4	PS-PI-$(PI)_2$ 33/33/$(57.8)_2$	33	149	1.14	0.199	1.15×10^{-8}	0.73

[a]obtained from Polymer Source, Inc.; [b]results obtained from static and dynamic light scattering at C_o = 30 μg/mL in n-hexane.

Stock solutions having a concentration of 300 μg/ml were prepared by adding 60 ml of n-hexane 99% (Alfa Aesar) to 18 mg of bulk polymer. The n-hexane was filtered through Millipore 0.2 μm PTFE filters prior solution preparation. The stock solutions were sealed and gently shaken for at least 10 days at room temperature in order to allow for equilibration. 48 to 72 hours prior to an experiment, an aliquot was taken from the stock solution and diluted with filtered n-hexane to achieve the desired experimental concentration in which the kinetics experiments were performed. Concentrations of 30 and 3 μg/ml were employed for the adsorption studies.

Diced silicon wafers (1.2 cm × 1 cm) obtained from Silicon Quest were cleaned by immersing them in 'piranha acid', which is a 70/30 (v/v) sulfuric acid (98%)/ hydrogen peroxide (30%) mixture, at 110°C for 30 min. *Piranha acid is a strong oxidizer; contact with organic solvents must be avoided and the solution should not be left unattended.* After the wafers were extracted from the piranha acid bath, they were rinsed with copious amounts of distilled water and dried with filtered N_2. This cleaning process leaves a native silicon dioxide, SiO_2, layer of thickness between 13-15 Å as checked by ellipsometry. These wafers were used within 4 hours of preparation. The glass fluid cell used to conduct the kinetics experiments was also cleaned in 'piranha acid' in the same

manner as the silicon wafers, except it was also rinsed with filtered acetone (0.2 μm PTFE Millipore) before the N_2 drying.

Phase Modulated Ellipsometry The kinetics of self-assembly at the solid/liquid interface were monitored using a Beaglehole Picometer Ellipsometer, which uses a He-Ne laser light source (λ = 632.8nm) and a photoelastic birefringent (quartz) element to modulate the phase of the incident light beam. Phase modulation provides a higher sensitivity, lower signal-to-noise ratio, and a time resolution as short as 1 ms. Ellipsometry is a technique measures the real and imaginary components of the ellipsometric ratio, ρ, which is defined as:[16]

$$\rho = \frac{r_p}{r_s} = \tan\Psi e^{i\Delta} = \mathrm{Re}(\rho) + i\,\mathrm{Im}(\rho) \tag{3.1}$$

where $\mathrm{Re}(\rho) = \tan\Psi\cos\Delta$ and $\mathrm{Im}(\rho) = \tan\Psi\sin\Delta$, and r_p and r_s are the complex overall reflection coefficients of the *p* and *s* polarization states, respectively.

At the start of the experiment, a clean silicon wafer is mounted on a home-built stage that fits in a cylindrical fluid cell made of high-quality optical glass. The entire fluid cell assembly sits on an x-, y-, z- translation stage that can also be tilted (rotated) about principal axes coincident with and perpendicular to the plane formed by the *p* and *s* polarization states of the incident light beam. This allows the sample to be aligned such that the laser beam enters (and exits) normal to the walls of the fluid cell, impinges on the center of the wafer and cleanly enters the detector through a pinhole. The alignment procedure is performed at incident angles of 75° and 40°. Then the fluid cell is filled with approximately 13 mL of filtered (Millipore PTFE 0.2μm) n-hexane and, if necessary,

realigned so the laser beam again passes cleanly through the pinhole at 75° and 40°. After the system is aligned, the arms that hold the incident and detector optics and electronics are moved in tandem to the Brewster angle, defined by $\theta_B = \tan^{-1}\left(n_{substrate}/n_{solvent}\right)$, where $n_{substrate}$ is the refractive index of silicon (3.875) and $n_{solvent}$ is the refractive index of n-hexane (1.372); thus for this system $\theta_B \approx 70.5°$ and at this condition $\Delta = 90$ and $\mathrm{Re}(\rho) = 0$. Experimentally, the Brewster angle is determined by finding the angle at which $\mathrm{Re}(\rho) < 1 \times 10^{-3}$, nominally $\theta_B = 70.5° +/- 0.3°$. After θ_B is determined, the imaginary signal, $\mathrm{Im}(\rho)$, is followed for about 1000 s in order to establish a baseline and determine if any contamination has adsorbed on the surface. If the baseline remains stable, the solvent is drained from the cell, replaced with a polymer solution (filtered through a Millpore PTFE 0.2 μm filter) at the desired concentration, and the measurement quickly started. The $\mathrm{Im}(\rho)$ signal is recorded every 3 seconds until a pseudo-plateau in its signal is reached. An illustration of the micellar adsorption process is shown in Figure 3.1B, and data showing the evolution of the imaginary signal from the baseline determination to the pseudo-equilibrium is shown in Figure 3.2. The adsorbed amount $\Gamma(\mathrm{mg/m^2})$, that is the areal density of polymer adsorbed on the substrate, is calculated from $\mathrm{Im}(\rho)$ using the following equation:[16]

$$\mathrm{Im}(\rho) - \mathrm{Im}(\rho)_{baseline} = \frac{2\pi}{\lambda} \frac{\sqrt{n_{solvent}^2 + n_{substrate}^2}}{n_{solvent}} \left(\frac{dn}{dc}\right) \Gamma \qquad (3.2)$$

Here the λ is the laser beam wavelength and the refractive index increment, *dn/dc*, values were determined independently at 25°C for each sample using a Wyatt Technology Optilab rEX refractive index detector (λ = 658 nm) in conjunction with a Harvard

Apparatus PHD 2000 Infusion syringe pump. The experimentally determined *dn/dc* values are reported in Table 3.1.

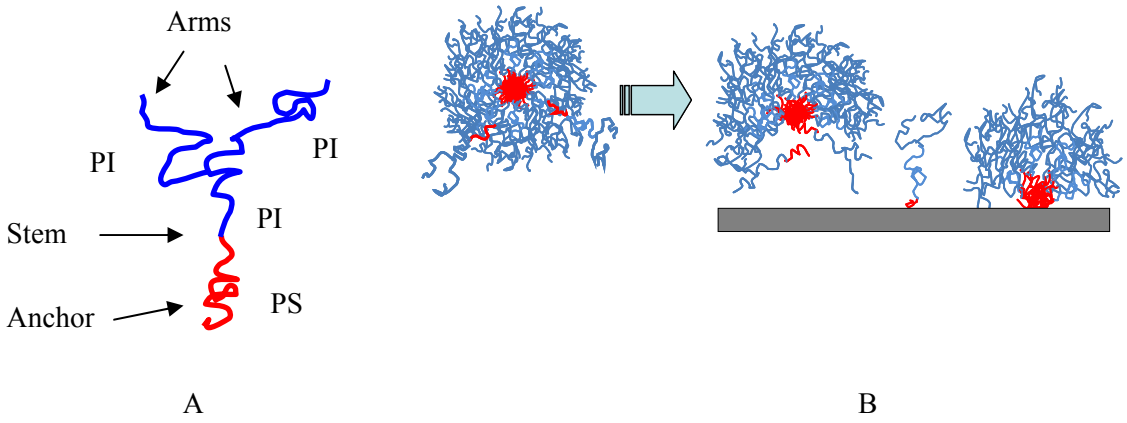

Figure 3.1. (A) Illustration of a single PS-PI-$(PI)_2$ miktoarm copolymer, and (B) scheme for preferential adsorption of macromolecular ensembles.

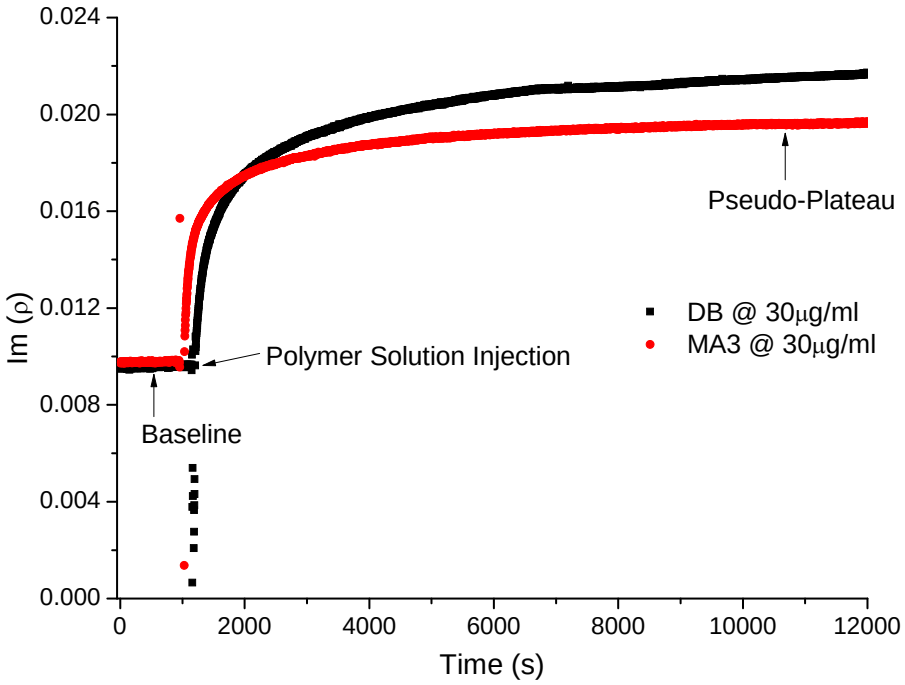

Figure 3.2. Measured Im(ρ) signal for the adsorption of PS-PI 26/141 (DB) and PS-PI-$(PI)_2$ 29.6/70/$(43)_2$ (MA3) in n-hexane.

3.3 Results and Discussion

Figure 3.3 shows the adsorption profiles for the polymers at C_o = 30 μg/mL with an inset log-log plot showing the first 500 s of the adsorption process. For comparison purposes, the kinetics of adsorption predicted for MA3 based on a Fickian diffusion-limited model using the experimentally found diffusion coefficient, $\langle D \rangle_z$, is also shown (see Table 2.2). The adsorption at early times, < 100 s, is very fast due to the large number of available sites, the diffusion of the macromolecular ensembles and the rapid introduction of the polymer solution into the fluid cell. Following this initial period, there is a transition marked by the continuously slowing adsorption rate until a pseudo-plateau is reached at ~12000 s. At these long times the layer is considered to be fully formed, as repulsion between the coronal PI chains of the adsorbed layer shields the surface, creating a significant barrier to penetration and tethering of additional chains. As seen in the inset of Fig. 3.3, the adsorption profile calculated using a Fickian diffusion-limited model, $\Gamma(t) = 2C_0\sqrt{Dt/\pi}$, for sample MA3 shows a substantial and increasing deviation from the data after the first 30 s, suggesting both the end of the diffusion-limited regime and the limit of applicability of the model. It is interesting to note that the adsorption behavior of sample MA1, which has the shortest PI-$(PI)_2$ block ($M_{w,PI}$ = 60 kDa) and smallest M_w and R_h, exhibits an extended transition period in its approach to pseudo-equilibrium and achieves the largest Γ at long times (12000 s).

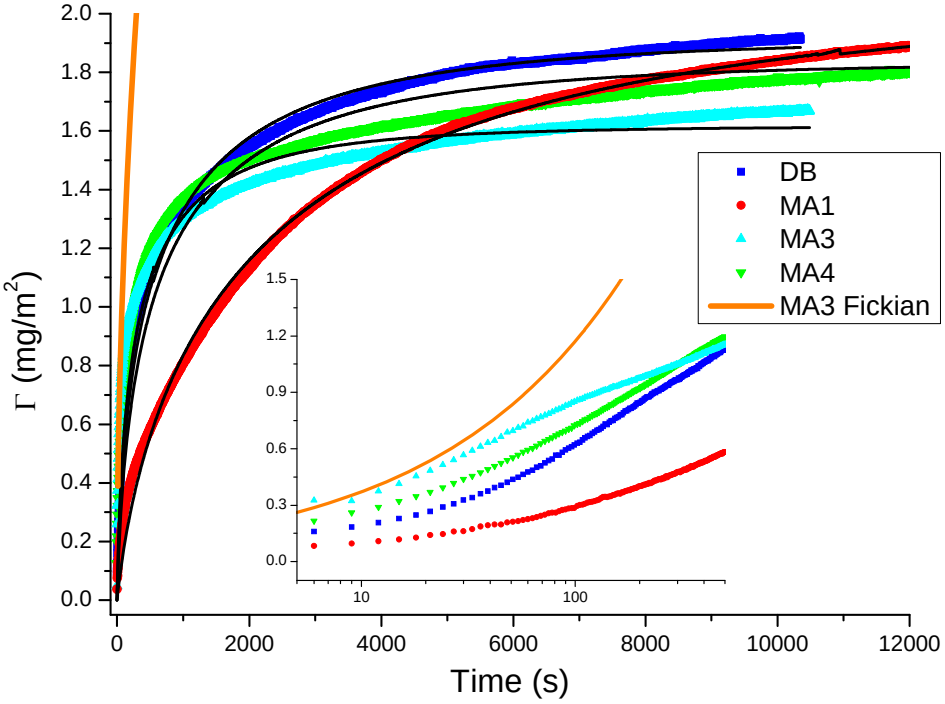

Figure 3.3. Profiles showing kinetics of adsorption of PS-PI micelles formed in n-hexane. The solid colored lines (which are formed from datum points measured every 3 seconds) are the experimental data and the black lines are the fitting results obtained using Eq. (2.3). The solid orange line corresponds to a calculated adsorption profile using a Fickian diffusion-limited model. The inset presents a log-log plot of the adsorption profiles up to 1000 s.

Control experiments using a PI hompolymer (M_w = 145 kDa) showed negligible adsorption (Γ = 0.14 mg/m^2 at 10000 s) at the highest concentration studied (30 μg/mL); these findings, along with a positive spreading coefficient for PS,[20] suggest that the PS blocks of the micellar core are responsible for the layer formation (see Figure 3.4 and Appendix A). Static and dynamic light scattering experiments (SLS and DLS) were carried out to determine $\langle D \rangle_z$, hydrodynamic radius, R_h, and radius of gyration, R_g, in the selective solvent n-hexane. As seen from the values shown in Table 3.1 and as discussed in Chapter 2, the ratios $R_g/R_h \approx 0.7$ suggest that the branched PS-PI-(PI)$_2$ copolymers

form spherical star-like micelles in n-hexane, having corona made of the PI-$(PI)_2$ blocks and a solvophobic PS core.

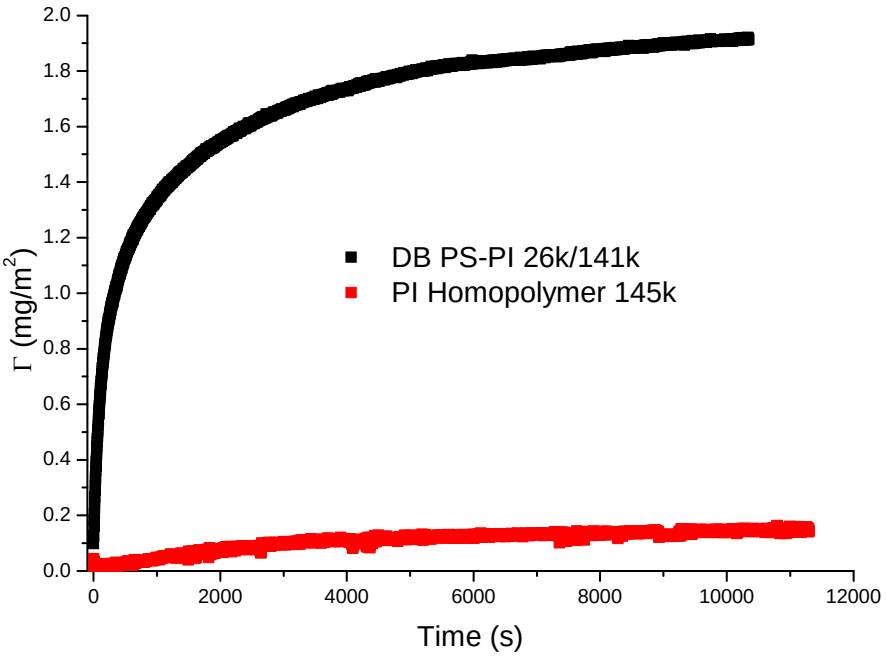

Figure 3.4. Adsorption profiles for the PS-PI diblock copolymer and PI homopolymer from n-hexane solutions at 30 μg/mL onto silicon substrates. At t = 10000 s, $\Gamma(t)_{DB}$ = 1.94 mg/m^2 and $\Gamma(t)_{PI}$ = 0.14 mg/m^2, indicating the important role of the PS block in promoting adsorption.

Given that the diffusion-limited regime ends within a few seconds and there is negligible homopolymer adsorption, I now test the suitability of the model proposed by Hubbard and coworkers,[21] which was conceived to describe the formation of hybrid bilayer membranes by adsorption, rupture and surface fusion of vesicles, as a framework for characterizing the dynamic processes by which complex macromolecular surfactant-like systems self-assemble at the solid-fluid interface. To the best of my knowledge, this model has been used only by the original authors to explain the formation of biomimetic cell membranes[21] and tested in limiting cases by Tirrell and coworkers[23] to describe the

kinetics of bilayer formation by vesicle adsorption on silicon dioxide surfaces. The model allows the evolution of Γ to be followed as a function of t with the adsorption rate depending on the fraction of surface sites available:[21]

$$\Gamma(t) = \Gamma_m \left\{ 1 - \exp \frac{-KC_o}{\Gamma_m} \left[\frac{D_{eff}}{K^2} \left(\exp\left[\frac{K^2 t}{D_{eff}} \right] erfc\left[\left(\frac{K^2 t}{D_{eff}} \right)^{1/2} \right] - 1 \right) + \frac{2}{K} \left(\frac{D_{eff} t}{\pi} \right)^{1/2} \right] \right\} \quad (3.3)$$

Here Γ_m is the maximum adsorbed amount, D_{eff} is a near-surface (effective) diffusion coefficient, and the surface reorganization parameter, K, accounts for the variety of dynamic relaxation/reorganization processes, described previously, that may occur at the interface during adsorption. Eq. 3.3 is derived based on an imperfectly adsorbing substrate having a near-surface concentration gradient, and also satisfies the initial condition $\Gamma_{(t\,=\,0)} = 0$ and boundary condition $\Gamma_{(t\,=\,\infty)} = \Gamma_m$.[23] The parameter K^2/D_{eff} represents the relative contribution of mass transport to surface relaxation/reorganization effects. Larger values of K^2/D_{eff} correspond to a mass transport limited regime, whereas smaller values of K^2/D_{eff} imply that layer formation is governed by complex surface relaxation/reorganization events. Based on this, two limiting cases are predicted. For larger values of K^2/D_{eff}, surface reorganization processes are fast and the adsorption is diffusion-limited:[21]

$$\Gamma(t) = \Gamma_m \left[1 - \exp\left(\frac{-2C_o}{\Gamma_m} \left(\frac{D_{eff} t}{\pi} \right)^{1/2} \right) \right] \quad (3.4)$$

On the other hand, when the evolution of the layer is limited by surface relaxation/reorganization events the adsorption process is modeled by:[21]

$$\Gamma(t) = \Gamma_m \left[1 - \exp\left(\frac{-KC_o t}{\Gamma_m} \right) \right] \tag{3.5}$$

To characterize the adsorption of the branched block copolymer micelles, Eq. 3.3 was used to fit the adsorption profiles using the Marquardt-Levenberg algorithm with K, D_{eff} and Γ_m as fitting parameters. The model is parameterized using an initial value of D_{eff} = 1×10^{-7}cm^2/s, which is obtained from DLS measurements reported in Chapter 2, and Γ_m is set equal to the Γ measured from the pseudo-plateau at ~ 12000 s. The parameter C_o is known and not allowed to vary. Finally, an initial value of $K = 1\times10^{-5}$ cm/s is used, which is similar to what was obtained previously by Hubbard et al.[21] and Strompoulis et. al.[22] to describe vesicle adsorption. Values of K, D_{eff} and Γ_m obtained by fitting the adsorption profiles at C_o = 30 μg/mL and 3 μg/mL are shown in Table 3.2. All of the parameters showed low correlation coefficients (0.2 - 0.5) providing evidence that Eq. 3.3 is not over-specified and the parameters D_{eff}, K and Γ_m are needed to effectively characterize the self-assembly of these macromolecular aggregates at the solid/fluid interface.

Table 3.2. Preferential adsorption kinetics fitting results

Sample ID	C_o (μg/mL)	K (cm/s)	D_{eff} (cm^2/s)	Γ_m (mg/m^2)	K^2/D_{eff} (s^{-1})
DB	30	6.00 x 10^{-5}	5.67 x 10^{-8}	1.92	6.35 x 10^{-2}
MA1	30	8.76 x 10^{-5}	2.39 x 10^{-8}	2.08	3.21 x 10^{-1}
MA3	30	7.00 x 10^{-5}	7.91 x 10^{-8}	1.62	6.19 x 10^{-2}
MA4	30	4.00 x 10^{-5}	5.54 x 10^{-8}	1.84	2.88 x 10^{-2}
MA1[a]	3	3.56 x 10^{-6}		1.51	
MA3	3	1.29 x 10^{-5}	1.42 x 10^{-7}	1.07	1.17 x 10^{-3}
MA4	3	8.00 x 10^{-5}	5.51 x 10^{-7}	1.49	1.16 x 10^{-2}

[a] fitting results obtained using Eq. (3.5) were better than those obtained using Eq. (3.3).

It is clear from Figure 3.3 and Table 3.2 that the "mixed-controlled" model embodied by Eq. 3.3 accurately predicts the entire adsorption kinetics profiles. The predicted Γ_m values are slightly lower than (within 10% of) the experimentally-measured values and

the adsorption behavior at early times has been adequately captured. In agreement with experimental results, the model also predicts that adsorption of MA1 yields the largest Γ_m, which is consistent with the idea that its smaller micelle size allows more micelles to pack along the solid/fluid interface. This result is in agreement with the work of Bijsterbosch et al.[23] who studied the effect of micelle size on adsorption using micelles made from poly(dimethyl siloxane)-*block*-poly(2-ethyl-2-oxazoline) copolymers in aqueous solution and concluded that the adsorption kinetics are governed by an interchange between the micelles and the free chains in solution and, at constant concentration, as the size of each block is reduced, Γ_m increases.

The constituent polymers of the micelles formed from DB, MA3 and MA4 have a similar M_w and PDI, and their micellar aggregates show similar trajectories in their adsorption behavior, with the surface layers made from the branched macromolecules having lower Γ_m and K^2/D_{eff}. I point to this as supporting the idea that differences in micellar aggregate structure (e.g., size, aggregation number, core and coronal solvation) affect both mass transport and dynamics of surface relaxations/reorganizations, which in concert give rise to layer evolution. It is interesting to note that the linear analog of the miktoarm copolymers reaches a pseudo-equilibrium Γ value only slightly less than that of the smallest miktoarm (MA1). One of the relaxation/reorganization processes that might occur during the adsorption process is the release of single chains, and it has been shown that the passage of the chain through the corona is the rate determining step in this type of relaxation.[24] Therefore, it is reasonable to assume that it would be easier for a linear chain

embedded in a micelle to extract itself from the ensemble and influence the preferential adsorption process.

It is worth noting that the D_{eff} values obtained from the fits at 30 μg/mL are almost one order of magnitude (<5x) smaller than $\langle D \rangle_z$ measured by dynamic light scattering and reported in Chapter 2 (see Table 2.2). The values for the reorganization parameter K are of the same order of magnitude, ~10^{-5} cm/s, as those obtained from studies of adsorption of lipid vesicles,[21,22] suggesting commonality with the adsorption behavior of surfactant-based bioinspired systems. Despite substantial differences in molecular complexity (e.g., size, topology), it is possible to affirm that the preferential adsorption of these macromolecular ensembles share the same underlying physical features: mass transport towards the solid/fluid interface and a variety of dynamic surface relaxation/reorganization processes. These include effects such as micelle break-up to supply single chains, adsorption and subsequent redistribution of the micellar ensemble in order to expose core blocks, and reflection of micelles that fail to adsorb. The surface morphology is presumed to be a layer of surface hemi-micelles and preferentially adsorbed single chains, as has been theoretically predicted by Ligoure[25] for block copolymer micelles adsorbed from selective solvents and experimentally observed by techniques such as atomic force microscopy as shown in Appendix E.

Further demonstration of the need to include both the diffusive and dynamic surface relaxation/reorganization contributions to properly describe the adsorption kinetics is obtained from experimental results at a lower concentration. Figure 3.5 depicts the adsorption profile for MA3 at C_o = 3 μg/mL, with the inset scaled to highlight the early

stages of the adsorption. A clear indication of the effect of reduced adsorbate concentration is that the time required to reach the pseudo-equilibrium in Γ is now ~45,000 s, as compared to ~12,000 s required at C_o = 30 µg/mL. It is also evident that a diffusion-controlled model (Eq. 3.4) provides a better description during the very early stages of adsorption at this concentration; however; the diffusion-limited fit yields a Γ_m = 1.25 mg/m^2, which differs substantially from the measured value, $\Gamma_{m,\text{measured}}$ = 0.97 mg/m^2. On the other hand, the kinetically-controlled model (Eq. 3.5) yields a slightly lower Γ_m than what is measured at the pseudo-plateau, but as shown in by the inset in Figure 3.5, the agreement between the data and this limiting-case model at early times is rather poor. Consequently, a mixed-controlled model provides a much better description of the entire preferential adsorption process, closely following the evolution of the kinetic profile up to its pseudo-equilibrium.

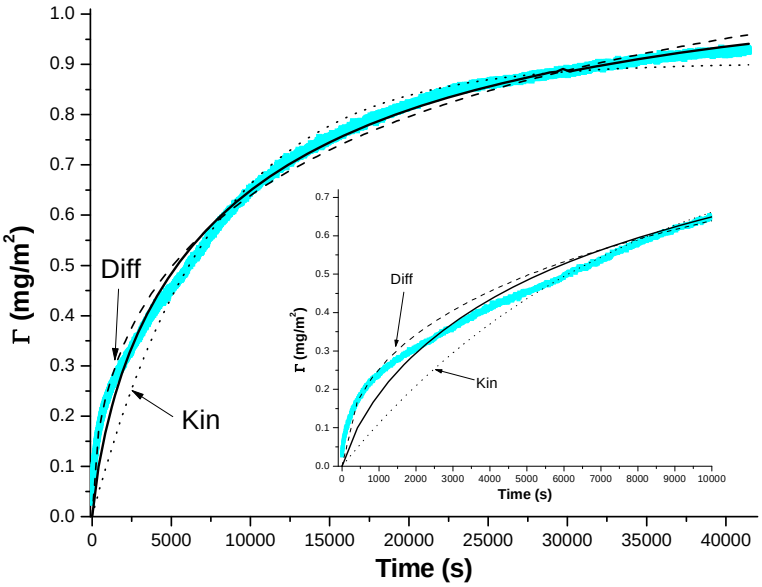

Figure 3.5. Adsorption profile for MA3 at C_o = 3 µg/ml. The light blue solid line is the experimental data, the solid black line is the fitting result using Eq. 3.3 while dashed line is the best fit using Eq. 3.4, and the dotted line represents the fit using Eq. 3.5. The inset shows the same profile and fits up to t = 10000 s.

Figure 3.6 shows the adsorption profiles for all of the miktoarm samples at C_o = 3 μg/mL. The D_{eff} values obtained at 3 μg/mL are an order of magnitude higher than the ones obtained at 30 μg/mL, showing the increasing effect of surface reorganization with respect to mass transport. Here the parameter K^2/D_{eff} also provides evidence of the importance of dynamic relaxation/reorganization phenomena as the overall solution concentration decreases. Comparing the results at C_o = 30 μg/mL and C_o = 3 μg/mL for samples MA3 and MA4, the decrease in K^2/D_{eff} in conjunction with the larger D_{eff} values (~10^{-7} cm^2/s) shows the enhanced role of surface relaxation/reorganization processes on the adsorption kinetics. This is also reflected in the long times required (~45000 s) to reach pseudo-equilibrium at low concentration since the characteristic time scale of the dynamic relaxation/reorganization events are long and the flux of new ensembles to the surface is low. It is also found that the adsorption of the smallest copolymer, MA1 at C_o = 3 μg/mL, is best described by the limiting case where adsorption is dominated by dynamic processes at the surface (Eq. 3.5), rather than a diffusion-limited model or the mixed-controlled model. Thus for small size micelles at a lower concentration the K^2/D_{eff} is smaller, suggesting that relaxation or reorganization of the micelles becomes a more prominent factor in the adsorption process.

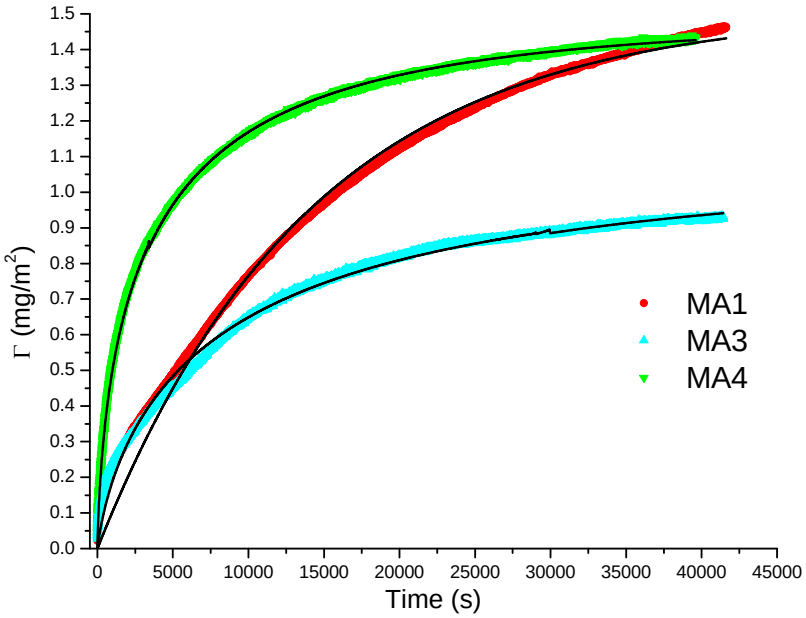

Figure 3.6. Adsorption profiles of PS-PI-$(PI)_2$ miktoarm copolymers at C_o = 3 µg/ml. Black solid lines are the best-fits obtained using Eq. 3.3 for MA3 and MA4 and Eq. 3.5 for MA1.

The initial fast increase in Γ observed at both concentrations comes from the large availability of surface sites because there is no competition or interaction between absorbing molecules. During these initial stages the near-surface concentration profile evolves, mainly controlled by the diffusion of material towards the solid/fluid interface, but also because micelle adsorption is neither instantaneous nor assured. While the near-surface concentration profile changes throughout the adsorption process, the dynamic relaxation/reorganization events occurring between the micellar solution, the free chains and the adsorbed chains at the interface dominate the evolution of the interfacial layer. As the overall solution concentration decreases, the flux of polymer to the interface decreases; thus, longer times are required to reach pseudo-equilibrium. However the

same diffusion and relaxation/reorganization processes take place in order to generate the polymer layer on the surface.

3.4 Conclusions

This body of work clarifies the important and controlling role of dynamic relaxation/reorganization that occurs throughout self-assembly (adsorption) of soft matter at the solid/fluid interface. In these micellar systems, the evolution of the interfacial layer towards pseudo-equilibrium is a product of both the diffusion of macromolecular ensembles and the relaxation events required to expose the PS core blocks, affected by chains at the already-populated surface and imperfect adsorption, with the diffusion-limited regime ending quickly, even at ultra low concentrations. The mixed-controlled model successfully describes the kinetics of preferential adsorption from early stages to pseudo-equilibrium and provides a quantitative basis for understanding the physical phenomena governing interfacial layer formation. A clear challenge remaining is to link ensemble structure, dynamics and specific surface relaxation processes to the rate constant that represents these complex processes. Such closure would bring a fundamental understanding that connects macromolecular design, (supra)molecular assembly and formation of polymer-modified interfaces by self-assembly.

3.5 References

1. Hadjichristidis, N.; Pispas, S.; Floudas, G. *Block Copolymers : Synthesis Strategies, Physical Properties, and Applications*; Wiley-Interscience: Hoboken, 2003; p. 195.

2. Hamley, I.W. *The Physics of Block Copolymers*; Oxford University Press: Oxford, 1998; p. 131.

3. Awan, M.; Dimonie, V.; Ou-Yang, D.;El-Aasset, M. *Langmuir* **1997**, *13,* 140.

4. Zhulina, E.; Adam, M.; LaRue, I.; Sheiko, S.; Rubinstein, M. *Macromolecues* **2005**, *38*, 5330.

5. Johner, A.; Joanny, J. *Macromolecules* **1990,** *23*, 5299.

6. Gohy, J-F. *Adv. Polym. Sci.* **2005,** *190*, 65.

7. Sakai, K.; Smith, E.; Webber, G.; Schatz, C.; Wanless, E.; Bütün, V.; Armes, S.; Bigss, S. *J. Phys. Chem. B* **2006**, *110*, 14744.

8. Toomey, R.; Mays, J.; Yang, J.; Tirrell, M. *Macromolecules* **2006,** *39*, 2262.

9. Munch, M.; Gast, A. *Macromolecules* **1990,** *23*, 2313.

10. Amiel, C.; Sikka, M.; Schneider, J.; Tsao, Y-H.; Tirrell, M.; Mays, J. *Macromolecules* **1995,** *28*, 3125.

11. Toomey, R.; Mays, J.; Holley, D.; Tirrell, M. *Macromolecules* **2005,** *38*, 5137

12. Zhan, Y.; Mattice, W. *Macromolecules* **1994,** *27*, 638.

13. Hamley, I.W. *Block Copolymers in Solution: Fundamentals and Applications*; Wiley: West Sussex, 2005; p. 226.

14. Dorgan, J.; Stamm, M.; Toprakcioglu, C.; Jérôme, R.; Fetters, L. *Macromolecules* **1993,** *26*, 5321.

15. Motschmann, H.; Stamm, M.; Troprakcioglu, C. *Macromolecules* **1991,** *24*, 3681.

16. Toomey, R.; Mays, J.; Tirrell, M. *Macromolecules* **2004,** *37,* 905.

17. Alonzo, J.; Huang, Z.; Liu, M.; Mays, J.; Toomey, R.; Dadmun, M.; Kilbey II, S.M. *Macromolecules* **2006,** *39,* 8434.

18. Brandani, P.; Stroeve, P. *Macromolecules* **2003,** *36*, 9502.

19. Erban, R.; Champman, J.; *Phys. Rev. E* **2007,** *75,* 041116.

20. Parsonage, E.; Tirell, M.; Watanabe, H.; Nuzzo, R. *Macromolecules* **1991**, *24*, 1987.

21. Hubbard, J.; Silin, V.; Plant, A. *Biophys. Chem.* **1998,** *75,* 163.

22. Stroumpoulis, D.; Parra, A.; Tirrell, M. *AIChE J.* **2006,** *52,* 2931.

23. Bijsterbosch, H.; Cohen Stuart. M.; Fleer, G. *Macromolecules* **1998,** *31,* 9281.

24. Halperin, A.; Alexander, S. *Macromolecules* **1989,** *22,* 2403.

25. Ligoure, C. *Macromolecules* **1991,** *24,* 2968.

CHAPTER 4

HYDRODYNAMIC PROPERTIES OF A_NB_N HETEROARM STAR COPOLYMERS

4.1 Introduction

Branched copolymers in which all branches (arms) emanate from a common junction point or core are usually referred to as stars. These branched structures are made of linear segments but they represent a special morphological class of polymers that have dynamics, structure and properties different from the more common linear polymers.[1] With the advent of anionic polymerization techniques, nowadays it is possible to synthesize star-like copolymers that have narrow polydispersities and controlled architecture.[2,3] In addition, the flexibility of anionic synthesis methods allows stars having arms made of diblock copolymers to be made, as well as stars having different types (monomeric building blocks) of arms, as illustrated in Figure 4.1. These novel copolymer architectures can be studied as models for colloidal systems and modifiers of rheological behavior in polymer blends, for example.[4,5]

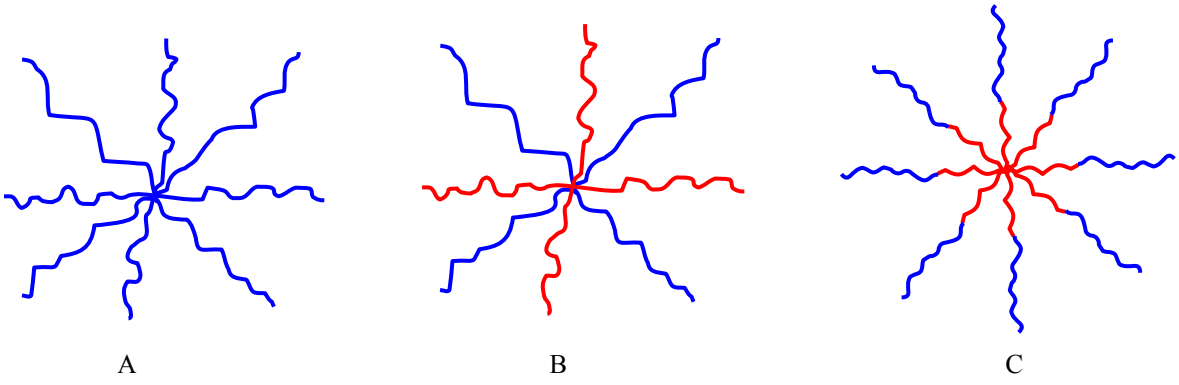

Figure 4.1. Illustration of different types of star polymers, including (A) star homopolymers, (B) A_nB_n heteroarm star copolymers (arms of different monomers emanating from the core), and (C) $(A\text{-}B)_n$ star block copolymers. The focus of this Chapter is on heteroarm star copolymers.

A considerable amount of work has been done to enhance our understanding of the structure and dynamics of homopolymer stars in solution (see Figure 4.1 A).[1,6-15] In the dilute solution regime, the radius of gyration of symmetrical homopolymer stars, $R_{g,s}$, scales with the number of arms, f, in the fashion $R_{g,s} \sim R_{g,l} f^{(1-3\nu)/2}$, where $R_{g,l}$ is the radius of gyration of a linear homopolymer of same total molecular weight, $M_{w,tot}$. In this expression, ν is the solvent quality parameter from the well-known relationship, $R_{g,l} \sim N^{\nu}$, where N is the degree of polymerization of the chain and $\nu \approx 0.6$ for self-avoiding chains (good solvent conditions) and $\nu = 0.5$ for Gaussian chains (θ-solvent conditions).[7] The scaling behavior for the stars implies that the overall size of a star homopolymer does not increase linearly with the number of arms, and it will eventually reach an asymptotic limit as f increases.[1] It also shows that stars are more compact than linear analogs. In the semi-dilute regime, star homopolymers have shown liquid-like ordering, as evidenced in computer simulations[13], in small-angle neutron scattering (SANS) studies and in light scattering experiments (LS).[7,11] Regarding the effect of f, Willner and coworkers[9] showed that the dependence of R_g on N were similar for a centro-symmetric 18 arm polyisoprene (PI) star and a linear PI chain; however, as f increased to 64 arms, the scaling of R_g with N is closer to the predictions for hard-spheres. This behavior can be attributed to increased intramolecular interactions as the crowding inside the star increases.

Intramolecular interactions also play a key role in the dynamics and structure of heteroarm star copolymers, which have different blocks emanating from the common junction point (as shown Figure 4.1 B). Glazer[16] synthesized A_nB_n (n stands for the number of arms of each constituent) stars with polystyrene (PS) and poly(2-

vinylpyridine) (PVP) constituent blocks. Gel permeation chromatography (GPC) studies in THF (a common good solvent) showed that for $(PVP)_3(PS)_3$ (A_3B_3) stars having similar sized PS and PVP blocks, the molecular dimensions are not that different from θ-solvent conditions. This contrasts with the typical behavior of linear block copolymers, which expand when the solvent is changed from theta to good. The fact that the stars do not readily expand was attributed to the constraints posed by their branched configuration. Similar $(PVP)_n(PS)_n$ stars have been studied by Procházka and coworkers.[17,18] Two $(PVP)_6(PS)_6$ with $M_{w,tot}$ = 507 and 330 kg/mol, and 66 and 47.7 wt % PVP, respectively, were used in these studies. By dissolving these heteroarm star copolymers in a 0.1 M HCl water solution, supramolecular assemblies are obtained, with the core being composed of the unsolvated PS blocks and the corona formed by the well-solvated, charged PVP blocks.[17] It is argued that the core is kinetically "frozen" in aqueous media because PS is insoluble in water and it has a high glass transition temperature, T_g. They found that the aggregation number, Q, is smaller for micelles made of the stars in comparison to Q of micelles formed from PVP-PS diblock copolymers of similar $M_{w,tot}$ and composition. For the star with 60 wt % PVP, Q = 8 whereas for a star with 48 wt % PVP, Q = 29. R_h values measured by dynamic light scattering for the aggregates were 57 nm and 75 nm, respectively. The strong segregation of the PS blocks is argued to be responsible for the increase in Q and R_h as the weight fraction of PVP decreases. Additionally, a $(PVP)_{20}(PS)_{20}$ star showed the coexistence of single stars in solution with small aggregates having Q = 4, which they called tetramers. Based on these findings, the authors proposed two aggregation states for the micellized heteroarm star

copolymers: i) very strong segregation of the PS blocks into the core, resulting in the formation of micelles having all of the core junction points localized at the core/corona interface; and ii) weak segregation because of the branched architecture, resulting in the presence of PVP blocks in the core (~ 20%) and a more homogeneous core/corona interface. Nevertheless, the authors affirmed that there is not enough evidence to elucidate the true structure of the aggregates.[17]

Later the same group studied the self-assembly of a $(PVP)_{20}(PS)_{20}$ heteroarm star where each PS arm has M_w = 3000 g/mol and each PVP arm has M_w = 23000 g/mol.[18] This heteroarm star was studied in 1,4 dioxane, a non-selective solvent, and mixtures of 1,4-dioxane and methanol, which tend to increase selectivity towards PVP as the content of methanol increases. In pure 1,4-dioxane the stars exists as unimers, i.e., there is no aggregation because there is no selectivity. However, as the methanol content is increased, changes in the dynamics and aggregation are observed: When the volume fraction of methanol is greater than 20%, micellization of the stars is observed, and as found previously,[17] Q = 4. At 50 vol % methanol, the R_h distribution obtained by dynamic light scattering changes from a single distribution peak at a concentration, c, of 0.32 mg/mL to a double distribution at c = 10.2 mg/mL, providing evidence that the critical micelle concentration, *cmc*, has been crossed. Since there is a clear coexistence of aggregates and single stars in solution and the position of the peaks did not change with concentration, it is suggested that these $(PVP)_{20}(PS)_{20}$ heteroarm stars follow the closed association model discussed in Section 1.1.

A similar $(PVP)_6(PS)_6$ heteroarm star and a PVP-PS diblock copolymer dissolved in toluene, a solvent selective for PS, were studied by light scattering and viscometry.[19] The $(PVP)_6(PS)_6$ heteroarm star had a $M_{w,tot}$ of 32900 g/mol and was 53.3 wt % of PVP and the diblock a $M_{w,tot}$ = 4600 g/mol and was 47 wt % PVP. As expected, the PVP-PS diblock readily micellizes at $c = 2.2 \times 10^{-4}$ mg/mL, whereas the stars only show evidence of micelles at $c = 7.4 \times 10^{-1}$ mg/mL. This implies that the *cmc* for the stars is three orders of magnitude higher than for the diblocks. The concentration range over which coexistence of single stars and star aggregates is observed is rather large, 7.4×10^{-1} mg/mL $< c <$ 7.5 mg/mL; only at very high concentrations are micelles uniquely observed in solution. The researchers were able to cover the three different zones of closed association model (see Figure 1.1) and showed that Q is significantly smaller for micelles formed from the star in comparison to the diblocks while R_h shows the opposite trend.[19] The thermodyamics of micellization were also studied, and they found that the Gibbs free energy is less negative for the stars. This, in conjunction with the higher values of the *cmc*, suggest that the micellization of heteroarm star copolymers is less favorable and that the soluble PS arms are able to shield the insoluble PVP blocks better in the case of the stars than in the case of diblock copolymers.[19]

A_nB_n systems with PS and polyisoprene (PI) constituents have been also synthesized by anionic polymerization techniques[20] and their solution behavior studied by light scattering techniques.[21] Studies in both selective and non-selective solvents for a $(PS)_8(PI)_8$ symmetric heteroarm star copolymer have suggested an expansion in molecular dimensions in comparison to star homopolymers having similar f and $M_{w,tot}$.

The larger values of R_h for the $(PS)_8(PI)_8$ heteroarm stars are attributed to the increased probability for heterocontacts between the incompatible PS and PI chains. Two samples with 50 wt % PS showed an increase in both R_h and the viscometric radius, R_v, as $M_{w,tot}$ increases.[21] Due to the lower monomer molecular weight of PI (68 g/mol), the PI blocks exert a greater influence on the overall hydrodynamic behavior of the stars. Solid films of these stars were cast from a 2 wt % solution of toluene, a common good solvent, and analyzed by small-angle x-ray scattering (SAXS) and transmission electron microscopy (TEM).[22] These experiments revealed lamellar morphologies for all the three stars studied. Similarly, $(PS)_2(PI)_2$ heteroarm stars were cast from a 5 wt % toluene solution and imaged by TEM.[23] These films also showed strong ordering and segregation into lamellar morphologies. This behavior was in accord with the theoretical predictions of Milner for A_2B copolymers in the melt state.[24]

Despite these previous works, systematic studies of architectural and compositional impact on the properties of stars are rather scarce. In an effort to better understand the effects of copolymer architecture on the hydrodynamic interactions of A_nB_n heteroarm star copolymers, I have used dynamic light scattering to study four symmetric $(PS)_n(PI)_n$ heteroarm star copolymers with 2, 4, 8 and 16 arms (n = 1, 2, 4, 8). These are depicted in Figure 4.2. Systematically doubling the number of arms results in a systematic doubling of $M_{w,tot}$ while keeping the composition fixed. This scheme allows the effects of increasing the branching and intermolecular interactions between incompatible blocks inside the star to be elucidated.

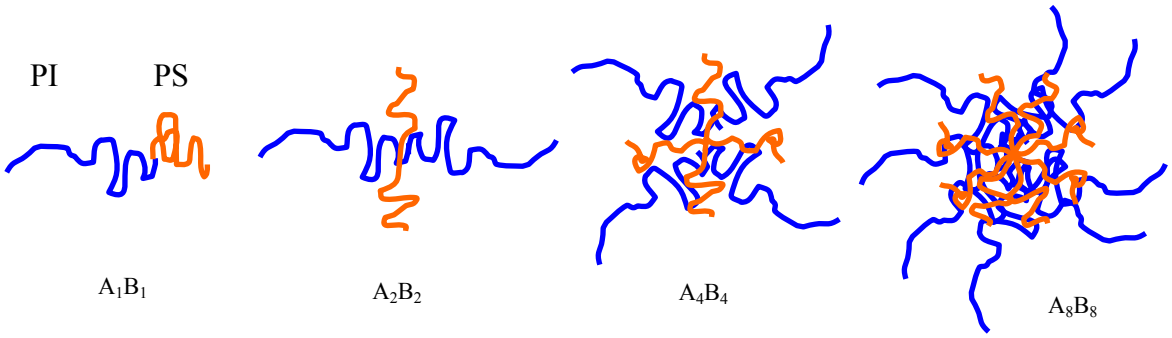

Figure 4.2. Illustration of the arm arrangements for the $(PS)_n(PI)_n$ (A_nB_n) heteroarm star copolymers made from PS (orange) and PI (blue).

4.2 Experimental

Synthesis of A_nB_n stars. The $(PS)_n(PI)_n$ stars were synthesized anionically using a strategy of sequential incorporation of macromolecular anions to multichlorosilane linking agents.[25-27] Styrene and isoprene were polymerized from sec-BuLi in benzene to obtain solutions of polystyryllithium (PS^-Li^+) anions and polyisoprenyllithium (PI^-Li^+) anions in benzene of known concentration. Fractionation in toluene-methanol mixtures yielded clean star copolymer products.

The A_nB_n star copolymer products were characterized using ^1H nuclear magnetic resonance (NMR) spectroscopy in $CDCl_3$ and by SEC-UV in THF to determine the composition and by SEC-RI to determine the $M_{w,tot}$ and polydispersity, PDI. Molecular properties of the heteroarm star copolymers and precursor arms are shown in Table 4.1.

Table 4.1. Properties of $(PS)_n(PI)_n$ (A_nB_n) heteroarm star copolymers

Sample ID	SEC-LS M_w (kDa)	SEC-RI PDI	N_{PI}	N_{PS}	SEC-UV & ^{1}H NMR wt % PS
PS arm	10.1	1.01		97	
PI arm	56.4	1.02	829		
A_1B_1	64.0	1.03	829	97	15.8
A_2B_2	129.0	1.02	1601	193	15.6
A_4B_4	261.3	1.02	3247	389	15.5
A_8B_8	505.4	1.02	6243	777	16.0

Solution Preparations and Dynamic Light Scattering. The solvent used in these studies is n-hexane, a solvent selective towards PI, as discussed in Chapter 2 and Appendix A. n-Hexane was previously filtered using Millipore PTFE 0.2 μm filters and tested in the ALV equipment to assure no dust was present. Concentrated stock solutions of about 5 mg/mL were prepared gravimetrically and allowed to equilibrate in sealed vials for at least 10 days at room temperature. Solutions at lower concentrations were prepared by diluting these stock solutions at least 72 hours prior to the dynamic light scattering (DLS) experiments and these solutions were allowed to equilibrate at room temperature. A_nB_n heteroarm star copolymers solutions having concentrations of 0.25, 0.5, 0.75, 1, 1.5 and 2 mg/mL were studied.

The DLS experiments were run in the same manner as described in Section 2.2. However, here the solution diffusion coefficient, D_s, is obtained from the slope of the plot of the mean decay rate or first cumulant, Γ_i, versus the square of the scattering wave vector, q. The linear fittings were forced through $\Gamma_i = 0$ at $q^2 = 0$. Once these D_s values are obtained, R_h is calculated from the Stokes-Einstein equation as $R_h = kT/6\pi\eta_o D_s$ where k is the Boltzmann constant, T is the absolute temperature and η_o is the solvent viscosity.

4.3 Results and Discussion

Here the analysis of the DLS results is divided in two separate sections: First the effects of polymer concentration on the behavior of the $(PS)_n(PI)_n$ heteroarm stars will be treated, since these results provide an understanding of their structure in solution. Second, the effects of branching and increased intramolecular interactions will be discussed through comparisons of results from different stars at a similar concentration.

Effects of Concentration. Figure 4.3 shows the hydrodynamic radii distributions for the A_nB_n heteroarm star copolymers at all the concentrations studied. For sample A_1B_1, the R_h distributions show one peak at the two lowest concentrations (0.25 and 0.50 mg/mL) but two peaks are observed at c = 0.75 and higher concentrations. The most prominent peak at $R_h \approx 8$ nm remains constant throughout the concentration range studied but its breadth reduces as c increases – a result that may arise due to the higher coherence obtained in the light intensity autocorrelation function, $g_2(q,\tau)$, as c increases (see Appendix F). The smaller second peak observed at larger R_h at and after c = 0.75 mg/mL is rather broad and its contribution to the total scattered intensity increases as c increases. The mean R_h values for this second peak are ≈ 38 nm, indicating the possibility of micellar aggregates.

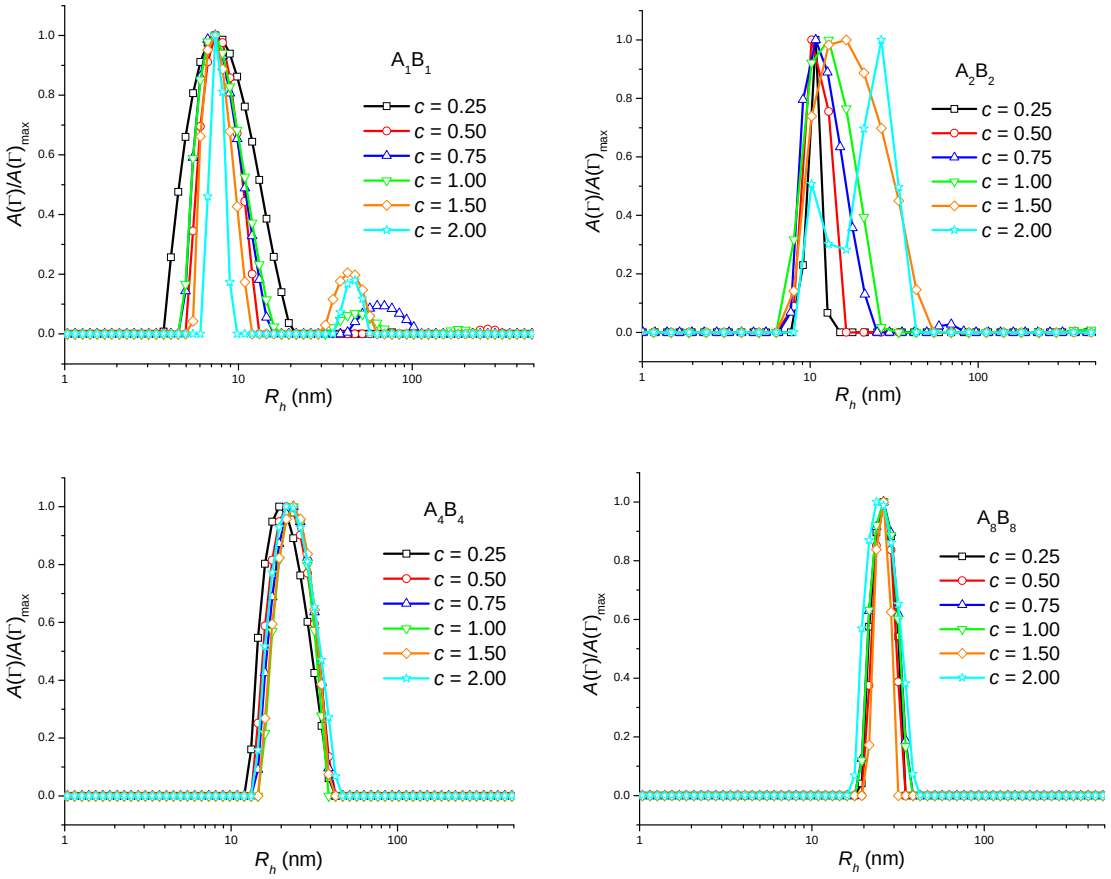

Figure 4.3. Hydrodynamic radii, R_h, distributions for A_nB_n heteroarm star copolymers at the six concentrations studied. Concentrations given in the legends are in units of mg/mL.

Plots of the mean decay rate, Γ, versus the square of the scattering vector, q, for sample A_1B_1 at the lowest and the highest concentrations studied are shown in Figure 4.4. At the lowest concentration, only one decay mode is observed for the 15 scattering angles analyzed and the data can be easily fit with a straight line intersecting the origin. This suggests a diffusion dominated behavior for this $(PS)_1(PI)_1$ (A_1B_1) diblock copolymer in n-hexane. On the contrary, at the highest concentration studied two distinct diffusive decay modes are observed requiring that the normalized light intensity autocorrelation function, $[g_2(q,\tau)\text{-}1]^{1/2}$, be fit using a double exponential decay (Equation 2.4).

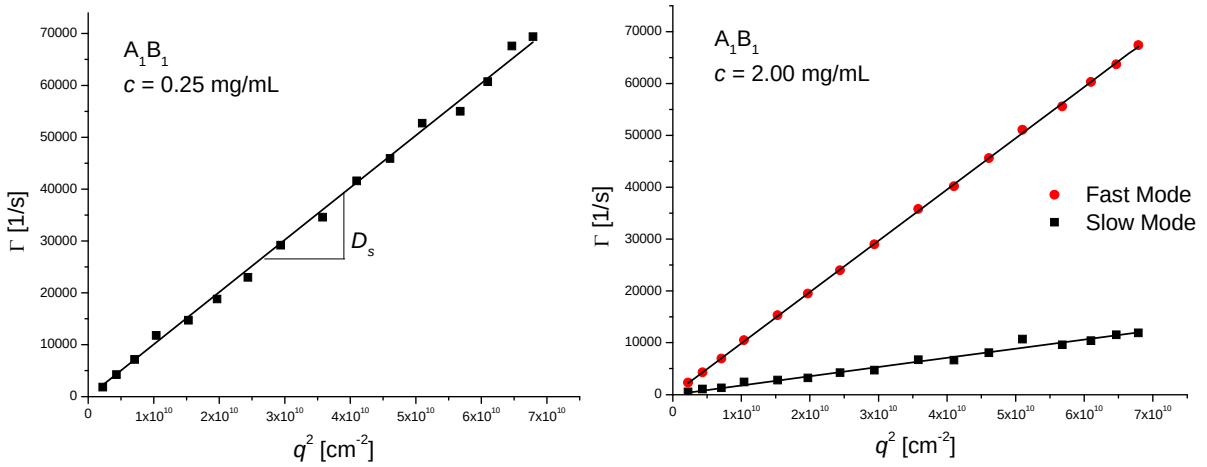

Figure 4.4. Γ versus q^2 plots for sample A_1B_1 at the lowest (left) and highest (right) concentrations studied. The solution diffusion coefficient, D_s, can be obtained from the slope of the line force fit through Γ = 0.

Based on the information from the hydrodynamic distribution and the fits of the Γ versus q^2 plots, it is possible to affirm that below a concentration of 0.75 mg/mL, the A_1B_1 heteroarm star copolymers exists as isolated chains in solution, as described in zone I of the closed association model (see section 1.1). After the concentration threshold for micellization is crossed at $c \approx 0.75$ mg/mL, ensembles of larger R_h start to form in solution and the amount of these larger aggregates increases as concentration is increased further. Therefore the "slow" mode found at $c \geq 0.75$ mg/mL is attributed to micellar aggregates, most likely spherical in structure. Here the insoluble PS blocks try to avoid contact with the solvent and form the micellar core and the soluble PI blocks form the corona. The coexistence of single chains and micelles in solution suggest that the system is in zone II of the closed association model (see Section 1.1).

It is intriguing that for such high concentrations in sample A_1B_1, the mass fraction of micelles is solution is rather small, as judged by the areas under the peaks of the R_h

distributions shown in Figure 4.3. Clearly single $(PS)_1(PI)_1$ diblocks are the predominant species. This behavior may be explained by the slight solubility of PS in n-alkanes, which has been shown to increase with a decrease in PS M_w and an increase in T.[28-31] Because the size of the PS arms of the A_1B_1 sample is small (N_{PS} = 97, as seen in Table 4.1), it is believed that n-hexane is able to partially solubilize the PS blocks. This phenomenon is responsible for the predominance of single A_1B_1 chains in solution, even at c = 2 mg/mL.

Similarly for sample A_2B_2, two distributions of hydrodynamic sizes are observed at concentrations of 1.5 and 2 mg/mL; however, in this case the two peaks are convoluted, i.e, partially overlapping one another. It is also noted that the breadth of the peaks increases as concentration increases from 0.25 to 1 mg/mL, which is a pattern opposite of what is seen for the A_1B_1 copolymer. Concentrations of 0.75 and 1 mg/mL could be at the brink of the onset of micellization and the observance of the broadening of the peak may indicate the formation of aggregates. Therefore, it is necessary to consider two scenarios for the structure of this $(PS)_2(PI)_2$ heteroarm star in n-hexane: Two peaks may signal i) a very polydisperse sample with only one species in solution, or ii) two separate species in which the smaller R_h peak corresponds to single A_2B_2 stars in solution and the larger R_h peak corresponds to a few aggregated stars. In order to sort out the origin and implications of these convoluted R_h distributions for the A_2B_2 stars in n-hexane, results for Γ at c = 0.25 and 2 mg/mL are compared in Figure 4.5. The fits of the Γ versus q^2 plots yield D_s values of 6.93×10^{-7} and 6.36×10^{-7} cm^2/s for the one mode seen at c = 0.25 mg/mL and for the "fast" diffusing mode observed at c = 2 mg/mL, respectively. On the other hand, the slow diffusing mode for the A_2B_2 star at c = 2 mg/mL yields D_s = 2.72

$\times 10^{-7}$ cm^2/s giving an R_h = 27.4 nm. Also shown in Figure 4.5 is a single exponential fit of the autocorrelation function measured at c = 2 mg/mL. This single exponential fit describes the average diffusive behavior of all of the polymers in solution. This fit is closer to the mean decay rate assigned to the slow diffusing mode because this mode dominates the normalized amplitude modes shown in Figure 4.3 for this heteroarm star. However, based on the quality of the fits, the agreement between D_s obtained from the fast mode at c = 2 mg/mL and that obtained for the single mode observed at c = 0.25 mg/mL, it is believed that the A_2B_2 heteroarm stars coexist as single chains and small aggregates at the concentrations of 1.5 and 2.0 mg/mL. Below 1.5 mg/mL, the A_2B_2 heteroarm stars remain in a non-aggregated state. At this moment the exact conformation of the A_2B_2 aggregates is uncertain, but I speculate that there may be either in a "classical" micellar conformation or in an aggregated state without well defined PS or PI domains. In the classical micellar state, the PS blocks are trapped in the core and the PI blocks form a corona. In this case a well defined core/corona interface is likely. However because the PS blocks are small in comparison to the length of the PI blocks, the latter can form a protective shell around the small PS blocks, thereby preventing the formation of proper micellar aggregates. Additionally due to the high entropic cost of bringing the PS block together in order to overcome the shielding of the PI blocks, the A_2B_2 stars may just adopt an aggregated conformation where the PS and PI blocks are mixed together resembling a heteroarm star having higher degree of branching. The same two scenarios were proposed by Procházka and coworkers[18] for the micelization of $(PVP)_6(PS)_6$ heteroarm stars in toluene.

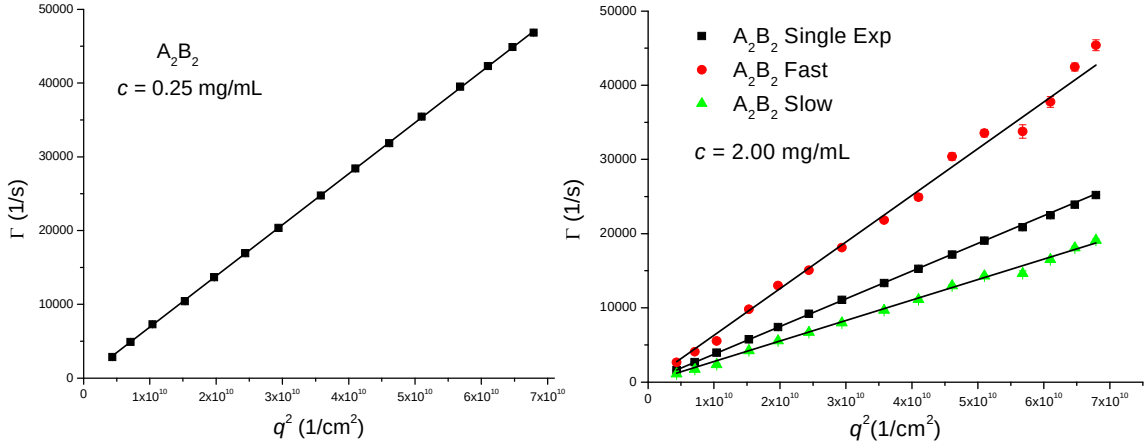

Figure 4.5. Γ versus q^2 plots for sample A_2B_2 at the lowest (left) and highest (right) concentrations studied. For c = 2 mg/mL fits of both single and double exponential decays are shown.

The hydrodynamic radii distributions (Figure 4.3) for heteroarm stars A_4B_4 and A_8B_8 show narrow peaks at all the concentrations studied and due to the R_h values obtained there is no evidence of any type of aggregation. Figure 4.6 shows the results of fitting of the autocorrelation function with a single exponential decay (Equation 2.4) at c = 2 mg/mL for A_4B_4 and A_8B_8 samples. The fact that no aggregates were found in these samples may be due to the crowded structure of the stars and relative size of the blocks: larger PI blocks may create a shell around the insoluble PS blocks, preventing self-assembly. The possibility of micelization at c > 2 mg/mL is likely, based on other results for similar A_nB_n heteroarm star copolymers.[2,11,19]

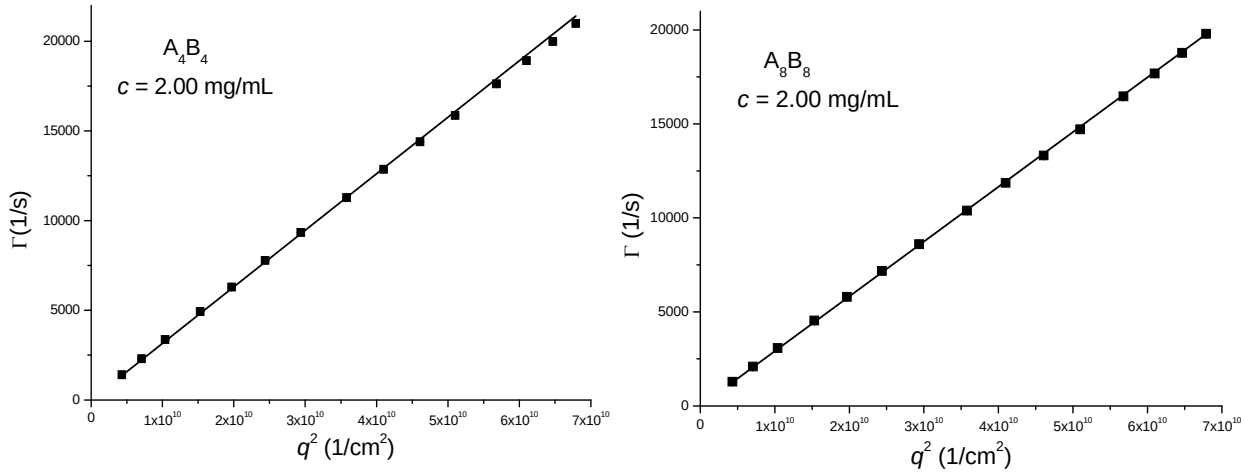

Figure 4.6. Γ versus q^2 plots for samples A_4B_4 (left) and A_8B_8 (right) at c = 2 mg/mL. Only a single decay mode is seen at these and lower concentrations.

Figure 4.7 shows the concentration dependence of D_s for the fast diffusing modes of samples A_1B_1 and A_2B_2 as well as for A_4B_4 and A_8B_8 stars for each of the six concentrations studied. The behavior of D_s with respect to concentration can be analyzed using the following expansion:[1]

$$D_s = D_0(1 + k_D c + ...) \tag{4.1}$$

where D_0 is the diffusion coefficient at infinite dilution and k_D is a concentration coefficient that provides information about the balance between thermodynamic and frictional interactions between the polymers and the solvent. Yamakawa defined k_D as:[32]

$$k_D = 2A_2M_w - k_f - \tilde{\upsilon} \tag{4.2}$$

Here A_2 is the second virial coefficient from static light scattering measurements, $\tilde{\upsilon}$ the specific partial molar volume of the polymer and k_f is a frictional coefficient that arises due to hydrodynamic interactions:[32]

$$F = f_0(1 + k_f c) \tag{4.3}$$

with F being the friction coefficient at a given concentration and $D_0 = kT/f_0$. In good solvent conditions, $2A_2M_w > k_f + \tilde{\upsilon}$, implying that the thermodynamic interactions are stronger than the hydrodynamic (frictional) ones. As solvent quality becomes poorer, A_2 decreases and k_D eventually becomes negative. Also for high enough M_w, $\tilde{\upsilon}$ can be neglected.[33] Experimental values of D_0 and k_D extracted from the slope of the D_s versus c data shown in Figure 4.7 are presented in Table 4.2. The k_D value obtained for sample A_1B_1 is slightly positive, which is an indication of good solvent conditions and swollen chains, and it is similar to the result found by Pispas and coworkers for PS-PI diblocks in n-decane[34] but rather small in comparison to the k_D values found by Tsunashima et al.[35] for PI in cyclohexane at 25°C. For the other heteroarm stars, $k_D \sim 0$ (within the error bounds). This result implies larger frictional interactions between the A_2B_2, A_4B_4 and A_8B_8 heteroarm star copolymers at constant solvent conditions. Similar results have been observed for PI[7] and PS[36] hompolymer stars in good solvent. For the systems studied here it may be necessary to cover a broader concentration range to properly determine the balance between thermodynamic and hydrodynamic (frictional) interactions, staring from the very dilute regime and going into the semidilute regime.

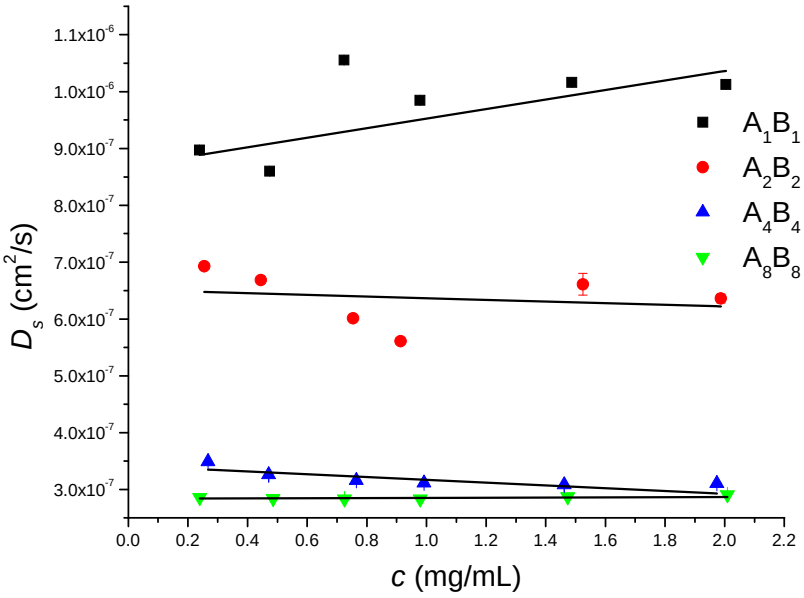

Figure 4.7. Dependence of D_s on solution concentration, c. Solid lines are fits obtained using Equation 4.1. Only data for the fast diffusion mode of stars A_1B_1 and A_2B_2 are used.

Table 4.2. Hydrodynamic properties of $(PS)_n(PI)_n$ (A_nB_n) heteroarm star copolymers in n-hexane at c = 2 mg/mL, and concentration dependant parameters D_0 and k_D.

Sample ID	D_s (cm^2/s)	R_h (nm)	D_0 (cm^2/s)	k_D
A_1B_1 fast	1.01×10^{-6}	7.4	8.67×10^{-7}	0.11
A_1B_1 slow	1.95×10^{-7}	38.3		
A_2B_2 fast	6.36×10^{-7}	11.7	6.51×10^{-7}	- 0.02
A_2B_2 slow	2.72×10^{-7}	27.4		
A_4B_4	3.10×10^{-7}	24.0	3.41×10^{-7}	-0.07
A_8B_8	2.90×10^{-7}	25.7	2.83×10^{-7}	0.01

Previous results from star hompolymers have shown that at the same $M_{w,tot}$ the size of a star is much smaller than the size of its linear analog polymer;[37] thus, in order for the stars to be of constant size, the $M_{w,tot}$ needs to be increased as branching increases. Now that there is a good idea of the structure of the stars in n-hexane and how concentration affects the organization, the effects on hydrodynamic properties of systematically increasing $M_{w,tot}$ by doubling the number of arms are discussed in the following section.

Effects of Branching. Figure 4.8 show the R_h distributions for the heteroarm star copolymers studied at c = 2 mg/mL. At this c, heteroarm stars A_1B_1 and A_2B_2 show the presence of aggregates and coexistence with single chains. On the other hand, samples A_4B_4 and A_8B_8 each show a single size distribution. These size distributions are very similar to one another and suggest that these copolymers do not form aggregates. The R_h values obtained at 2 mg/mL are shown in Table 4.2. While a complete list of D_s and R_h values at all of the concentrations studied are shown in Appendix F, the results show that the hydrodynamic size does not change considerably when the number of PI arms is increased from 4 to 8. However, as previously discussed, the PS blocks have some solubility in n-hexane; thus, they may contribute to the hydrodynamic size of the stars. In light of this, A_4B_4 and A_8B_8 could be conceptualized as 8 and 16 arms stars, respectively, and it has been shown that size does not significantly change when $f \geq 8$.[1] Additionally, the free space needed for the motions of the chains is strongly limited near the core; consequently, both the PS and PI arms would have the tendency to stretch out in order to alleviate crowding.[38]

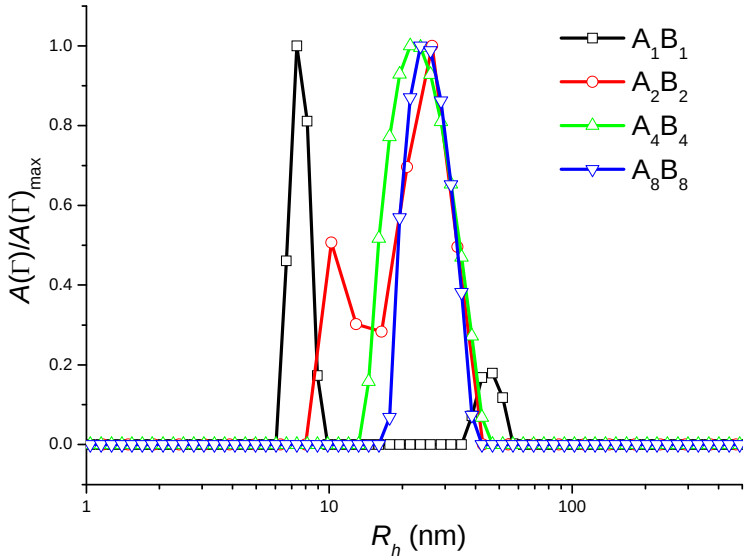

Figure 4.8. Hydrodynamic size, R_h, distributions for A_nB_n heteroarm stars studied at c =2 mg/mL and θ = 78°. The x-axis scale is the same as that used in Figure 4.3.

Further insight into the hydrodynamics of the system can be obtained by calculating the reduced decay rate, Γ*, from the experimentally measured decay rate, Γ:[39]

$$\Gamma^*(q) \equiv \left(\frac{\Gamma}{q^3}\right)\left(\frac{\eta_o}{kT}\right) = \frac{1}{6\pi q \xi_h(q)} \tag{4.4}$$

where ξ_h is the hydrodynamic correlation length, which is defined as:[39]

$$\xi_h^{-1} = \lim_{q\to 0} 6\pi\eta_o \Gamma / kTq^2 \tag{4.5}$$

ξ_h can also be related to D_s by $D_s = kT/6\pi\ \eta_o\xi_h$. It should be noted that the hydrodynamic correlation length, ξ_h, is not directly proportional to the static correlation length, ξ, obtained from the picture of a polymer chain divided into a string of independent blobs.[40] Also Γ* is a dimensionless quantity that does not depend on parameters specific to the polymer. As observed in Figure 4.9, as branching (number of arms about the central core) increases, the values of Γ* at a given q decrease, suggesting a slowing down of the

segmental motions and a loss of flexibility of the stars. This is an expected result due to the constraint imposed by attaching more arms to the core. The entropic cost associated with attaching more chains about a common junction point (similar to the tethering of polymer chains to a solid substrate to form polymer brushes) will reduce the flexibility of the stars as a whole ensemble. The loss of flexibility as crowding increases from A_4B_4 to A_8B_8 is much smaller than the loss observed when the number of arms is doubled from A_2B_2 to A_4B_4. This behavior again shows that after a certain degree of branching, the hydrodynamic behavior of the stars does not change significantly. Because the mass fraction of PS is kept (nearly) constant in all the samples, the reduction in Γ* arises from increases in the degree of branching of the A_nB_n heteroarm star copolymers.

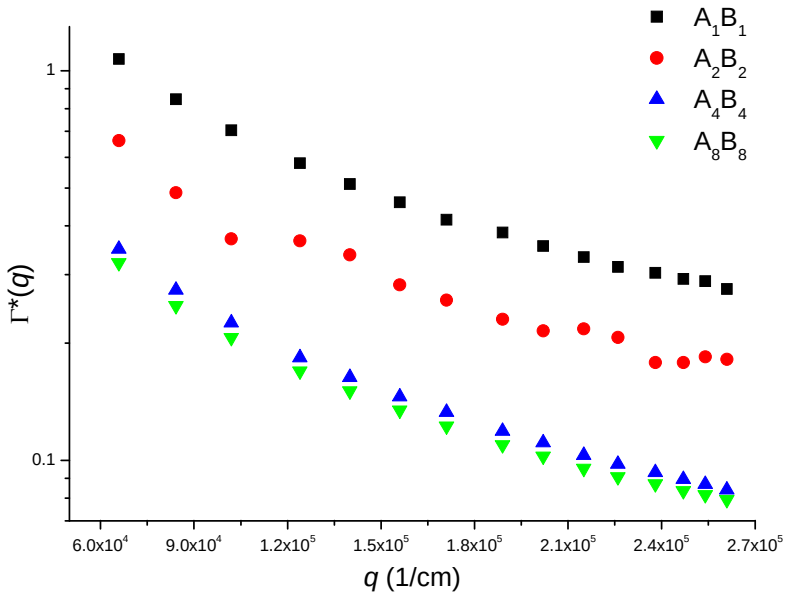

Figure 4.9. Reduced decay rate, Γ*, for the A_nB_n heteroarm stars at 2 mg/mL. For the stars A_1B_1 and A_2B_2 results are based on the fast modes observed in DLS. In doing so, these results compare the behavior of individual $(PS)_n(PI)_n$ stars in n-hexane.

The reduced decay rate, Γ*, can be scaled by the hydrodynamic correlation length ($\xi_h \approx R_h$) by plotting Γ* versus qR_h. Figure 4.10 shows the plot of Γ* versus qR_h for all of the

heteroarm stars, and it is seen that the data collapse onto a common curve. This shows how the effects of molecular weight and branching are embedded in the diffusion properties of the systems and that Γ* for the stars is only a function of qR_h. Similar patterns of behavior have been obtained for PS linear homopolymers in toluene[39] and degraded starch samples in 0.5 M NaOH solutions.[41] As argued by Galinsky and Burchard,[41] the fact that Γ* does not reach an asymptotic behavior may come from two factors. It could be that the qR_h range covered is not large enough, especially for light scattering measurements, or it is possible that because of the high branch density, loss of internal flexibility and the incompatibility between the blocks makes Γ* decrease continuously.

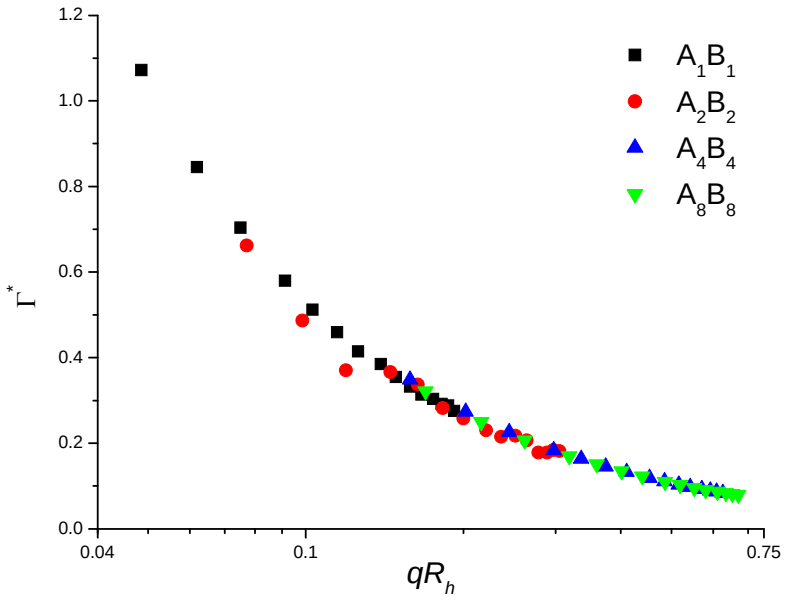

Figure 4.10. Reduced decay rate, Γ*, versus qR_h for the A_nB_n heteroarm stars studied at 2 mg/mL. Only data for the fast diffusion mode observed for stars A_1B_1 and A_2B_2 are shown.

Lastly, it is interesting to compare the experimental R_h results with predictions based on linear PI homopolymers in similar good solvent conditions. To make the comparisons

I consider the PI blocks only, viewing the star as being made of n PI arms of molecular weight $M_{w,PI\ arm}$ (see Table 4.1). For the various A_nB_n heteroarm star copolymers studied, n = 1, 2, 4 and 8. Measurements of R_h of linear PI chains in cyclohexane were performed by Tsunashima et al., and they found:[35]

$$R_h(\text{cm}) = 9.03\times10^{-10} M_w^{0.61} \tag{4.6}$$

The M_w exponent, v = 0.61 indicates that cyclohexane is a better solvent for PI than n-hexane, which has a v = 0.57 (see Appendix C, Equation C.1). To calculate values for linear PI chains in n-hexane, it is possible to combine the prediction of R_g for PI in n-hexane, R_g = (1.68Å)$N_{PI}^{0.57}$ with the expected relationship between R_g and R_h for monodisperse linear chains in a good solvent: R_g/R_h = 1.78.[1] It is worth noting that Tsunashima et al. found a R_g/R_h ratio of 1.5 for all of the PI linear homopolymers they studied in cyclohexane.[35] Here I do not attempt to resolve this conflict, but rather use the former relationship.

Comparisons of the experimentally measured R_h values and the predictions for linear PI chains in both cyclohexane and n-hexane are shown in Figure 4.11. The R_h values measured for the stars are very similar to the ones predicted for linear PI chains in cyclohexane, with the exception of sample A_4B_4. A plausible explanation for the discrepancy observed for A_4B_4 is that the crowding within the star makes the PI chains adopt a stretched conformation (resembling a spherical polymer brush) in comparison to their conformation in free solution (in n-hexane); however, if internal stretching were the only effect on the hydrodynamics of the stars, the result for A_1B_1 should more closely

match to the predictions for a linear chain in n-hexane. Therefore, I also believe that there is a contribution to R_h from the slightly soluble PS blocks, as previously indicated.

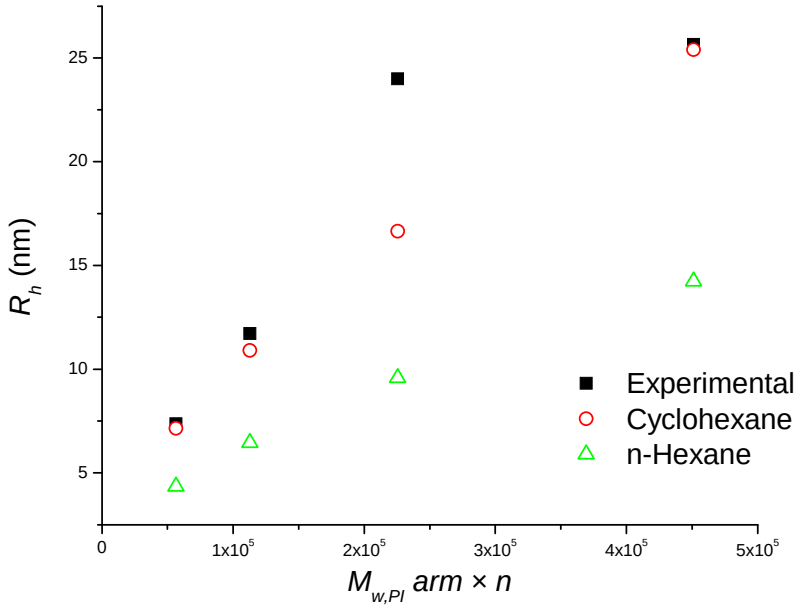

Figure 4.11. Comparisons of experimentally obtained R_h with predictions for PI linear chains in cyclohexane and n-hexane.

4.4 Conclusions

The effects of concentration and increase in branching on the hydrodynamic properties of $(PS)_n(PI)_n$ (A_nB_n) heteroarm star copolymers are studied in n-hexane, a solvent selective for PI. These asymmetric stars have larger PI arms; thus, their hydrodynamic properties are largely controlled by these blocks. However, over the concentration range studied, samples $(PS)_1(PI)_1$ (A_1B_1) and $(PS)_2(PI)_2$ (A_2B_2) show evidence of coexistence of single stars with aggregates in solution, with this aggregation driven by the desire of the PS insoluble blocks to avoid contact with the solvent. For star A_1B_1 the aggregates are likely to be 'classical' spherical micelles having cores composed

of the insoluble PS blocks and the corona formed by the soluble PI blocks. For star A_2B_2, the conformation of the aggregates is uncertain because the branched configuration may impose a barrier for the PS blocks to come together and create a well-formed micelle. On the other hand, A_4B_4 and A_8B_8 stars remain as single stars (over the concentration range studied), a behavior enabled if the much larger PI arms shield the smaller and possibly collapsed PS blocks. This behavior may restrict the self-assembly of these heteroarm stars, though micelles may be formed at higher concentrations. Interestingly, the contribution from micelles observed for sample A_1B_1 at the highest concentration studied is rather small and the chains predominantly exist as single diblocks in the n-hexane solution. This result can be explained in light of the fact that low molecular weight PS is slightly soluble in n-hexane. This solubility of PS also contributes to the larger hydrodynamic sizes observed for the stars in comparison to predictions for linear PI chains in n-hexane.

By studying the reduced decay rate it is possible to see that as branching increases, the heteroarm star copolymers lose flexibility – they behave like "soft colloids". This phenomenon is related to the constraints imposed by attaching several arms about the small molecule core. It is enhanced by the incompatibility between PS and PI arms and also because PS has a high glass transition temperature. It is also shown that the reduced decay rate is an universal function of the product of the scattering wave-vector and the hydrodynamic correlation length. The data from the four stars collapse to a single curve, indicating similar hydrodynamic interactions with the solvent.

In addition to revealing new insights into the structure and dynamics of architecturally complex heteroarm copolymers, the results shown here will ultimately be beneficial to the design of drug delivery carriers based on branched copolymers, as well to the homogenization of polymer blends of incompatible homopolymers.

4.5 References

1. Burchard, W. *Adv. Polym. Sci.* **1999**, *143*, 113.

2. Pitsikalis, M.; Pispas, S.; Mays, J.; Hadjichristidis, N. *Adv. Polym. Sci.* **1998**, *135*, 1.

3. Hadjichristidis, N.; Pisikalis, M.; Pispas, S.; Iatrou, H. *Chem. Rev.* **2001**, *101*, 3747.

4. Chang, K.; Macosko, C.W.; Morse, D.C.; *Macromolecules* **2007**, *40*, 3819.

5. Pavlopoulou, E.; Anastasiadis, S.H.; Iatrou, H.; Moshakou, M.; Hadjichristidis, N.; Portale, G.; Bras, W. *Macromolecules* **2009**, *42*, 5285.

6. Burchard, W. *Adv. Polym. Sci.* **1983**, *48*, 1.

7. Adam. M.; Fetters, L.J.; Graessley, W.; Witten, T. *Macromolecules* **1991**, *24*, 2434.

8. Dozier, W.; Huang, J.; Fetters, L.J. *Macromolecules* **1991**, *24*, 2810.

9. Willner, L.; Jucknischke, O.; Richter, D.; Roovers, J.; Zhou, L.; Toporowski, P.; Fetters, L.J.; Huang, J.; Lin, M.; Hadjichristidis, N. *Macromolecules* **1994**, *27*, 3821.

10. Willner, L.; Jucknischke, O.; Richter, D.; Farago, B.; Fetters, L.J.; Huang, J.S. *Europhys. Lett.* **1992**, *19*, 297.

11. Roovers, J.; Toporowski, P.; Douglas, J. *Macromolecules* **1995**, *28*, 7064.

12. Bauer, B.; Fetters, L.; Graessley, W.; Hadjichristidis, M.; Quack, G. *Macromolecules* **1989**, *22*, 2337.

13. Mayer, C.; Zaccarelli, E.; Stiakakis, E.; Likos, C.N.; Sciortino, F.; Munam, A.; Gauthier, M.; Hadjichristidis, N.; Iatrou, H.; Tartaglia, P.; Löwen, H.; Vlassopoulos, D.; *Nat. Mater.* **2008**, *7*, 780.

14. Daoud, M.; Cotton, J-P. *J. Physique (France)* **1982**, *43*, 531.

15. Higo, Y.; Ueno, N.; Noda, I. *Polymer* **1983**, *15*, 367.

16. Glazer, J. *J. Polym. Sci.* **1954**, *14*, 225.

17. Tsitsilanis, C.; Voulgaris, D.; Štěpánek, M.; Podhájecká, K.; Procházka, K.; Tuzar, Z.; Brown, W. *Langmuir* **2000**, *16*, 6868.

18. Štěpánek, M.; Matějíček, P.; Humpolíčková, J.; Havránková, J.; Podhájecká, K.; Špírková, M.; Tuzar, Z.; Tsitsilanis, C.; Procházka, K. *Polymer* **2005**, *46*, 10493.

19. Voulgaris, D.; Tsitsilanis, C.; Esselink, F.J.; Hadziioannou, G. *Polymer* **1998**, *39*, 6429.

20. Avegeropoulos, A.; Poulos, Y.; Hadjichristidis, N.; Roovers, J. *Macromolecules* **1996**, *29*, 6076.

21. Pispas, S.; Avgeropoulos, A.; Hadjichristidis, N.; Roovers, J. *J. Polym. Sci., Part B : Polym. Phys.* **1999**, *37*, 1329.

22.Beyer, F.; Gido, S.; Poulos, Y.; Avgeropoulos, A.; Hadjichristidis, N. *Macromolecules* **1997**, *30*, 2373.

23. Beyer, F.; Gido, S.; Uhrig, D.; Mays, J.; Tan, N.; Trevino, S. *J. Polym. Sci. Part B: Polym. Phy.* **1999**, *37*, 3392.

24. Milner, S. *Macromolecules* **1994**, *27*, 2333.

25. Morton, M.; Fetters, L. *J. Rubber Chem. Technol.*, **1975**, *48*, 359.

26. Hadjichristidis, N.; Iatrou, H.; Pispas, S.; Pitsikalis, M. *J. Polym. Sci. Part A: Polym. Chem.*, **2000**, *38*, 3211.

27. Uhrig, D.; Mays, J.W. *J. Polym. Sci. Part A: Polym. Chem.* **2005**, *43*, 6179.

28. Lairez, D.; Adam, M.; Carton, J.-P. Raspaud, E. *Macromolecules* **1997**, *30*, 6798.

29. Lund, R.; Willner, L.; Lindner, P.; Richter, D. *Macromolecules 2009*, *42*, 2686.

30. Qin, X.; Chang, W. *J. Adhes. Sci. Techol.* **1995**, *9*, 823.

31. Nicolais, L.; Drioli, E.; Hopfenberg, H.B.; Apicella, A. *Polymer* **1979**, *20*, 459.

32. Yamakawa, H. *Modern Theory of Polymer Solutions*; Harper and Row: New York, 1971.

33. Selser, J. C. *Macromolecules* **1981**, *14*, 346.

34. Pispas, S.; Hadjichristidis, N.; Potemkin, I.; Khokhlov, A. *Macromolecules* **2000**, *33*, 1741.

35. Tsunashima, Y.; Hirata, M.; Nemoto, N.; Kurata, M. *Macromolecules* **1987**, *20*, 1992.

36. Huber, H.; Burchard, W.; Fetters, L.J. *Macromolecules* **1984**, *17*, 541.

37. Roovers, J.; Zhou, L.; Toporowski, P.; van der Zwan, M.; Iatrou, H.; Hadjichristidis, N. *Macromolecules* **1993**, *26*, 4324.

38. Huber, K. Burchard, W.; Bantle, S.; Fetters, L. *Polymer* **1987**, *28*, 1997.

39. Wiltzius, P.; Cannell, D. *Phys. Rev. Lett.* **1986**, *56*, 61.

40. de Gennes, P-G. *Scaling Concepts in Polymer Physics*; Cornell: Ithaca, 1979.

41. Galinski, G.; Burchard, W. *Macromolecules* **1997**, *30*, 6966.

CHAPTER 5

CONCLUSIONS AND RECOMMENDATIONS

5.1 Conclusions

The solution properties, self-assembly and preferential adsorption at the solid/fluid interface of architecturally complex block copolymers have been studied. Copolymers with polystyrene (PS) and polyisoprene (PI) constituents were used because their monomers are among the best behaved for anionic polymerization techniques, yielding well-defined polymers that enable studies of fundamental relationships between chain connectivity, composition and molecular weight. Two different types of branched copolymers were used in my thesis work, including miktoarm block copolymers with a PS-PI-$(PI)_2$ configuration (as shown in Figure 2.1) and symmetric heteroarm star copolymers with an equal number of PS and PI arms emanating from a common junction point (as seen in Figure 4.2). Static and dynamic light scattering, *in-situ* phase modulated ellipsometry and atomic force microscopy techniques were used in these studies.

Static and dynamic light scattering measurements and analysis show that the PS-PI-$(PI)_2$ miktoarm copolymers self-assemble into spherical micelles when dissolved in n-hexane, a solvent selective for PI. The organization of the ensembles is such that the insoluble PS blocks form the core and the soluble PI chains form the micellar corona (see Figure 2.1). Comparisons of the micelles formed from the branched miktoarms with micelles formed from a linear diblock of similar molecular weight and composition show that micelles formed from the diblock have larger sizes, a property attributed to the

branching of the PI blocks of the miktoarms, leading to more compact structures. The aggregation number, i.e. the number of single chains self-assembled into the micelle, for the self-assembled miktoarms is found to be highly dependant of the length of the insoluble PS block, as theoretically predicted (see Table 1.1). However, the organization of the branched PI chains in the corona plays an important role in the equilibrium properties of the ensembles. It is speculated that denser packing at the core/corona interface may promote additional stretching of the PI "stem" that increases the overall size of the micelle. On the other hand, micelles with lower aggregation numbers may arrange their stem and arms (see Figure 2.1) such that one of the arms may configure itself such that it points towards the core/corona interface. These micellar systems are likely to follow the closed association model (see Section 1.1), as revealed by the bimodal size distribution obtained for one of the samples. Unfortunately, the critical micelle concentration for these copolymers in n-hexane could not be experimentally determined by light scattering.

Comparisons of the hydrodynamic sizes and aggregation numbers of the PS-PI-$(PI)_2$ miktoarms obtained experimentally with predictions for spherical micelles formed from linear block copolymers show noteworthy discrepancies. The predicted hydrodynamic radii are smaller than those measured, although the predicted aggregation numbers are rather similar to the experimental results. These differences may be explained by the internal arrangement of the branched PI blocks in the micellar corona and/or by the use of numerical prefactors experimentally determined for linear self-assembled block

copolymers. In the predictions, variations in solvent quality have a stronger effect on the equilibrium properties than the polymer volume fraction inside the core.

The preferential adsorption of the micellized PS-PI-$(PI)_2$ miktoarm block copolymers from n-hexane solutions onto silicon substrates show the classical two step profile: i) There is an initial fast increase in the adsorbed amount, a process that is dominated by mass transport of material towards the solid/fluid interface, followed by ii) a transition towards pseudo-equilibrium, where further adsorption is continually diminished by the presence of an already adsorbed layer. The transition from one regime to the other was found to occur at earlier times for the micelles formed from the branched copolymers in comparison to the ones formed from the linear analog PS-PI diblock. Solution concentration plays an important role in the kinetics of adsorption: as the concentration is reduced, the adsorbed amount decreases and the time to reach pseudo-equilibrium becomes longer.

A complete description of the kinetics of adsorption profiles was achieved by incorporating both mass transport and relaxation/reorganization events occurring at the solid/fluid interface into a model for preferential adsorption. Surface events are important to consider because adsorption is driven by the desire of the PS blocks trapped in the micellar core to avoid contact with the solvent. Therefore, events such as micelle break-up, adsorption through the PI corona chains and reorganization after adsorption, and release of single chains from the micellar ensemble are responsible for the layer formation. The result of the analysis also shows that these macromolecular ensembles follow an adsorption behavior similar to that displayed by biomimetic vesicles.

The hydrodynamic properties of a series of symmetric $(PS)_n$-$(PI)_n$ hetero-arm star copolymers solvated in n-hexane were studied by dynamic light scattering. The results show that there is a loss of flexibility in the stars as the number of arms increase. (Hetero-arm stars with n = 1, 2, 4 and 8 were studied.) This behavior arises from the crowding of chains around a common junction point, which considerably limits free movement of each arm. For hetero-arm stars with lower degrees of branching (A_1B_1 and A_2B_2), coexistence between single stars and aggregates of stars is observed at high concentrations (≈ 2 mg/mL). On the other hand, samples with larger degrees of branching (A_4B_4 and A_8B_8) did not show evidence of aggregation (micellization) over the concentration range studied. This phenomenon is explained by shielding of PS blocks by the larger PI chains, which prevents these stars from self-assembling.

In summary, through this body of results, my research has shown specifically that copolymer architecture can have an impact on the solution behavior, self-assembly and preferential adsorption of block copolymers at the solid/fluid interface. Additionally, effects such as molecular weight and solution concentration play a key role in governing the interactions of the copolymers both in solution and adsorbed onto solid substrates. Therefore, by controlling these parameters, tailor-made structures can be achieved and responses to external stimuli can be predicted, setting the base for future developments of functional nanomaterials based on branched macromolecules.

5.2 Recommendations

Detailed insight into the effects of macromolecular architecture on the behavior of block copolymer systems have been gained through this work; however, there are many possible further studies that may help to advance the understanding the self-assembly of complex macromolecular nanomaterials. The following research is recommended:

I. A more detailed picture of the structure of the micelles formed from PS-PI-$(PI)_2$ miktoarms and the $(PS)_n(PI)_n$ heteroarm star copolymers could be achieved if one of the blocks was isotopically labeled. By doing this, the conformation and location of each block, both in single stars and micellized assemblies, can be better determined using, for example, small-angle neutron scattering techniques.[1] In the case of the PS-PI-$(PI)_2$ micelles, the volume fraction of PS inside the core and the organization of the branched PI blocks in the corona could be resolved. In the case of the $(PS)_n(PI)_n$ heteroarm star copolymers, the extent of solvation of the PS blocks and the organization of the aggregates formed from sample A_2B_2 may be obtained. Both of these areas would help clarify certain issues remaining from my studies.

II. Previously it has been discussed that the manner in which the copolymer solutions are prepared may affect the self-assembly and equilibrium properties of the system.[2,3] Therefore, it would be interesting to make a comparison between block copolymers solutions prepared gravimetrically and solutions made by dissolution into a non-selective solvent and then subsequent dialysis against a solvent selective for one of the blocks.

III. Comparisons of the experimental results for the micelles formed from the PS-PI-$(PI)_2$ miktoarm copolymers with predictions for micellar systems of linear block copolymers were rather unsatisfactory. The predicted hydrodynamic sizes were rather different from those determined in my experiments, though the aggregation numbers were somewhat close. Consequently, it would be useful to develop a new model that includes the effect of branching on the thermodynamic stability and structure of micelles formed from branched block copolymers, similar to what Milner showed for A_2B block copolymers in the melt state.[4]

IV. Theoretical predictions for branched systems may need to be experimentally validated using different sets of architecturally complex block copolymers that vary in systematic ways. For example, in the case of the PS-PI-$(PI)_2$ miktoarms, the length of the PS block and the PI stem could be kept constant while varying the length of the $(PI)_2$ blocks. In the case of the A_nB_n stars, the number of arms can be systematically increased while keeping the molecular weight of the whole star constant. Intuitively, there are many possibilities and variations for block copolymers having complex, non-linear architectures. In principle, the necessary copolymers can be synthesized by anionic polymerization techniques, but they may be tedious and expensive to prepare.[5] Additionally, due to the marked differences in behavior observed with different branched arrangements, a general theoretical framework for branched materials may not be achievable.

V. In Chapter 3, I showed that the kinetics of preferential adsorption and relaxation/reorganization events at the solid/fluid interface are dependant on the

polymer solution concentration. Consequently, studies over a broader concentration range are recommended.

VI. The adsorbed PS-PI-$(PI)_2$ miktoarm block copolymers are believed to be in the form of surface hemi-micelles and some preferentially adsorbed single chains (see Chapter 3). A better picture of the actual structure of the solvated interfacial layer may be achieved by techniques such as atomic force microscopy and neutron reflectivity. The former would yield topological information about the layer, but problems such as chains sticking to the silicon nitride tip and solvent evaporation are likely to arise.[6] (And these problems arose in my attempts.) Neutron reflectivity is useful for determining the density profile of the adsorbed layer with nanoscale resolution in the direction normal to the surface; however, the "patchy" nature of the layer formed by surface hemi-micelles (see Figure E.1 in Appendix E) may make modeling of the reflectivity profile very difficult because of in-plane inhomogeneties.[7]

VII. As revealed by Awan et al.,[8] the preferential adsorption of PS-PEO block copolymers onto silicon substrates was enhanced by covering the substrates with a PS film prior to the adsorption process. Therefore, adsorption experiments using polymer-modified substrates, instead of bare silicon, could improve the amount of material adsorbed and reveal new insights in the kinetics of adsorption processes as well as the impact of surface energy on surface reorganizations and near-surface diffusivity, as described in Chapter 3.

5.3 References

1. Hammouda, B. *The SANS Toolbox;* National Institute for Standards and Technology: Gaithersburg, MD, 2004.

2. Gohy, J-F. *Adv. Polym. Sci.* **2005**, *190*, 65.

3. Riess, G. *Prog. Polym. Sci.* **2003**, *28*, 1107.

4. Milner, S. *Macromolecules* **1994**, *27*, 2333.

5. Hadjichristidis, N.; Pitsikalis, M.; Pispas, S.; Iatrou, H. *Chem. Rev.* **2001**, *101*, 3747.

6. Hamley, I.W.; Connell, S.; Collins, S. *Macromolecules* **2004**, *37*, 5337.

7. Higgins, J.; Benoît, H. *Polymers and Neutron Scattering* Oxford University Press: Oxford, 1994.

8. Awan, M.; Dimonie, V.; Ou-Yang, D.; El-Aasset, M. *Langmuir* **1997**, *13,* 130.

APPENDICES

APPENDIX A

INTERFACIAL TENSION AND SPREADING COEFFICIENT FOR POLYSTYRENE-POLYISOPRENE POLYMERS IN N-HEXANE

The interfacial tension, γ, is defined as the excess energy per unit area due to the formation of an interface or the reversible work required to generate a unit area surface. In the work of van Krevelen,[1] there are several equations for predicting the interfacial tension between two substances (liquid, solid or a combination), γ_{12}, and it can be written as:[1]

$$\gamma_{12} = \left[(\gamma_1^d)^{1/2} - (\gamma_2^d)^{1/2}\right]^2 + \left[(\gamma_1^h)^{1/2} - (\gamma_2^h)^{1/2}\right]^2 \quad \text{(A.1)}$$

Here γ_i^d corresponds to the interfacial tension due to dispersive forces and γ_i^h corresponds to the one due to hydrogen bonding. The values for γ_i^d and γ_i^h for PS, PI, n-hexane and silicon are shown in Table A.1.

Table A.1. Interfacial tension parameters for PS, PI, n-hexane and silicon

	γ_i^d (mJ/m^2)	γ_i^h (mJ/m^2)	Reference
Polystyrene (PS)	41.4	0.6	[1]
Polyisoprene (PI)	32.0		[2]
n-hexane	18.4		[1]
Silicon	76.0		[3]

Using Eq. A.1, it is possible to determine the interfacial tension of the different pairs used in this study of PS-PI architecturally complex block copolymers both dissolved and when adsorbed onto silicon substrates from n-hexane. The calculation results using Eq. A.1 are shown in Table A.2. From Table A.2 is seen that the energy cost to generate a PI-n-hexane interface is smaller than to generate a PS-n-hexane one. This implies that the interactions between PI and the solvent are favored, and the micelization of the the PS

blocks tend to minimize contacts with the solvent. However the value for $\gamma_{PS\text{-}n\text{-}hex}$ is non-negative which may indicate certain solubility of PS in n-hexane.

Table A.2. Interfacial tension, γ_{12}, values for pairings considered in this study

Pair	γ_{12} (mJ/m^2)
Silicon – n-hexane	19.6
Silicon – PS	5.8
Silicon – PI	9.4
PS – n-hexane	5.2
PI – n-hexane	1.9

For the preferential adsorption of block copolymers onto solid substrates from solution, the spreading coefficient, *S*, provides an idea of the affinity block for a given substrate. *S* is defined as:[4]

$$S = \gamma_{WL} - \gamma_{PL} - \gamma_{WP} \tag{A2}$$

Here *W* refers to the wall (silicon), *P* to the polymer (PS or PI) and *L* to the solvent (n-hexane in this case). A positive value of *S* indicates that the polymer has affinity for the substrate whereas a negative value of *S* suggests that the interaction of the substrate with the solvent would be more favorable compared to a substrate-polymer interaction.

Using the values in Table A.2 it is possible to calculate *S* for the W-PS-L and W-PI-L systems, yielding values of S_{WPSL} = 8.6 mJ/m^2 and S_{WPIL} = 5.6 mJ/m^2. The positive values of *S* indicate that the adsorption of both PS and PI are thermodynamically favorable; however, the larger value of S_{WPSL} suggests a more energetically favorable situation for the adsorption of the PS blocks. On the other hand, there is some adsorption of PI as seen by the adsorption profile for PI homopolymer shown in Fig. 3.4 Consequently, the interaction of the micellar ensembles of PS-PI-(PI)$_2$ miktoarm block copolymers with the silicon substrate is likely to initially include the micellar corona chains followed by a

rearrangement in order to expose the PS insoluble blocks; thus, this type of relaxation/reorganization needs to be taken into account in the analysis of adsorption kinetics discussed in Chapter 3.

References

1. van Krevelen, D.W. *Properties of Polymers: Their Estimation and Correlation with Chemical Structure.* Elsevier: Amsterdam, 1976.

2. Kikuchi, H.; Kuwajima, S.; Fukuda, M. *J. Chem. Phys.* **2001**, *115*, 6528.

3. Himenz, P. *Principles of Colloid and Surface Chemistry.* Marcel Dekker: New York, 1977.

4. Marques, C.; Joanny, J.; Leibler, L. *Macromolecules* **1988**, 21, 1051.

APPENDIX B

CUMULANT FITTING AND HARD-SPHERE FORM FACTOR FOR PS-PI-$(PI)_2$ MIKTOARM COPOLYMERS IN N-HEXANE

Cumulant fitting

Light intensity autocorrelation functions, expressed as $[g_2(q,\tau)\text{-}1]^{1/2}$, for the all copolymers studied in n-hexane at 30 μg/mL can be fit using the method of cumulants (Eq. 2.3).[1] Data and fitting results of up to 90% of the correlation function decay are shown in Figure B.1 for sample MA1 at 30 μg/mL at four scattering angles.

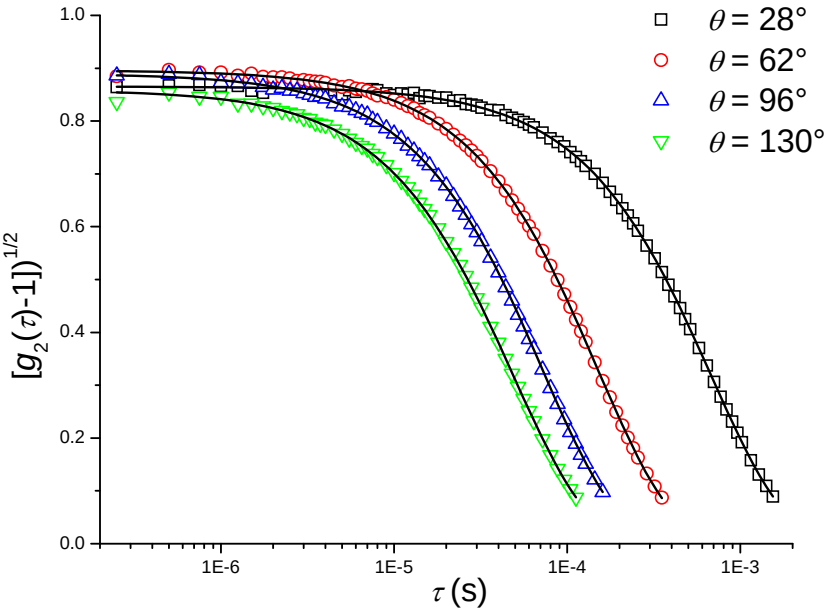

Figure B.1. Light intensity autocorrelation functions and cumulant fits (black solid lines) at four scattering angles for sample MA1 at 30 μg/mL in n-hexane.

Hard-sphere form factor for micellized PS-PI-$(PI)_2$ miktoarm block copolymers

Further insight into the morphology of the self-assembled miktoarms can be gained by analyzing the scattered intensity $I(q)$ from the SLS experiments. Figure B.2 shows a

plot of $I(q)$ defined as $I(q) = I(q = 0)*P(q)$, where $I(q = 0)$ is the intensity at zero scattering angle, for the copolymers studied at c = 30 μg/mL. Although the q-range covered is not sufficient to see fringes in the $I(q)$ profiles, the data can be fit using the particle form factor derived for hard-sphere morphologies:[2]

$$P(q) = \left\{ \frac{3}{(qR_g)^3} \left[\sin(qR_g) - (qR_g)\cos(qR_g) \right] \right\}^2 \qquad \text{(B.1)}$$

By using this approach the same results for R_g and $M_{w,app}$ are obtained as when Eq. 2.6 is used (Berry plot). This analysis provides additional support for the conclusion that a spherical morphology is adopted by the micelles formed by the PS-PI and PS-PI-$(PI)_2$ miktoarm block copolymers.

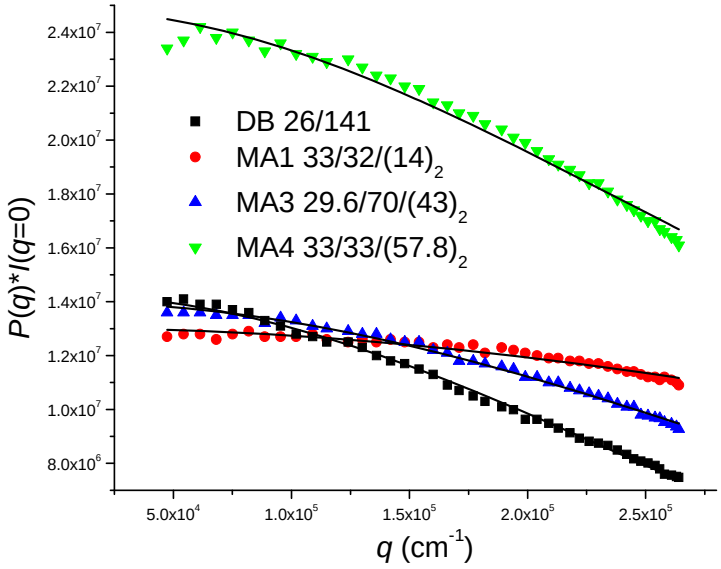

Figure B.2. Scattered intensity $I(q)$ for PS-PI-$(PI)_2$ miktoarm and PS-PI block copolymers at c = 30 μg/mL. Solid black lines are the fits produced using a hard-sphere particle form factor (Eq. B.1).

References

1. Koppel, D. *J. Chem. Phys.* **1972**, *57*, 4814.

2. Schärtl, W. *Light Scattering from Polymer Solutions and Nanoparticle Disperions*; Springer: Berlin, 2007.

APPENDIX C

DETERMINATION OF RADIUS OF GYRATION FOR SINGLE PS-PI-$(PI)_2$ MIKTOARM COPOLYMERS IN N-HEXANE

The radius of gyration of single branched miktoarm polystyrene (PS) and polyisoprene (PI) block copolymers (see Figure 2.1), $R_{g,br}$, in n-hexane could not be determined by light scattering methods at concentrations below 3 μg/mL due the low $I(q)$ and incoherent scattering. However $R_{g,br}$ can be calculated from three different approaches based on chain statistics: i) star homopolymer branching parameter ii) Yamakawa's branching parameter and iii) average arm calculations. Each approach is discussed and the equations required to determine $R_{g,br}$ are developed. The first two methods incorporate Flory's branching parameter, g, in the determination of geometric size for branched chains, where the $R_{g,br}$ of a branched PI homopolymer in n-hexane can be written as:[1]

$$R_{g,br} = g^{1/2} b_{PI} N_{PI}^{\nu}, \text{ where } b_{PI} = 1.68\text{Å} \text{ and } \nu = 0.57 \qquad \text{(C.1)}$$

Here b_{PI} is the statistical segment size for PI and N_{PI} the degree of polymerization of the PI block. The values for b_{PI} and ν were calculated from intrinsic viscosity measurements.[39] Because n-hexane is a poor solvent for PS, it is assumed that the PS block is collapsed and, in the case of an isolated single chain, it does not contribute significantly to $R_{g,br}$ (see Figure C.1). Therefore, the calculations treat the branched PI-$(PI)_2$ blocks only, and the results for each method are presented in Table C.1. Knowing $R_{g,br}$ would be of use when interpreting the light scattering results, specifically whether

the copolymers exist as isolated chains or as micellar aggregates in solution. Also, by determining g for each of the miktoarm samples, it is possible to properly 'rescale' the values of N_{PI} used in the comparisons of our experimental results with theoretical predictions for block copolymer micelles in dilute solution. As stated in Chapter 2, this rescaling helps to elucidate whether an 'equivalent' diblock copolymer would show the same micellar properties as the miktoarms. The first two approaches allow the g parameter that properly describes the effects of branching in a polymer chain to be found while the third approach uses a formula directly derived for PI homopolymer stars to determine $R_{g,br}$.

Star Homopolymer Branching Parameter. The branching parameter, g, for any type of branched copolymer is defined as the ratio between the mean-squares of the radius of gyration of the branched polymer, $R_{g,br}$ and that of a linear polymer of the same molecular weight, $R_{g,l}$. Specifically, for monodisperse star homopolymers with f symmetrical arms, g can be written as:[2]

$$g = \frac{\left\langle R_{g,br}^2 \right\rangle}{\left\langle R_{g,l}^2 \right\rangle} = \frac{3f-2}{f^2} \tag{C.2}$$

Equation C.2 works well for θ–solvent conditions, but in the case of a good solvent, g is found to be ≈ 6% greater than the experimental value.[1] f is also called the functionality and it is defined as:

$$f = M_{w,star} / M_{w,a} \tag{C.3}$$

Where $M_{w,star}$ is the total molecular weight of the star and $M_{w,a}$ is the molecular weight of a single arm (or branch). Considering the PI-$(PI)_2$ blocks of the miktoarms as a

symmetric 3-arm star, $g = 0.77$. This value is used in Eq. (C.1) to calculate $R_{g,br}$ for each of the samples studied based on their N_{PI}. The main drawback of this approach is that it does not take into account the asymmetry of the macromolecules. To address this shortcoming, a manner proposed by Yamakawa is used to determine g. This approach is based on the dividing the branched structure into subsegments between branching points.[3]

Yamakawa's Calculation of the *g* Branching Parameter. This method takes into account the size of each segmenr of the branched polymer; consequently, it can be used for non-symmetrical arrangements. Yamakawa's g parameter is defined by:[3]

$$g = \frac{1}{N^p}\left[\sum_{\lambda=1}^{p}\left(3NN_\lambda^2 - 2N_\lambda^3\right) + 6\sum_{(\lambda,\mu)} N_\lambda N_{\lambda\mu} N_\mu\right] \tag{C.4}$$

where N is the total number of segments or degree of polymerization of the whole branched polymer, N_λ the number of segments in the λ^{th} subsegment, p is the total number of subchains or branches. $N_{\lambda\mu}$ the number of segments in subchains that lie between the λ^{th} and μ^{th} subchains. For the PI-$(PI)_2$ miktoarm stars, the second summation in Eq. C.4 is zero because there are no segments between the subchains, which allows Eq. C.4 for the PI-$(PI)_2$ branched homopolymer to be rewritten simply as:

$$g = \frac{1}{N^3}\left[(3NN_1^2 - 2N_1^3) + 2(3NN_2^2 - 2N_2^3)\right] \tag{C.5}$$

Figure C.1 identifies subchain 1 as the stem, while the two arms constitute the second subchains (which are labeled as 2 since both have the same N_{PI}). By using Eq. C.5 it is possible to calculate g for the miktoarm stars and then use Eq. C.1 to find $R_{g,br}$. These results are also given in Table C.1.

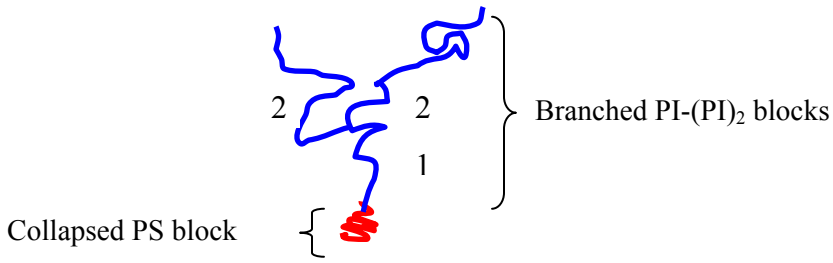

Figure C.1. Representation of a PS-PI-$(PI)_2$ miktoarm copolymer. In the $R_{g,br}$ calculations only the branched PI-$(PI)_2$ blocks is taken into account.

Average Arm Calculations. The third approach is based on an average arm molecular weight, $M_{w,avg}$, which is calculated by dividing $M_{w,tot}$ by f. ($f = 3$ in the case of PI-$(PI)_2$.) $R_{g,br}$ is then calculated using the following formula derived from light scattering and intrinsic viscosity measurements of star PI homopolymers in cyclohexane, and it is applicable to stars of $f \geq 3$:[4]

$$R_{g,br} = 1.37 f^{0.175} R_{g,avg} \tag{C.6}$$

Here the radius of gyration of the average arm, $R_{g,avg}$, is calculated by Eq. C.1 using an average arm degree of polymerization, $N_{A,avg}$ and assuming $g = 1$. The $R_{g,br}$ results for the three approaches are summarized and the comparison of the g values obtained by each method is shown in Table C.1.

Table C.1. Radius of gyration and branching parameter for PS-PI and PS-PI-$(PI)_2$ miktoarm block copolymers in n-hexane.

Sample ID	N_{PS}	N_{PI}	Star Homopolymer		Yamakawa		Avg. Arm	
			$R_{g,br}$ (nm)	G	$R_{g,br}$ (nm)	g	$R_{g,br}$ (nm)	g
DB	250	2073	13.1	1.00				
MA1	317	882	6.2	0.77	6.6	0.83	7.1	0.89
MA3	285	2294	10.6	0.77	11.0	0.80	12.3	0.89
MA4	317	2185	10.4	0.77	10.7	0.80	11.9	0.89

The calculated $R_{g,br}$ values for the PI-$(PI)_2$ branched polymers show the expected trend, with sample MA1 having smallest value and sample MA3 having a slightly larger value of $R_{g,br}$ in comparison to MA4, which comes from the larger N_{PI} of the former. Due to its linear architecture, sample DB has a larger R_g in comparison to branched samples MA3 and MA4. (Again it is noted that samples DB, MA3 and MA4 have similar N_{PI}.) Concerning the g values obtained by each approach, the ones determined using the average arm approach are larger than those calculated using the two other approaches. In consideration of all the three methods, it is seen that $g \approx 0.8$, and therefore this value is used to 'rescale' N_{PI} for use as parameter N_A in the calculations developed by Zhulina et al.[5] to compute Q and R_h^s of spherical micelles based on a equivalent-sized linear diblock as discussed in Chapter 2.

References

1. Tian, P. Structure and Scaling of Polymer Brushes Formed by Branched Copolymers. Ph.D. Dissertation, Clemson University, Clemson, SC, 2004.

2. Mazur, J; McCrakin, F. *Macromolecules* **1977**, *10*, 326.

3. Yamakawa, H. *Modern Theory of Polymer Solutions*; Harper and Row: New York, 1971.

4. Bauer, B.; Fetters, L.; Graessley, W.; Hadjichristidis, M.; Quack, G. *Macromolecules* **1989**, *22*, 2337.

5. Zhulina, E.; Adam, M.; LaRue, I.; Sheiko, S.; Rubinstein, M. *Macromolecues* **2005**, *38*, 5330.

APPENDIX D

CALCUTION OF THE CONTRIBUTION FROM TWO DIFFUSING SPECIES TO STATIC AND DYNAMIC LIGHT SCATTERING EXPERIMENTS

The DLS measurements of sample MA3 at 3 μg/mL show two distinct peaks in the hydrodynamic radii distribution, as seen in Figure D.1. Due to the presence of the two hydrodynamic radii peaks, a double exponential decay (Eq. 2.4) is used to fit the autocorrelation function in order to obtain amplitudes $A_1$and A_2, and mean decay rates Γ_1 and Γ_2. It is necessary to normalize A_1 and A_2 to properly determine the relative contribution of each diffusing species to $I(q)$. The normalized amplitudes of the fast and slow diffusing species, A_f and A_s, respectively, can be calculated from:[1]

$$A_f = \frac{A_1}{A_1 + A_2} \quad \text{and} \quad A_s = \frac{A_2}{A_1 + A_2} \tag{D.1}$$

Because the DLS experiments were run at 16 angles and SLS experiments at 44 angles, the dependence of A_f and A_s on q^2 are obtained by a linear fit of the normalized amplitude data, as shown in Figure D.2. The fitting of the normalized amplitudes from the DLS results yields $A_f = 0.089 + (3.012\times10^{-13})q^2$ and $A_s = 0.911 - (3.012\times10^{-13})q^2$. These two results then can then be used to predict the contribution of the fast and slow diffusing species to $I(q)$ measured at each scattering angle in the SLS experiments using the following formalism:[1]

$$\left(\frac{Kc}{\Delta R}\right)_{fast} = \frac{1}{A_f}\left(\frac{Kc}{\Delta R}\right)_{tot} \quad \text{and} \quad \left(\frac{Kc}{\Delta R}\right)_{slow} = \frac{1}{A_s}\left(\frac{Kc}{\Delta R}\right)_{tot} \tag{D.2}$$

The results of the contribution of each population of diffusing species to the SLS experiments are shown in Figure 2.9.

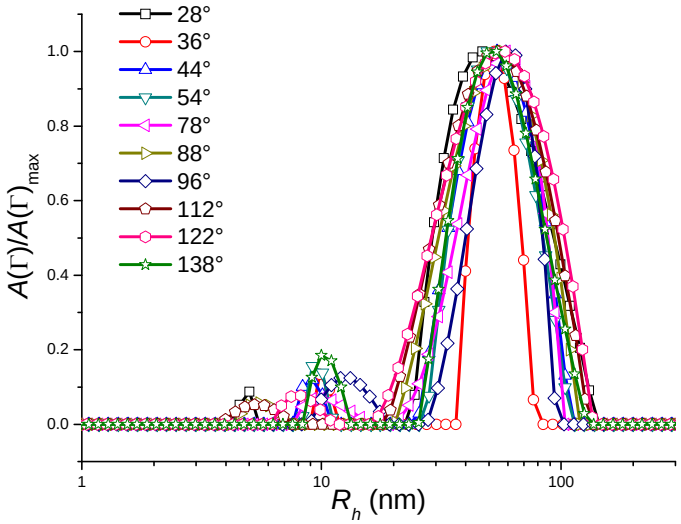

Figure D.1. Hydrodynamic size distribution from CONTIN analysis for sample MA3 at 3 μg/mL in n-hexane. Large peaks correspond to spherical micellar aggregates whereas small peaks are attributed to small copolymer aggregates.

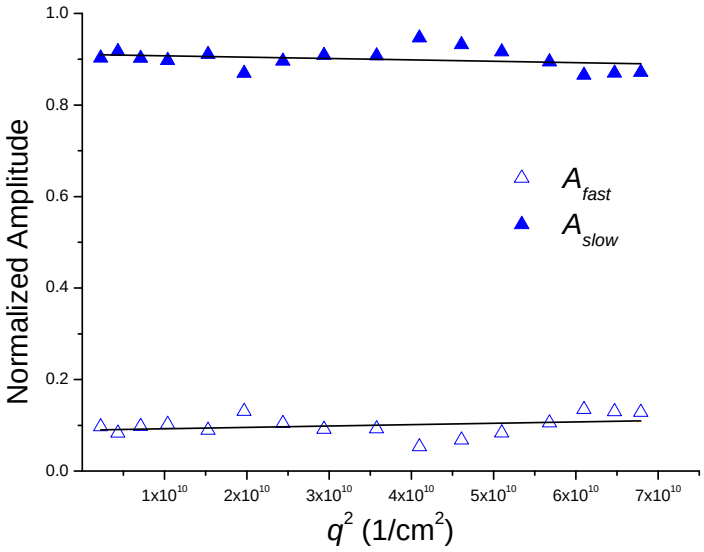

Figure D.2. Normalized amplitude for fast and slow diffusing modes for sample MA3 at 3 μg/mL in n-hexane. Solid black lines correspond to linear fits used to establish q^2-dependance of each mode.

References

1. Kawaguchi, T.; Kobayashi, K.; Osa, M.; Yosizaki, T. *J. Phys. Chem. B.* **2009**, *113*, 5440.

APPENDIX E

ATOMIC FORCE MICROSCOPY OF PS-PI-$(PI)_2$ MIKTOARM BLOCK COPOLYMERS PREFERENTIALLY ADSORBED ONTO SILICON SUBSTRATES FROM N-HEXANE SOLUTIONS

After measurements of kinetics of the preferential adsorption of the PS-PI-$(PI)_2$ miktoarm block copolymers were completed (as discussed in Chapter 3), the samples were removed from the fluid cell and allowed to dry in the ambient air for at least 5 minutes. It is worth noting that evaporation of n-hexane took place rather quickly and there was no visual evidence of solvent remaining on the substrate. The atomic force microscopy (AFM) experiments were carried out using a Veeco Instruments Nanoscope IIIa equipped with a silicon-nitride tip and in tapping mode. Images were single flattened to correct for the tilt and bow of the cantilever. A total of 256 lines at a rate of 1 Hz were taken for each image.

The height and phase images acquired from the miktoarm copolymer PS-PI-$(PI)_2$ $(29.6/70/(43)_2)$ (identified as MA3 in Table 3.1) adsorbed from solution in n-hexane at 30 μg/mL are presented in Figure E.1. The height image (on the left) shows spherical aggregates on the surface, likely corresponding to surface hemi-micelles as has been observed previously by Hamley and coworkers for polypropylene – poly(ethylene oxide) diblock copolymers adsorbed from water solutions.[1] Although there is some controversy about the interpretation of phase images obtained by AFM experiments,[2-4] it is believed the phase image (on the right in Figure E.1) shows differences in stiffness between the core and corona of the surface hemi-micelles: The bright center of each hemi-micelle

likely corresponds to the PS glassy core, whereas the surroundings darker halos correspond to the softer, rubbery PI corona. While we are unable to resolve whether the area between the aggregates is populated with adsorbed single chains or simply the bare silicon substrate, based on the brightness of the phase image between the aggregates, it is speculated there are some adsorbed chains as well as uncovered silicon. Figures E.2 and E.3 show the height and phase AFM images of PS-PI-$(PI)_2$ miktoarm copolymer samples MA1 $(33/32/(14)_2)$ and MA4 $(33/33/(58.8)_2)$, respectively, after they had been preferentially adsorbed onto silicon substrates. Unfortunately, the phase images for these two samples did not show the contrast between the PS core blocks and the PI coronas that was observed in Figure E.1. However, I believe these images show strong evidence for the presence of surface hemi-micelles on the silicon substrates. It is worth noting that these images were taken on dried layers, and during the solvent evaporation period some reorganization of the polymer may have occurred. Certainly the PI chains contract because air is a poor solvent. As a comparison, the height and phase AFM images for a freshly cleaned bare silicon wafer are shown in Figure E.4.

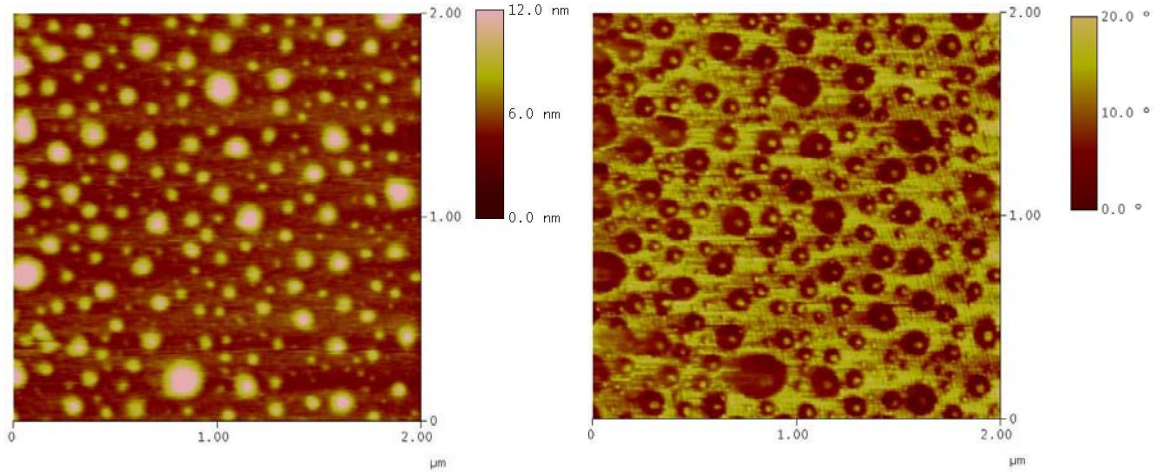

Figure E.1. Height and phase images obtained after adsorption of MA3 from n-hexane at 30 µg/mL.

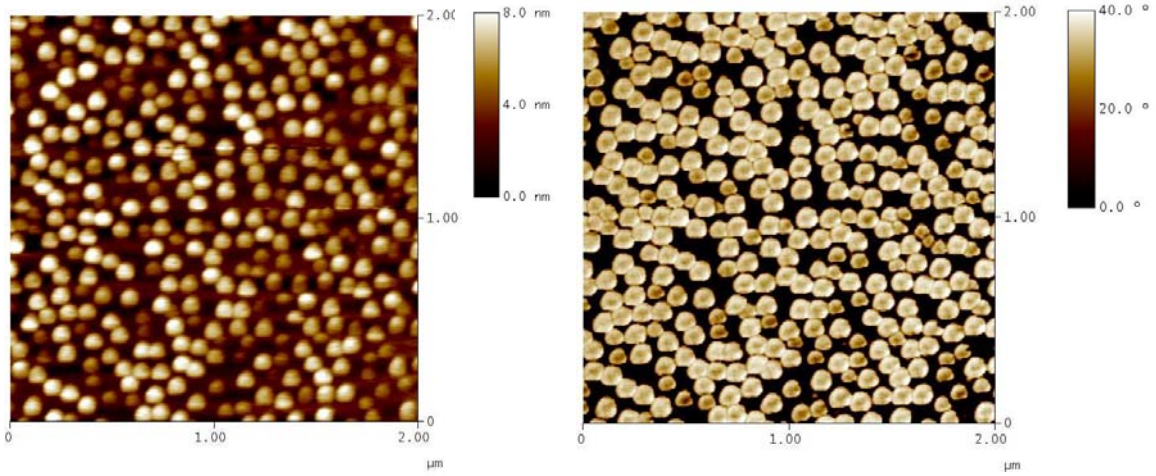

Figure E.2. Height and phase images obtained after adsorption of MA1 from n-hexane at 30 µg/mL.

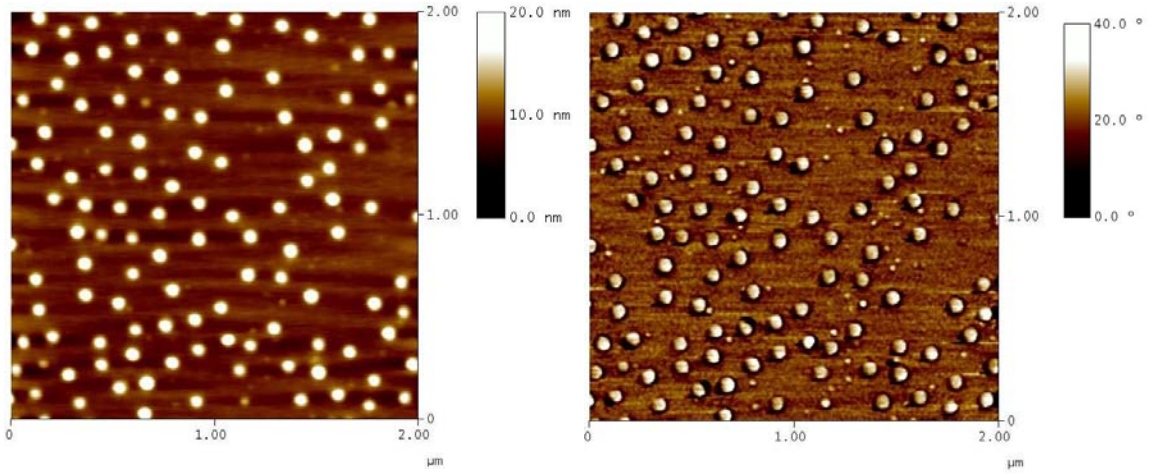

Figure E.3. Height and phase images obtained after adsorption of MA4 from n-hexane at 30 µg/mL.

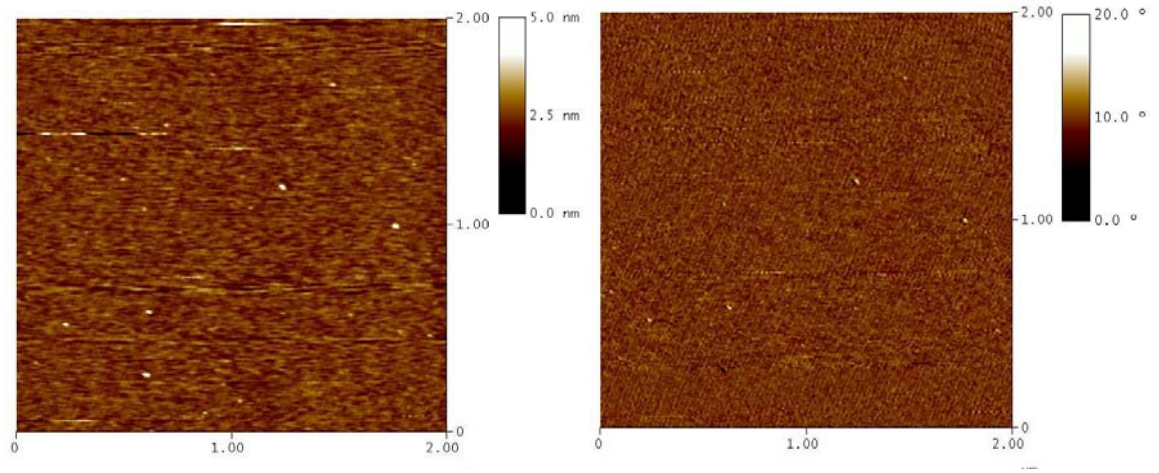

Figure E.4. Height and phase images obtained for a freshly cleaned, bare silicon wafer.

References

1. Hamley, I.W.; Connell, S.; Collins, S. *Macromolecules* **2004**, *37*, 5337.

2. Knoll, A.; Magerle, R.; Krausch, G.; *Macromolecules* **2001**, *34*, 4159.

3. Wang, Y.; Song, R.; Yingshun, L.; Shen, J. *Surf. Sci.* **2003**, *530*, 136.

4. Cleveland, J.P.; Anczykowski, B.; Schmid, A.; Elings, V. *Appl. Phys. Lett.* **1998**, *72*, 2613.

APPENDIX F

DYNAMIC LIGHT SCATTERING RESULTS FOR A_NB_N HETEROARM STAR COPOLYMERS

Figure F.1 shows a comparison of the normalized light intensity autocorrelation functions, $[g_2(q,\tau)\text{-}1]^{1/2}$, (see Equation 2.1) for the A_nB_n heteroarm star copolymers at all of the concentrations studied. It is seen clearly that as concentration increases, the values of $[g_2(q,\tau)\text{-}1]^{1/2}$ increase because there is less incoherent scattering from the solutions. This pattern of behavior is most strikingly observed in the smaller heteroarm star copolymers, A_1B_1 and A_2B_2.

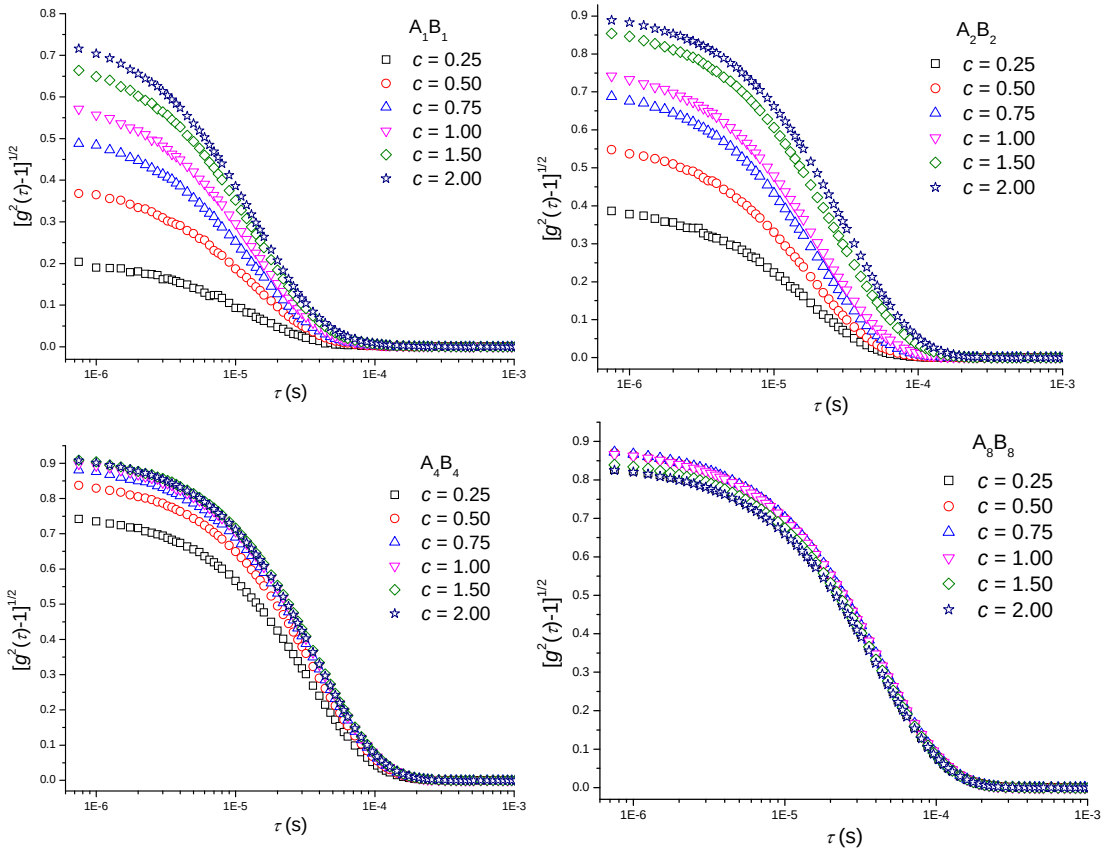

Figure F.1. Autocorrelation functions for A_nB_n heteroarm star copolymers at the six concentrations studied and $\theta = 96°$. Concentrations given in the legends are in units of mg/mL.

The following tables show all of the results for the solution diffusion coefficient, D_s, and the hydrodynamic radius, R_h, for the A_nB_n hetero-arm stars in n-hexane at the six concentrations studied. Fast modes for samples A_1B_1 and A_2B_2 correspond to the population of scatterers having smaller R_h found from dynamic light scattering experiments. These R_h values correspond to single $(PS)_1(PI)_1$ and $(PS)_2(PI)_2$ heteroarm stars in solution. The slow modes arise from the aggregation of the A_1B_1 and A_2B_2 heteroarm stars, which explains the larger R_h and smaller D_s. For stars A_4B_4 and A_8B_8, only single stars are observed over the concentration rage studied; thus, no fast or slow labeling is needed.

Table F.1. Hydrodynamic properties of $(PS)_1(PI)_1$ (A_1B_1) heteroarm star copolymers in n-hexane at several concentrations.

Sample ID	c (mg/mL)	D_s (cm^2/s)	R_h (nm)
A_1B_1	0.24	8.97×10^{-7}	8.3
A_1B_1	0.47	8.60×10^{-7}	8.7
A_1B_1 fast	0.72	1.06×10^{-6}	7.1
A_1B_1 slow	0.72	2.46×10^{-7}	30.4
A_1B_1 fast	0.98	9.85×10^{-7}	7.6
A_1B_1 slow	0.98	1.69×10^{-7}	44.1
A_1B_1 fast	1.49	1.02×10^{-6}	7.3
A_1B_1 slow	1.49	1.96×10^{-7}	38.0
A_1B_1 fast	2.00	1.01×10^{-6}	7.4
A_1B_1 slow	2.00	1.95×10^{-7}	38.3

Table F.2. Hydrodynamic properties of $(PS)_2(PI)_2$ (A_2B_2) heteroarm star copolymers in n-hexane at several concentrations.

Sample ID	c (mg/mL)	D_s (cm^2/s)	R_h (nm)
A_2B_2	0.25	6.93×10^{-7}	10.8
A_2B_2	0.44	6.69×10^{-7}	11.1
A_2B_2	0.75	6.01×10^{-7}	12.4
A_2B_2	0.91	5.61×10^{-7}	13.3
A_2B_2 fast	1.52	6.61×10^{-7}	11.3
A_2B_2 slow	1.52	2.63×10^{-7}	28.3
A_2B_2 fast	1.99	6.36×10^{-7}	11.7
A_2B_2 slow	1.99	2.72×10^{-7}	27.4

Table F.3. Hydrodynamic properties of $(PS)_4(PI)_4$ (A_4B_4) heteroarm star copolymers in n-hexane at several concentrations.

Sample ID	c (mg/mL)	D_s (cm^2/s)	R_h (nm)
A_4B_4	0.27	3.49×10^{-7}	21.4
A_4B_4	0.47	3.26×10^{-7}	22.9
A_4B_4	0.77	3.16×10^{-7}	23.6
A_4B_4	0.99	3.11×10^{-7}	23.9
A_4B_4	1.46	3.08×10^{-7}	24.2
A_4B_4	1.97	3.10×10^{-6}	24.0

Table F.4. Hydrodynamic properties of $(PS)_8(PI)_8$ (A_8B_8) heteroarm star copolymers in n-hexane at several concentrations.

Sample ID	c (mg/mL)	D_s (cm^2/s)	R_h (nm)
A_8B_8	0.24	2.86×10^{-7}	26.1
A_8B_8	0.49	2.84×10^{-7}	26.3
A_8B_8	0.72	2.83×10^{-7}	26.3
A_8B_8	0.98	2.83×10^{-7}	26.3
A_8B_8	1.47	2.87×10^{-7}	26.0
A_8B_8	2.01	2.90×10^{-6}	25.7